A MOLECULAR LOOP WITH INTERSTITIAL CHANNELS IN A CHIRAL ENVIRONMENT AND STUDY OF FORMATION OF METAL-METAL BONDS IN DINICKEL, DIPALLADIUM AND DITITANIUM COMPLEXES

A Dissertation

by

SERGEY IBRAGIMOV

Submitted to the Office of Graduate Studies of
Texas A&M University
in partial fulfillment of the requirements for the degree of

DOCTOR OF PHILOSOPHY

May 2006

Major Subject: Chemistry

A MOLECULAR LOOP WITH INTERSTITIAL CHANNELS IN A CHIRAL ENVIRONMENT AND STUDY OF FORMATION OF METAL-METAL BONDS IN DINICKEL, DIPALLADIUM AND DITITANIUM COMPLEXES

A Dissertation

by

SERGEY IBRAGIMOV

Submitted to the Office of Graduate Studies of
Texas A&M University
in partial fulfillment of the requirements for the degree of

DOCTOR OF PHILOSOPHY

Approved by:

Chair of Committee,	F. A. Cotton
Committee Members,	E. E. Simanek
	R. E. Schaak
	R. Tribble
Head of Department,	Emile A. Schweikert

May 2006

Major Subject: Chemistry

ABSTRACT

A Molecular Loop with Interstitial Channels in a Chiral Environment

and

Study of Formation of Metal-Metal Bonds in Dinickel, Dipalladium and Dititanium Complexes. (May 2006)

Sergey Ibragimov, M.S., Chemistry, Lomonosov Moscow State University

Chair of Advisory Committee: Dr. F. Albert Cotton

This dissertation consists of two independent topics: (1) a molecular loop with interstitial channels in a chiral environment; (2) study of formation of metal-metal bonds in dinickel, dipalladium and dititanium complexes

On the first topic, a study of the reaction products of the interaction of *cis*-$Mo_2(DAniF)_2(CH_3CN)_4^{2+}$ corner pieces with *ortho*-, *meta*- and *para*- isomers of enatiomerically pure $^{-}O_2CCH(CH_3)C_6H_4CH(CH_3)CO_2^{-}$ dicarboxylate was performed. First, an enantiomerically pure molecular loop based on two dimolybdenum units and two *para*-dicarboxylate linkers was synthesized and structurally characterized. Similar reactions with isomeric *ortho*- and *meta*- dicarboxylate linkers, as well as with some nonchiral ligands, showed that the structure of the obtained products depends on the geometry of the ligand. *Meta*- dicarboxylate linker favors the formation of the chelated product and *ortho*- dicarboxylate linker produces the mixture of chelated molecules and loops.

On the second topic, an investigation of the formation of metal-metal bonds was performed. Study of the one-electron bond obtained upon oxidation of Ni_2^{4+} and Pd_2^{4+} to Ni_2^{5+} and Pd_2^{5+}, respectively, was made. The compounds synthesized were studied with various physical methods, such as X-ray crystallography, UV-visible spectroscopy and EPR spectroscopy. The nature of oxidized species as well as the dependence of metal-metal interactions on electron-donating abilities of bridging ligands was studied. It was shown that oxidation takes place on a metal center. The formation of one-electron bond in oxidized species is proposed.

Finally formation of Ti_2^{6+} single bonded compounds by the reduction of two Ti^{4+} monomers to Ti_2^{6+} dimer was studied. The nature of the species obtained in solution and in solid state is discussed. The crystal structure shows the presence of two types of hpp ligands – chelating and bridging. NMR study of this compound in solution proposes the rearrangement of this structure to a paddlewheel.

DEDICATION

To all those who gave their lives fighting for Russia.

ACKNOWLEDGEMENTS

I greatly thank Dr. Cotton for providing the opportunity to work in the LMSB. I also would like to thank him for explaining to me that "world does not pay you for trying, it pays you for succeeding." I guess I will live according to this expression until the day I die.

I am very grateful to Carlos for assigning me projects and for his guidance and help. Without his expertise in synthetic chemistry and his patience with me none of these projects would be finished.

I would like to acknowledge the great contribution that was made to this work by John F. Berry. I've never shared the lab with a person who is perfect in everything he does, including his hobbies. I would like to thank Dino for doing all the calculations, helping me with the computer when it was "offending" me and for being a good friend. I am very grateful to Liu for showing me various synthetic tricks and for teaching me how to grow nice crystals. Rongmin was very helpful in mounting the crystals. Xiaoping Wang taught me a lot about crystallography. Penglin gave me several very helpful suggestions. Vladimir Ivanovich Bahmutov is an NMR expert and spent a lot of time studying my spectra, helping me to carry out NMR experiments and teaching me about this method. Dr. Simanek helped me a lot in understanding organic chemistry. Liza Hillard was a great person to talk to when I had "non-chemical" problems. I also acknowledge the work of Julie and Beverly in the preparation of manuscripts. I also

thank all past and present members of the LMSB for their support and help through the years.

I would like to thank Erin, Charles, Jennifer, Jessie, Juan, Ivan, Juliya, Mikhail, Irina and all my friends in College Station for making it such a fun place to live. I would like to thank my parents and my grandmother for persuading me to come here to get my Ph.D. I would like to thank all my relatives in my hometown Baku for their support.

I, also, would like to thank Mila, Viktorija, Aleksey, Konstantin, Sergey, Igor' Aleksandrovich, Tanja, Nikolay, Sasha, Anna and all my friends back in Russia for staying great friends even after I moved away from Moscow.

TABLE OF CONTENTS

LIST OF FIGURES

FIGURE Page

FIGURE Page

FIGURE Page

LIST OF TABLES

CHAPTER I

INTRODUCTION

The discovery of the unsupported quadruple bond in $Re_2Cl_8^{2-}$ is a landmark for inorganic chemistry. During the past four decades, thousands of dimetal compounds have been synthesized and physically characterized.[1]

Those compounds are promising materials in various areas, two of which are catalysis and supramolecular chemistry. Their application as building blocks for large molecules was recently discovered in our research group.[2] A lot of interesting properties of these species such as stacking of molecules on top of each other when crystallized, empty spaces inside the compounds large enough to accommodate different molecules, ability to easily control the size of these empty spaces, etc. were observed. The first part of this dissertation is devoted to obtaining

these supramolecular compounds based on dimetal building blocks and chiral linkers. The aim of this research is to create a chiral environment in these supramolecules and to study the influence of geometry of the starting material on the structure of the obtained product.

The second part of this dissertation is the study of the formation and properties of one- and two-electron bond between two metal centers. This can be done in two ways (Scheme 1).

This dissertation follows the style of *Inorganic Chemistry*.

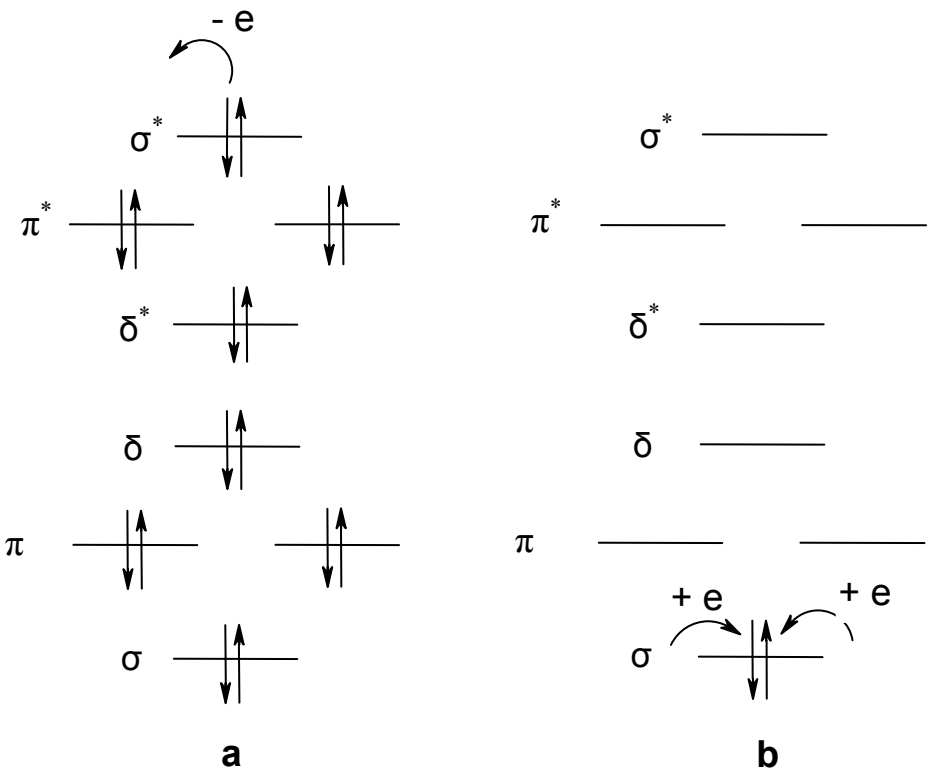

Scheme 1

For Pd_2^{4+} and Ni_2^{4+} compounds both bonding and antibonding orbitals are filled, (Scheme 1a) resulting in bond order of 0 and therefore no chemical bond between metal centers is to be expected. Upon oxidation one can remove 1 or 2 electrons from the compound. In our research we will try to answer the question whether this oxidation leads to formation of chemical bond between metal atoms and what are the electronic properties of the oxidized species.

Ti^{4+} has no electrons on its outer shell (Scheme 1b). By chemically reducing Ti(IV) – organometallic complexes such as $Ti(hpp)_2Cl_2$ to Ti(III) we aim at obtaining a Ti_2^{6+} paddlewheel molecule with single Ti-Ti bond.

CHAPTER II

A MOLECULAR LOOP WITH INTERSTITIAL CHANNELS IN A CHIRAL ENVIRONMENT

INTRODUCTION

Metal-metal bonded compounds have proven useful in many areas such as catalysis,[3] medicine[4] and for building supramolecular arrays.[2] Some of the most notable catalytic processes employ chiral ligands that induce optical activity in the products.[5] Chirality is also of great importance in medicine as many processes, e.g., enzymatic processes,[6] are controlled by optically active centers. In the field of supramolecular chemistry some efforts have been made to study the use of chiral ligands attached to metal centers[7] but often structural characterization is hampered by difficulties in crystallizing large chiral molecules.[8] Only two systems having chiral species bound to metal–metal bonded centers have been structurally characterized. One of them is a triangle made with $Ru_2(CO)_4L_2$ corner pieces, L = axial MeCN or PPh_3, with optically active tartrate dianions as linkers.[9] The other is a set of molecular pairs containing two $Mo_2(DAniF)_3^+$ units (DAniF = *N*,*N*′-di-*p*-anisylformamidinate) bridged by either L-tartrate or D-aspartate.[10]

A useful type of dimetal unit in the construction of polygonal supramolecules is *cis*-$M_2(DAniF)_2$, M = Mo, Ru and Rh, which can form loops, triangles, squares or more complex entities[11] depending on the nature of the linker and the presence or absence of

axial ligation. For example, we have shown that *cis*-$M_2(DAniF)_2$ corner pieces give squares with rigid dicarboxylate linkers such as the dianion of terephthalic acid,[12] triangles with the less constrained 1,4-dicyclohexyldicarboxylate[13] and loops with the more flexible or bent bridges such as homophthalate, phenylenedicarboxylate and malonate anions[14] as summarized schematically in Scheme 2.

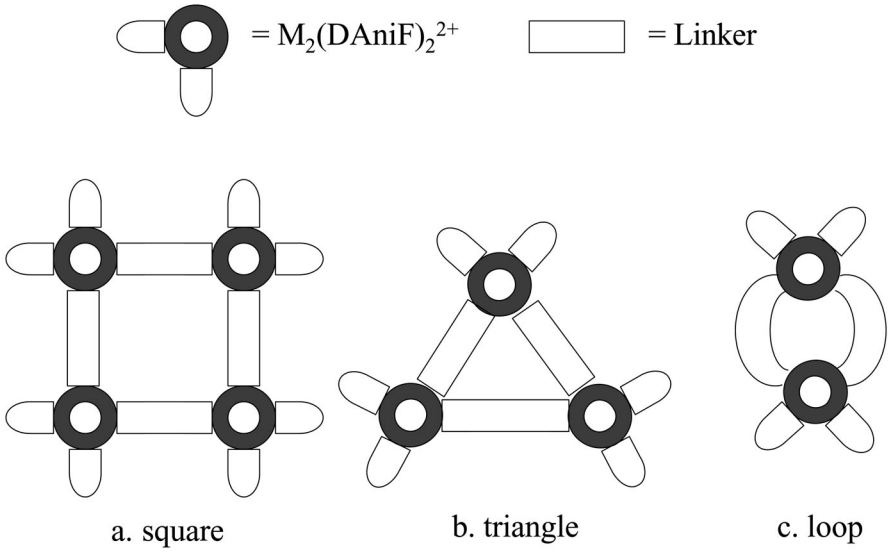

Scheme 2

Interestingly, most of these compounds crystallize in such way that the molecules stack to form channels,[2] which can be filled with other molecules, and the size of the channels can be controlled by the length of the linkers. For example, the $Ru_2(CO)_4L_2$ corner piece produces a molecular square and a molecular loop by using oxalate and malonate linkers, respectively.[15] Bonar-Law[16] and others[17] before him have shown that bidentate ligands with well separated carboxylate groups can be used to bind two *cis* equatorial positions of a dimetal unit. For example, with dirhodium units, the use of *m*-$HO_2CC(CH_3)_2O$-C_6H_4-$OC(CH_3)_2CO_2H$ dicarboxylic acid yields a chelated compound (Scheme 3). This chelated species reacts further with rigid dicarboxylic acids to form

squares,[16,18] or with pyridine to form π-stacked columns with hexagonal holes.[19] A similar tetracarboxylate has been used to link two dirhodium units into a dimer.[20] With a long rigid dicarboxylate ligand, these dimetal units can be linked together in a vertical manner along the Rh-Rh axis.[21]

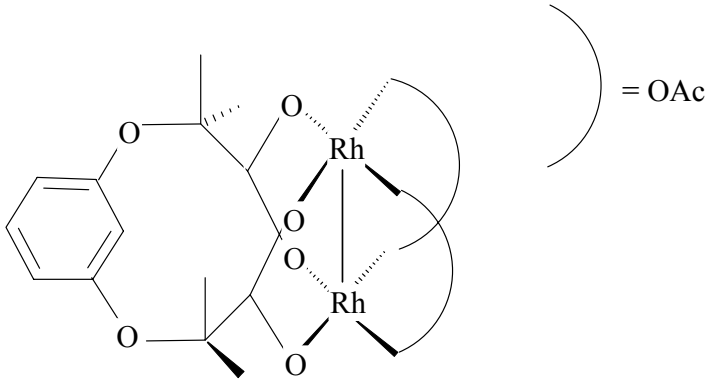

Scheme 3

In this report we describe exploratory work combining quadruply bonded $[Mo_2(DAniF)_2]^{2+}$ units with enantiomerically pure ligands[22, 23] of the type shown in Scheme 4 which will be labeled as *p*-H_2**L1**, *m*-H_2**L2** and *o*-H_2**L3** for the *para*-, *meta*- and *ortho*-substituted species, respectively. The *meta* ligand, $\mathbf{L2}^{2-}$, is akin to the one shown in Scheme 3. The latter has Me_2C units, whereas **L2** has chiral MeHC units. We report the first structural characterization of a chiral molecular loop and show that it crystallizes to form chiral cavities. We also report the structure of a related dinuclear species in which a dicarboxylate anion wraps around to chelate the dinuclear species.

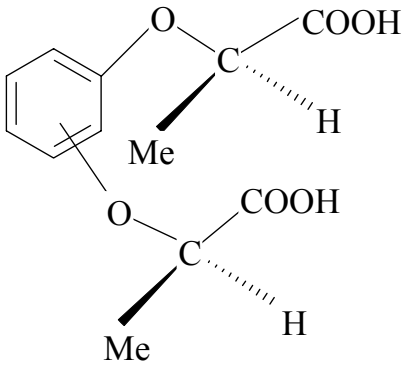

H_2**L1** - *para*

H_2**L2** - *meta*

H_2**L3** - *ortho*

Scheme 4

EXPERIMENTAL SECTION

General Comments. Unless otherwise stated, all operations were carried out in Schlenkware under an inert atmosphere and by using carefully dried and oxygen-free solvents. Acetonitrile was dried by distillation over CaH_2 in a nitrogen atmosphere. Ethanol was prepared by boiling it with $Mg(OEt)_2$ in a nitrogen atmosphere, followed by distillation. All other solvents were purified using a Glass Contour solvent purification system. *Cis*-$Mo_2(DAniF)_2(CH_3CN)_4 \cdot 2BF_4 \cdot 2CH_3CN$[24] (**0**), the chiral diacids[22, 23] *o*-H_2**L3**, *m*-H_2**L2** and *p*-H_2**L3**, and the non-chiral diacid *m*-$HO_2C(CH_3)_2O\text{-}C_6H_4\text{-}OC(CH_3)_2CO_2H$, [14] H_2**L4**, were prepared following published methods. The nonchiral *ortho*- ligand, H_2**L5**, was prepared as described below following a modified experimental procedure.[25] Commercially available chemicals were used as received. IR spectra were recorded on a Perkin-Elmer 16PC FTIR spectrometer using KBr pellets. ^{1}H NMR spectra were obtained on a Varian XL-300 spectrometer with chemical shifts (δ, ppm) referenced to the signal of the deuterated solvent. Elemental analyses were performed by Canadian

Microanalytical Services in British Columbia, Canada. The electrochemical measurements were recorded on a BAS 100 electrochemical analyzer with Bu_4NPF_6 (0.1 M) electrolyte, Pt working and auxiliary electrodes, an Ag/AgCl reference electrode, at a scan rate of 100 mV/s (for CV). UV-Vis measurements were taken on a UV2501 PC spectrophotometer.

Preparation of $(Et_4N)_2$L1, $(Et_4N)_2$L2, $(Et_4N)_2$L3 and $(Et_4N)_2$L4. The salts were obtained by adding a 0.1 M solution of Et_4NOH in MeOH (1.15 g,7.87 mmol) to a 1 M solution of the corresponding H_2**L** acid in MeOH (1.00 g, 3.94 mmol). After stirring for a few minutes the solvent was removed under vacuum and the residue was dried under vacuum overnight at 50 °C. For $(Et_4N)_2$**L1**, ^{1}H NMR ($CDCl_3$, δ): 1.16 (t, NCH_2CH_3, 24H), 1.54 (d, $CHCH_3$, 6H), 3.19 (q, NCH_2CH_3, 16H), 4.53 (q, $CHCH_3$, 2H), 6.61-6.94 (m, aromatic, 4H); for $(Et_4N)_2$**L2**, ^{1}H NMR ($CDCl_3$, δ): 1.22 (t, NCH_2CH_3, 24H), 1.48 (d, $CHCH_3$, 6H), 3.26 (q, NCH_2CH_3, 16H), 4.52 (q, $CHCH_3$, 2H), 6.33-6.99 (m, aromatic, 4H); for $(Et_4N)_2$**L3**, ^{1}H NMR (CD_3COCD_3, δ): 1.55 (t, NCH_2CH_3, 24H), 1.64 (d, $CHCH_3$, 6H), 3.68 (q, NCH_2CH_3, 16H), 4.47 (q, $CHCH_3$, 2H), 6.99 (s, aromatic, 4H); for $(Et_4N)_2$**L4** ^{1}H NMR ($CDCl_3$, δ): 1.20 (t, NCH_2CH_3, 24 H), 1.50 (s, $C(CH_3)_2$, 12 H), 3.25 (q, NCH_2CH_3, 16H), 6.47-6.77 (m, aromatic, 4H).

Preparation of $(Et_4N)_2$L5. A solution of $ICH_2CO_2C_2H_5$ (0.936 g, 4.37 mmol) in 10 ml of CH_3CN which was prepared in a flask protected from light by aluminum foil, was added via cannula to a suspension of catechol (0.2372 g, 2.156 mmol) and K_2CO_3 (0.716 g, 5.19 mmol) in 10 ml of CH_3CN. The mixture was stirred overnight in a flask wrapped with aluminum foil. The solvent was then removed under vacuum and the

residue was dissolved in 30 ml of CH_2Cl_2; an insoluble portion was removed by filtration. The CH_2Cl_2 was removed from a filtrate and yielded the corresponding diester Et_2**L5**.

Hydrolysis of the diester was performed as previously described[22, 23] for the $(H_5C_2)_2$**L1**, $(H_5C_2)_2$**L2** and $(H_5C_2)_2$**L3**, by stirring it for 2 h with NaOH in the H_2O/MeOH solution. The insoluble H_2**L5** was collected by filtration and used without further purification. Neutralization with Et_4NOH was performed as described above for the other chiral ligands. For $(Et_4N)_2$**L5**, ^{1}H NMR ($CDCl_3$, δ): 1.20 (t, NCH_2CH_3, 24 H), 3.30 (q, NCH_2CH_3, 16 H), 4.36 (s, CH_2, 4H), 6.68-6.85 (m, aromatic, 4H).

Preparation of $[Mo_2(DAniF)_2(L1)]_2$, 1. A mixture of **0** (0.300 g, 0.267 mmol), and $(NEt_4)_2$**L1** (0.137 g, 0.267 mmol) was placed in one flask. In another flask 10 ml of CH_3CN was degassed by freezing in liquid nitrogen and pumping under vacuum. The solvent was then added to the solid mixture via cannula. A yellow solid formed upon mixing. The mixture was stirred for 30 minutes, the solvent was then decanted via cannula and the yellow residue was washed with EtOH and hexanes. The yield was essentially quantitative. IR (KBr, cm^{-1}): 3448 (w, br), 2935 (w), 2832 (w), 1609 (w), 1542 (s), 1503 (vs), 1461 (m), 1441 (m), 1415 (w), 1292 (m), 1245 (s), 1217 (s), 1177 (m), 1103 (m), 1035 (s), 941 (w), 874 (w), 827 (m), 764 (w), 703 (w), 644 (w), 619 (w), 591 (w), 522 (w), 453 (w). Elemental analysis, calculated for $Mo_4C_{84}N_8O_{25}H_{94}$: C, 50.46; N, 5.60; H, 4.74%. Found: C, 50.37; N, 5.55; H, 4.47%. ^{1}H NMR (CD_3COCD_3, δ): 1.74 (d, $CHCH_3$, 12 H), 3.68 (s, OCH_3, 12 H), 3.70 (s, OCH_3, 12 H), 5.23 (q, $CHCH_3$, 4 H), 6.62-6.98 (m, aromatic, 40 H), 8.55 (s, CH, 4 H). Crystals of **1** were obtained by dissolving the yellow solid in 10 ml of CH_2Cl_2 and layering the solution with 40 ml of

hexanes. Needle-like yellow crystals, suitable for X-ray single crystal diffraction formed within 24 h.

Preparation of $Mo_2(DAniF)_2(L2)$, 2. This was prepared similarly to **1**. The yield was quantitative. IR (KBr, cm^{-1}): 3448 (w, br), 2935 (w), 2832 (w), 1609 (w), 1542 (s), 1503 (vs), 1461 (m), 1441 (m), 1415 (w), 1292 (m), 1245 (s), 1217 (s), 1177 (m), 1103 (m), 1035 (s), 941 (w), 874 (w), 827 (m), 764 (w), 703 (w), 644 (w), 619 (w), 591 (w), 522 (w), 453 (w). Elemental analysis, calc. for $Mo_2C_{42}N_4O_{13}H_{48}$: C, 50.01; N, 5.55; H, 4.80%. Found: C, 49.87; N, 5.29; H, 4.58%. ^{1}H NMR (C_6D_6, δ): 1.83 (d, CHC*H*$_3$, 6 H), 3.17 (s, OC*H*$_3$,6 H), 3.19 (s, OC*H*$_3$, 6 H), 5.02 (q, C*H*CH$_3$, 2 H), 6.39-7.26 (m, aromatic, 20 H), 8.48 (s, C*H*, 2 H).

Preparation of $Mo_2(DAniF)_2(L4)$, 4. This was prepared similarly to **1**. Yield: (90 %). (KBr pellet, cm^{-1}): 2986 (w), 2944 (w), 2905 (w), 2831 (w), 1696 (w), 1594 (m), 1534 (s), 1499 (s), 1467 (m) 1439 (w), 1413 (w), 1362 (w), 1312 (m), 1284 (m), 1244 (s), 1210 (m), 1176 (m), 1036 (m), 826 (m), 779 (w), 780 (w), 700 (w), 621 (w), 588 (w), 537 (w), 450 (w). Elemental analysis, calc. for $Mo_2C_{47}N_4O_{10}H_{49}$: C, 55.25; N, 5.48; H, 4.83%. Found: C, 55.46; N, 5.09; H, 4.85%. ^{1}H NMR (C_6D_6, δ): 1.96 (s, C(C*H*$_3$)$_2$, 12 H), 3.19 (s, OC*H*$_3$, 12 H), 3.19 (s, OC*H*$_3$, 6 H), 5.02 (q, C*H*CH$_3$, 2 H), 6.39-7.26 (m, aromatic, 20 H), 8.48 (s, C*H*, 2 H).

Reaction of 0 with $(NEt_4)_2L3$. This was carried out similarly to the preparation of **1**. IR (KBr, cm^{-1}): 3034 (w), 2933 (w), 3831 (w), 1560 (m), 1542 (s), 1500 (vs), 1459 (m), 1440 (m), 1291 (m), 1411 (m), 1291 (m), 1246 (s), 1214 (s), 1104 (m), 1031 (s), 940 (w), 878 (w), 825 (s), 762 (w), 590 (w), 532 (w), 449 (w). Elemental analysis, calc. for $Mo_4C_{84}N_8O_{25}H_{94}$: C, 50.46; N, 5.60; H, 4.74%. Found: C, 50.70; N, 5.91; H, 4.84%. ^{1}H

NMR (C_6D_6, δ): 1.91, 1.98 (two doublets, CHC*H*$_3$, 18 H), 3.11, 3.19 (two doublets of singlets, OC*H*$_3$, 36 H), 5.22, 5.51 (two quartets, C*H*CH$_3$, 6 H), 6.36-7.42 (m, aromatic, 60 H), 8.42, 8.49 (two singlets, C*H*, 6 H).

Reaction of 0 with $(NEt_4)_2$L5. This yellow solid was obtained similarly to the preparation of **1**. IR (KBr, cm^{-1}): 2947 (w), 2832 (w), 1623 (m), 1543 (s), 1534 (s), 1500 (vs), 1452 (m), 1426 (m), 1384 (w), 1341 (w), 1286 (s), 1246 (s), 1215 (s), 1176 (w), 1131 (w), 1106 (w), 1030 (m), 941 (w), 830 (m), 789 (w), 763 (w), 742 (w), 712 (w), 618 (w), 592 (w), 542 (w), 470 (w), 449 (w). Elemental analysis, calc. for $Mo_2C_{40}N_4O_{11}H_{40}$: C, 50.86; N, 5.78; H, 4.27%. Found C, 50.77; N, 5.57; H, 4.10%. ^{1}H NMR ($CDCl_3$, δ): 3.64, 3.68 (two singlets, OC*H*$_3$, 36 H), 5.18, 5.22 (two singlets, C*H*$_2$, 12 H), 6.44-7.10 (m, aromatic, 60 H), 8.39, 8.42 (two singlets, C*H*, 6 H).

X-Ray Crystallography

For **1**, a single crystal was mounted on the tip of a quartz fiber and transferred to the goniometer of an Enraf-Nonius FAST diffractometer. Two hundred and fifty strong reflections were indexed to a body-centered orthorhombic unit cell. The cell dimensions, lattice type, and Laue symmetry were confirmed from axial images. Data collection and integration were performed by the software program MADNES[26] and the integrated data were processed and corrected for Lorentz and polarization effects by the program PROCOR.[27] An absorption correction was applied by the program SORTAV.[28] The crystal showed broad reflections in ω indicative of a high degree of mosaicity. A single crystal of **4** was mounted on a nylon loop and transferred to the goniometer of a SMART APEX CCD diffractometer. Data collection and integration were performed by the software program SMART[29] and the integrated data were processed and corrected for

Lorentz and polarization effects by the program SAINT.[30] An absorption correction was applied by the program SADABS.[31] Both structures were solved by the Patterson method and refined by alternate cycles of full-matrix least squares and difference Fourier maps with the SHELXTL-97 package.[32] Except for the disordered aryl groups found in **1**, non-hydrogen atoms were refined anisotropically, and hydrogen atoms were added at calculated positions and included in the structure factor calculations. Selected bond distances for **1** and **4** are listed in Table 1. Crystal data are listed in Table 2.

Table 1 Selected interatomic distances[a] for **1**·4CH_2Cl_2 and **4**·C_6H_6

	1·4CH_2Cl_2	**4**·C_6H_6
Mo–Mo	2.081(2)	2.0812(7)
Mo–N	2.08[3]	2.112[2]
Mo–O	2.13[2]	2.141[2]
Overall torsion angle, deg.[b]	75.8	-

[a] Distances given in Å. Numbers in square brackets correspond to average values.
[b] The torsion angle is defined as the angle between the two Mo–Mo bonds. Since **4** has only one Mo_2 unit, no torsion angle is given.

Table 2 Crystal data for **1**·$4CH_2Cl_2$ and **4**·C_6H_6

	1·$4CH_2Cl_2$	**4**·C_6H_6
Formula	$Mo_4N_8O_{20}C_{88}Cl_8H_{92}$	$Mo_2N_4O_{10}C_{50}H_{52}$
Formula weight	2249.06	1060.84
Space group	*I*222 (No. 23)	$P2_1/c$ (No. 14)
a/Å	13.970(3)	16.837(5)
b/Å	20.450(5)	16.094(5)
c/Å	37.216(5)	19.036(6)
β/°	90	115.727(5)
V/Å^3	10632(4)	4647(3)
Z	4	4
D_c/g cm^{-3}	1.405	1.405
μ(Mo Kα)/mm^{-1}	0.726	0.597
Temp/°C	60	173
R1[a], *w*R2[b] ($I > 2\sigma(I)$)	0.1102, 0.2226	0.0334, 0.0746
R1[a], *w*R2[b] (all data)	0.1488, 0.2404	0.0457, 0.0796
Flack Parameter [c]	0.0 (1)	

[a]$R1 = \sum||F_o| - |F_c||/\sum|F_o|$. [b]$wR2 = [\sum[w(F_o^2 - F_c^2)^2]/ \sum[w(F_o^2)^2]]^{½}$, $w = 1/\sigma^2(F_o^2) + (aP)^2 + bP$, where $P = [\max(0 \text{ or } F_o^2) + 2(F_c^2)]/3$. [c]See: H. D. Flack, *Acta Cryst*., 1983, **A39**, 876.

RESULTS AND DISCUSSION

Synthesis. The first stage of the ligands ($(NEt_4)_2$**L1**, $(NEt_4)_2$**L2** and $(NEt_4)_2$**L3**) synthesis has been described as taking place via a nucleophilic attack, which inverts the *S*-conformation of the ethyl lactate triflate derivative to the *R*-conformation for the precursor of the linker. Effenberger and coworkers showed by chiral gas chromatography that the reaction occurs with 92% enantiomeric inversion.[23] We also determined the enantiomeric purity of the $(NEt_4)_2$**L1** salt by NMR spectroscopy and found it to be similar, that is, *ca*. 95%.

The quadruply-bonded corner-piece precursor [*cis*-$Mo_2(DAniF)_2(CH_3CN)_4](BF_4)_2$ (compound **0**) reacts with the tetraethylammonium salt of the chiral dicarboxylate, $(NEt_4)_2$**L1**, to give [*cis*-$Mo_2(DAniF)_2]_2$(**L1**)$_2$, **1**, in high yield according to eq. (1):

2[*cis*-$Mo_2(DAniF)_2(CH_3CN)_4](BF_4)_2$ + 2$(NEt_4)_2$**L1** → [*cis*-$Mo_2(DAniF)_2]_2$(**L1**)$_2$ + NEt_4BF_4 (1)

The ^{1}H NMR spectrum of **1** in acetone-d_6 shows the presence of one singlet at 8.55 ppm for the methine proton of the formamidinate ligands and two singlets in a 1:1 ratio for the OCH_3 groups of the anisyl groups at 3.68 and 3.70 ppm which is in agreement with D_2 being the highest possible symmetry of the molecule. A complicated multiplet in the range of 6.62 to 6.98 ppm corresponds to the aromatic protons of the anisyl groups and those of the linkers. The remaining signals for the chiral linkers are a quartet at 5.23 ppm for the CH unit and a doublet for CH_3 at 1.74 ppm. The ratio of carboxylate to formamidinate signals of 1:2 is consistent with a structure of D_2 symmetry.

Reactions similar to that in eq. (1) have been carried out for the isomeric *ortho*- and *meta*- ligands using the corresponding tetraethylammonium salts $(NEt_4)_2$**L2** and $(NEt_4)_2$**L3**. Because of the smaller bite of these ligands, it was considered less likely that these could form compounds similar to **1**. Nevertheless, we decided to investigate their reactivity towards the corner-piece precursor, **0**, to determine how the geometry of the ligands might impact the structure of the dimolybdenum compounds. This is of importance as small changes in the structures of the ligand can have a significant effect on the structure of the metal complexes and the manner in which they pack in the crystal.[2]

Reactions of **0** and $\mathbf{L2}^{2}$ or $\mathbf{L3}^{2-}$ proceeded similarly to that for the preparation of **1** with the formation of yellow solids, **2** and **3**, in high yields. Like those for **1**, the results of the elemental analysis were consistent with the empirical formula $Mo_2C_{42}H_{42}N_4O_{10}$ (i.e., 1:1 adduct of **L2** or **L3** with an $Mo_2(DAniF)_2$ unit). The ^{1}H NMR spectrum of **2** in C_6D_6 is similar to that of **1**, indicating the formation of a single product with a formamidinate to carboxylate ratio of 2:1. But whether this is a chelated dinuclear compound with C_2 symmetry, or a tetranuclear loop like **1** compound cannot be determined solely by analysis of the ^{1}H NMR spectrum.

Sharp signals in the ^{1}H NMR spectrum of **3** in C_6D_6 indicate that the product is diamagnetic as required by the presence of the quadruply-bonded Mo_2 unit. The spectrum is more complex, however, having two singlets at 8.42 and 8.49 ppm in a ratio of ca. 1:2 that correspond to methine groups. There are also two doublets in a similar ratio at 1.91 and 1.98 ppm for the CH_3 groups from the chiral centers, two quartets assigned to CH groups from the chiral centers at 5.22 and 5.51 ppm. A complicated

multiplet in the range of 6.50 to 6.64 ppm corresponds to the aromatic protons of the anisyl groups and those of the linkers. This doubling of the signals suggests the formation of two products which are isolated in a relative ratio of 1:2.

Because attempts at crystallizing **2** and **3** produced only amorphous materials unsuitable for single crystal X-ray diffraction, we tried to gain insight by looking at the type of product formed by analogous non-chiral ligands in which the $OCMeHCO_2$ groups

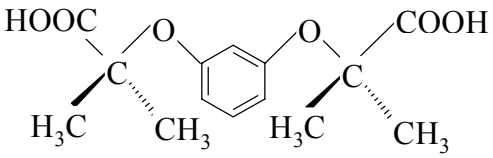

H_2**L4**

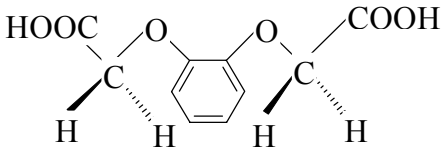

H_2**L5**

Scheme 5.

are replaced by $OCMe_2CO_2$ groups to give the *meta* analog H_2**L4**,[16] or by OCH_2CO_2 groups to give the *ortho* analog H_2**L5**[33] (Scheme 5).

Using $\mathbf{L4}^{2-}$, a reaction with **0** was performed in CH_3CN following eq. (1). A yellow solid which formed was dissolved in C_6H_6, and this solution was mixed with hexanes to produce crystals of *cis*-Mo_2(DAniF)$_2$(**L4**)·C_6H_6 (**4**·C_6H_6). The ^{1}H NMR spectrum in C_6D_6 shows the presence of one compound (**4**) with a carboxylate to formamidinate ratio of 1:2, as in **2**. A singlet at 8.46 ppm corresponds to the methine protons. We observed only one singlet for the OCH_3 groups at 3.19 ppm and a doublet for the methyl groups of the non-chiral dicarboxylate at 1.96 ppm, which is in agreement

with a molecule in an idealized C_{2v} symmetry (*vide infra*). The ^{1}H NMR spectrum, electrochemical measurements and elemental analysis indicate that the purity of the product is good.

A similar reaction of **0** with **L5**$^{2-}$ was performed in CH_3CN and a crystalline product (**5**) was obtained by extracting the product with hot CH_2Cl_2, then adding hexanes and storing at −10 °C. Unfortunately these crystals diffracted poorly and were twinned, which prevented a structural characterization, but the product was analyzed by ^{1}H NMR spectroscopy. The spectrum in $CDCl_3$ of either the crystals or the yellow powder shows the presence of the carboxylate and formamidinate ligands in a 1:2 ratio but as in the reaction with **L3**$^{2-}$, the signals show signs of doubling suggesting again the presence of two compounds but in a 1:3 ratio. There are two singlets at 8.42 and 8.40 ppm from methine groups (ratio of 1:3), two singlets at 3.64 and 3.67 ppm for two types of OCH_3 groups, and two singlets at 5.18 and 5.22 ppm assigned to the CH_2 groups. A complicated multiplet in the range of 6.47 to 7.10 ppm corresponds to the aromatic protons of the anisyl groups and those of the linkers. This suggests again the formation of two types of products, possibly a loop and a chelated product, analogous to those obtained with **L3**$^{2-}$.

X-Ray Crystallography. In the compound **1** two *cis*-$Mo_2(DAniF)_2$ units are held together by two of the carboxylate anions producing a molecular loop as shown in Fig. 1. It is clear that the dicarboxylate anions displace the labile equatorial acetonitrile groups and each of the two **L1** dianions has a carboxylate group attached to each of the two Mo_2^{4+} units resembling the claws of a crab as seen in Fig. 2.

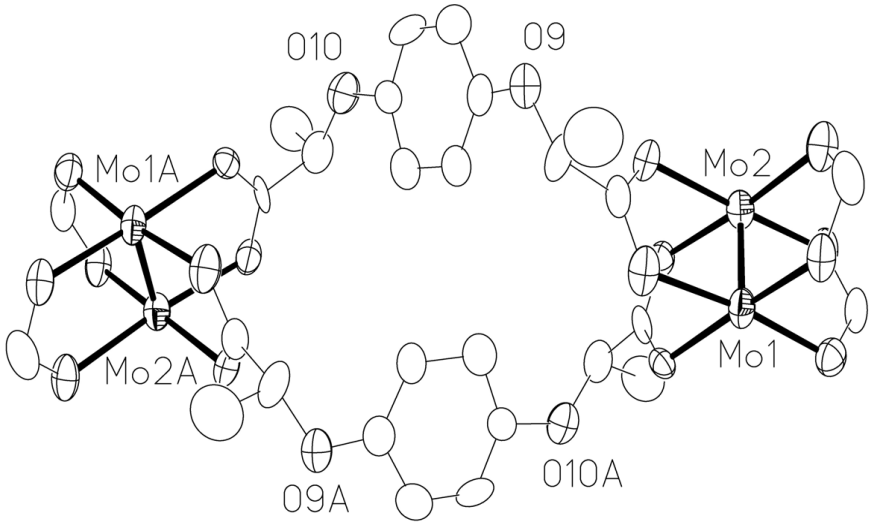

Fig. 1 Thermal ellipsoid plot of **1** drawn at 30 % probability level. Hydrogen atoms, solvent molecules and anisyl groups have been removed for clarity

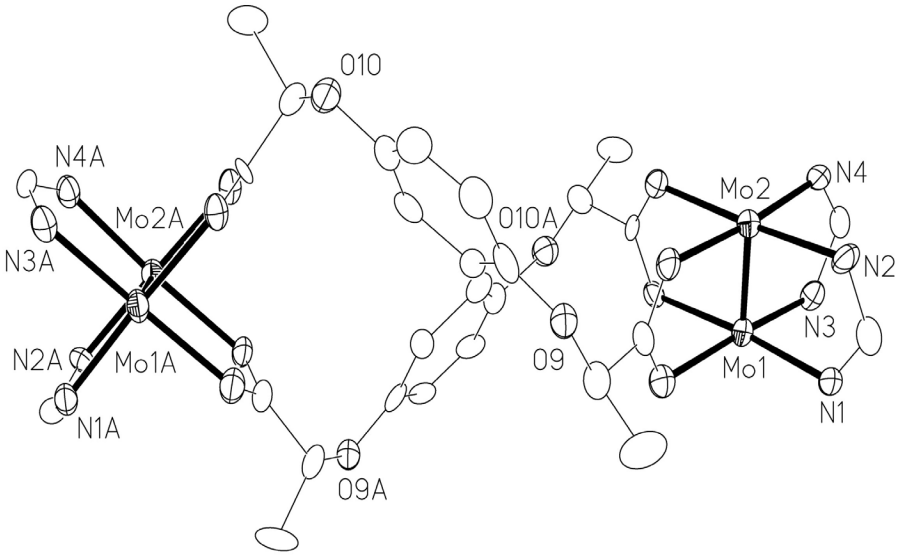

Fig. 2 Thermal ellipsoid plot of **1** showing the twisted nature of the loop. The torsion angle between the two Mo_2 units is 75 °. Ellipsoids are drawn at 30 % probabilty level; Hydrogen atoms, solvent molecules and anisyl groups have been omitted.

The entire molecule resembles a second-order Möbius strip, which is a Möbius type ring in which there are two twists (rather than one), both in the same direction. The idealized molecular symmetry would be 222 (D_2 in Schönflies notation). As noted above, the ^{1}H NMR spectrum is consistent with this symmetry.

Since the two Mo_2 units in each molecule are related by a crystallographic two-fold axis, they are equivalent and the Mo–Mo bond distance of 2.081(2) Å (see Table 1) is similar to those found in other paddlewheel compounds having carboxylate or formamididate bridging ligands.[1] The ligands are attached to each dimolybdenum unit by one carboxyl group, as in other molecular loops, though the conformation there is quite different from those previously described. Loops with the dianions 1,4-phenylenediacetate (p-$C_6H_4(CH_2CO_2)_2$), homophthlate (o-$C_6H_4(CH_2CO_2)(CO_2)$) and malonate ($CH_2(CO_2)_2$) have the two Mo_2 units essentially parallel to each other.[14] Because of the chiral nature of the ligands in **1**, there is a significant twist between the vectors of the two Mo_2 species which are at an angle of -75.8 °. This twist has consequences in the packing of the molecules, Fig. 3.

In the previously described molecular loops,[14] the molecules stacked with the Mo–Mo bonds aligned thus creating channels that can vary in size depending on the length of the linkers. This is not possible in **1** due to the S shape of the molecule. Here again the molecules stack but now, parallel stacks of loops form channels along the *a* axis. These channels, which provide a chiral environment because of the chirality of the dicarboxylate linkers, are large enough to allow interstitial solvent molecules to reside in them as shown in Fig. 3.[34] This could be of importance in enantiomer resolution or in catalysis and efforts are being made to prepare ruthenium and rhodium analogs for which catalytic activity should be highly relevant. In this context it is important to note that the chiral linker can be made in high purity and very cheaply from readily available commercial sources.[22, 23]

The structure of **4**, Fig. 4, shows that the dicarboxylate anion wraps around the dimetal unit to form a chelate in the same way as described by others for similar Rh_2^{4+} compounds. The Mo–Mo bond distance of 2.0812(7) Å (see Table 1) is similar to that in other paddlewheel compounds having mixed carboxylate and formamididate bridging ligands. Because of the similarity of $\mathbf{L2}^{2-}$ and $\mathbf{L4}^{2-}$, it is likely that the structure of **2** is similar to that of **4** and thus **2** has a chelated dicarboxylate anion and only one Mo_2^{4+} unit.

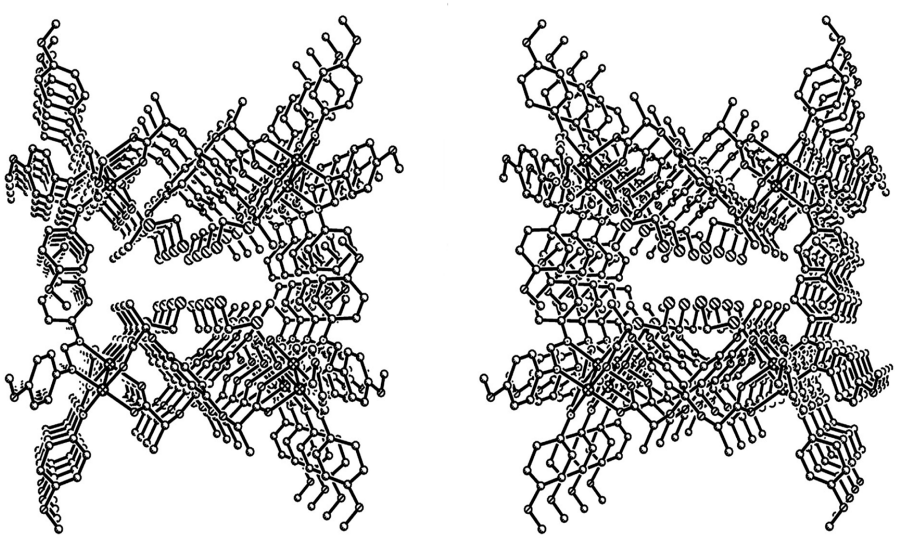

Fig. 3 A stereoscopic view of the packing of **1**·4CH_2Cl_2 showing channels filled with guest dichloromethane molecules.

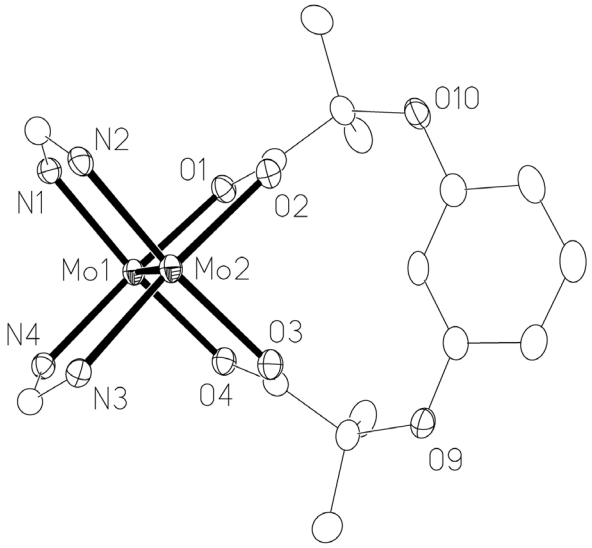

Fig. 4 Thermal ellipsoid plot of **4** drawn at 50 % probability level. Hydrogen atoms, solvent molecules and anisyl groups have been removed for clarity.

Electrochemistry and UV-visible spectra. For **1**, the cyclic voltammogram (CV) and differential pulse voltammogram (DPV) show a single reversible oxidation wave at 0.388 V versus Ag/AgCl which is similar to that in [*cis*-$Mo_2(DAniF)_2]_2(O_2CCH_2C_6H_4CH_2CO_2)_2$. The peak at 428 nm in CH_2Cl_2 observed for **1** in the UV-visible spectra can be interpreted as $\delta\rightarrow\delta^*$ transition. Similarly **2** and **3** show $\delta\rightarrow\delta^*$ transitions at 410 and 412 nm, respectively. Cyclic voltammogram of **2** is similar to **1** (0.380 V versus Ag/AgCl), but signal of **3** (0.284 V versus Ag/AgCl) is very broad and is consistent with the presence of two species in solution.

The CV and differential pulse voltammogram (DPV) of **4** show a single reversible oxidation wave at 0.344 V versus Ag/AgCl. The UV/vis spectra for **4** and **5** show $\delta\rightarrow\delta^*$ transitions at 430 and 431 nm, respectively, consistent with the presence of an Mo_2^{4+} core.

Conclusions. We have shown that the type of compound formed between quadruply-bonded Mo_2^{4+} units in a *cis*-$Mo_2(DAniF)_2$ species and chiral and non-chiral dicarboxylate anions derived from *ortho*, *meta* and *para* substitution of aromatic entities such as those in $\mathbf{L1}^{2-}$ - $\mathbf{L5}^{2-}$ is very dependent on the ligand configuration, with those having *para* substitution favoring the formation of molecular loops and those having the *meta* substitution favoring dinuclear complexes in which the dicarboxylate gives a chelate. Enantiomerically pure compounds **1** and **2** were obtained. Insight into the structure of **2** was obtained by making a non-chiral analog, namely **4**. The structure of the loop **1** shows channels capable of holding guest molecules. This opens the possibility for using dirhodium instead of dimolybdenum units which might be useful in catalysis.

CHAPTER III

NON-TRIVIAL BEHAVIOR OF PALLADIUM (II) ACETATE

INTRODUCTION

Palladium(II) acetate (**6**) is an important substance with many significant uses. It catalyses many organic reactions,[35] is easily reduced by light[36] or heat[37] to form thin films of Pd and can produce colloids[38] and nanowires.[39] The primary use of **6**, however, is as a starting material for the syntheses of other Pd(II) compounds as well as for the preparation of palladium catalysts and their precursors.[40] It is usually prepared by reaction of a slight excess of activated palladium metal, usually made by reduction of palladium dichloride with formic acid,[41] and a deficiency of nitric acid in acetic acid to assure the entire consumption of nitric acid.[42] In the solid state, the structure is generally trinuclear with nearly idealized D_{3h} symmetry, in which each of the three palladium atoms is in a square planar environment and there are six bridging acetate groups,[43] as shown in Scheme 6. The structures of four crystalline forms having five independent molecules show that the D_{3h} structure is persistent and there are only small variations in the non-bonded Pd···Pd distances in the $Pd_3(OAc)_6$ molecules. This unusual structure is known in only one other case,[44] *viz.* $Cu_3[O_2C(2,4,6\text{-}(Me_2CH)_3C_6H_3]_6$. Recently, a structure was reported of a polymeric, water-insoluble form (1').[45] The chain structure was determined from X-ray powder diffraction data of a pink substance formed upon prolonged heating of a mixture prepared by adding acetic acid to a solution of palladium dissolved in nitric

acid.

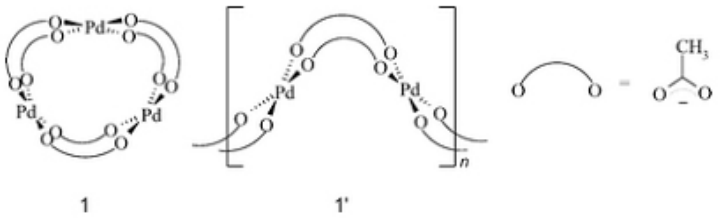

Scheme 6

In solution, the structure of palladium acetate has remained somewhat controversial. Claims have been made supporting the persistence of the trinuclear molecules in solution,[46] while other evidence is said[47] to support the formation of various aggregates of $[Pd(OAc)_2]_n$ (n = 1, 2, 3, *etc*.). The ^{1}H NMR spectrum of palladium acetate in methanol has been reported[48] to show a large number of signals in the range where a single acetate signal would be expected for the symmetrical triangular structure. This was said to be indicative of a variety of aggregates and possibly even the occurrence of ionic species. More recently in a paper describing the use of palladium acetate for the preparation of a catalyst and entitled "Too many precautions in making a catalyst is never a loss of time: A lesson we learned at our own expense", a discussion was provided for the importance of the nature of the palladium acetate in solution and the solvent used for the preparation of catalysts.[49]

Because of our interest in metal–metal bonded dipalladium compounds such as those containing Pd_2^{6+}[50] and Pd_2^{5+} units,[51] we have recently initiated a broad study of these compounds. Although we had a considerable amount of palladium dichloride available, its low solubility in common organic solvents limits the utility of $PdCl_2$ as a starting material for the preparation of such complexes, and we preferred to use the soluble

palladium acetate. Therefore, we sought a good method for the preparation for **6** from $PdCl_2$. What we expected to be a trivial synthetic exercise has led us to believe that not all of the so-called preparations of palladium acetate indeed lead to the desired compound in good purity. Here we report the structure of $Pd_3(OAc)_5NO_2$, **7**, which has a structure similar to that of $Pd_3(OAc)_6$ except that one acetate ion has been replaced by a bridging nitrite ion. We can now also shed some light on the solution behavior of $Pd_3(OAc)_6$ in both wet and carefully dried NMR solvents. We also provide a reliable and reproducible synthesis of $Pd_3(OAc)_6$ using $PdCl_2$ as starting material.

EXPERIMENTAL SECTION

General Comments. Unless otherwise stated, operations were carried out in air. Solvents were purified using a Glass Contour purification system. Deuterated solvents were used as received, except for samples that were carefully dried using freshly dried molecular sieves. $Pd_3(OAc)_6$ was purchased from Aldrich and deuterated solvents were purchased from Cambridge Isotope Laboratories, Inc.

Physical measurements. The IR spectra were recorded on a Perkin-Elmer 16PC FTIR spectrometer using KBr pellets. Elemental analyses were carried out by Canadian Microanalytical Services in British Columbia, Canada. Samples were vacuum dried prior to elemental analyses in order to remove the interstitial solvent molecules of the crystals. ^1H and ^{13}C NMR spectra were obtained on a VXR-300 NMR spectrometer.

Synthesis of $Pd_3(OAc)_6$ (6). A mixture of sodium hydroxide (1.0 g, 25 mmol) and HCOONa (0.80 g, 11.7 mmol) was added to a solution of $PdCl_2$ (0.500 g, 2.86 mmol)

in 50 ml of water. Formation of a palladium powder occurred immediately. The suspension was stirred for 30 min to allow the palladium particles to coagulate. The palladium was separated by filtration, washed with acetone and dried under vacuum. The solid was then suspended in 20 ml of glacial acetic acid, and 0.3 ml of concentrated nitric acid was slowly added with stirring. The resulting solution was heated to reflux for 30 min while N_2 was bubbled through the reaction mixture and the volume of the solution was then reduced to a third of the original volume by slow evaporation using mild heating. After cooling to room temperature, an orange powder was isolated by filtration. Yield: 0.605 g (94.4%). ^{1}H NMR (very dry $CDCl_3$, 300 MHz, δ, ppm): 2.006 (s); IR (KBr, cm^{-1}): 1600 vs, 1430 vs, 1350 w, 1157 vw, 1047 vw, 951 vw, 696 m, 625 vw.

Crystals of **6** were obtained by addition of 50 mg of the $Pd_3(OAc)_6$ synthesized as just described to a mixture of 10 ml of CH_2Cl_2 and 10 ml of hexanes. After filtration, slow evaporation of the solvent under a N_2 stream produced orange plates the following day.

Synthesis of $Pd_3(OAc)_5(NO_2)$ (7). This was prepared similarly to 6 but when the palladium metal was allowed to react with a mixture of acetic acid and nitric acid, no N_2 flow was applied to eliminate the brown gases formed. Concentration of the solution by a factor of 3 was accomplished by slow evaporation under mild heating, and cooling to room temperature yielded an orange powder. To this powder was added a mixture of 10 ml of CH_2Cl_2 and 10 ml of hexanes. A small amount of solid was eliminated after filtration. Slow evaporation of the solution was performed by passing a constant N_2 flow over it. Two types of crystals were obtained. Orange plates were $Pd_3(OAc)_6$ and purple cubes were $Pd_3(OAc)_5(NO_2)$. The products were separated manually. Yield of 7: 0.2601

g (40.0%). ^{1}H NMR ($CDCl_3$, 300 MHz, δ, ppm): 1.960 (s, 1H), 2.004 (s, 1H), 2.043 (s, 1H), 2.072 (s, 1H), 2.081 (s, 1H); IR (KBr, cm^{-1}): 1608 vs, 1560 s, 1541 s, 1517 s, 1420 vs, 1351 m, 1261 m, 1197 m, 1153 w, 1098 s, 1024 s, 949 w, 867 w, 800 m, 696 m, 622 w. X-Ray quality crystals of **7** were obtained by recrystallization of 50 mg of the purple solid from the reaction in a mixture of 10 ml of CH_2Cl_2 and 20 ml of hexanes.

X-Ray Crystallography

A suitable crystal of **6**·CH_2Cl_2 was placed inside a loop using a small amount of stopcock grease, and was mounted on the goniometer of a Bruker SMART 1000 CCD area detector diffractometer. The crystal was centered in the goniometer, and cooled to –60 °C in a stream of cold nitrogen. Geometric and intensity data were collected using SMART software.[28] The data were processed using SAINT software,[29] and corrections for absorption were applied using the program SADABS.[30] Crystal data are presented in Table 3. Table 4 lists pertinent bond distances and angles for **6**·CH_2Cl_2 and **7**. The positions of the Pd atoms were determined using the Patterson method available in the SHELX-97 software package.[31] This was followed by least squares refinement and difference Fourier synthesis to determine the positions of the remaining heavy atoms. Hydrogen atoms were placed in calculated positions based on a riding model.

Table 3 Crystal data and structure refinement for **6**·CH_2Cl_2 and **7**

	6·CH_2Cl_2	**7**
Empirical formula	$Pd_3C_{13}H_{20}O_{12}Cl_2$	$Pd_3C_{10}H_{15}O_{12}N$
Formula weight	758.39	660.43
Space group	*Pbcm*	*Pna*2_1
a/Å	8.139(2)	15.854(4)
b/Å	15.891(4)	11.608(3)
c/Å	17.500(5)	10.109(3)
V/Å^3	2263.5(11)	1860.5(8)
Z	4	4
Density (calcd.)/g cm^{-3}	2.226	2.358
μ(Mo–Kα)/mm^{-1}	2.649	2.927
R1[a], *w*R2[b] [$I > 2\sigma(I)$]	0.0214, 0.0563	0.0280, 0.0717
R1[a], *w*R2[b] (all data)	0.0244, 0.0583	0.0309, 0.0736

[a] R1 = ∑ Fo| – |Fc‖/∑|Fo|. b wR2 = [∑[w(Fo2 – Fc2)2]/ ∑[w(Fo2)2]]½, w = 1/σ2(Fo2) + (aP)2 + bP, where P = [max(0 or Fo2) + 2(Fc2)]/3.

Table 4 Selected interatomic distances[a] for **6**·CH_2Cl_2 and **7**

	6·CH_2Cl_2	**7**
Pd···Pd[b]	3.1678[7]	3.103[1]
Pd–O	1.995[2]	2.011[5]
Pd–N	—	1.949(7)

[a] Distances given in Å. Numbers in square brackets correspond to average values.

[b] In trinuclear forms the reported Pd···Pd separations are in the range of 3.081(2) to 3.203(1) Å (see ref. 43) while the unique distance in the polymeric form is 2.9192(1) Å (see ref. 45).

RESULTS AND DISCUSSION

Synthesis. Although palladium(II) acetate is commercially available, there are several recent reports describing its preparation.[52] We originally selected the reaction of activated Pd metal in nitric acid described by Zhang and coworkers,[52a] because it appeared to be a straightforward, high yield method. This method is summarized by the following pair of reactions:

$$PdCl_2 + NaHCO_2 + NaOH \rightarrow Pd + CO_2 + 2\ NaCl + H_2O \quad (1)$$

$$3Pd + 6HNO_3 + 6HOAc \rightarrow Pd_3(OAc)_6 + 6NO_2 + 6H_2O \quad (2)$$

The first reaction occurs as reported with rapid formation of finely divided palladium metal. The freshly formed powder is subsequently oxidized by a mixture of HNO_3 and acetic acid, and the product is extracted in a 1 : 2 mixture of CH_2Cl_2 : hexanes. Crystals are obtained by evaporation in a stream of N_2. However, this produced a mixture of purple and orange crystals which can be separated manually. The ^{1}H NMR spectrum of the orange crystals in $CDCl_3$ was identical to that of a commercial sample of **6** (Aldrich) and shows five resonances of various intensities at around 2 ppm as shown in Fig. 5a. This is not consistent with the D_{3h} symmetry of $Pd_3(OAc)_6$ in the solid state but is consistent with literature reports.[48] The ^{1}H NMR spectrum of the purple crystals shows five resonances of essentially equal intensities at 1.961, 2.004, 2.045, 2.073 and 2.082 ppm (Fig. 5b). The spectrum of the bulk product from the reaction mixture, shown in Fig.

5c, is a superposition of the two spectra shown in Figs. 5a and 5b which indicates that these are the only soluble species produced in the reaction.

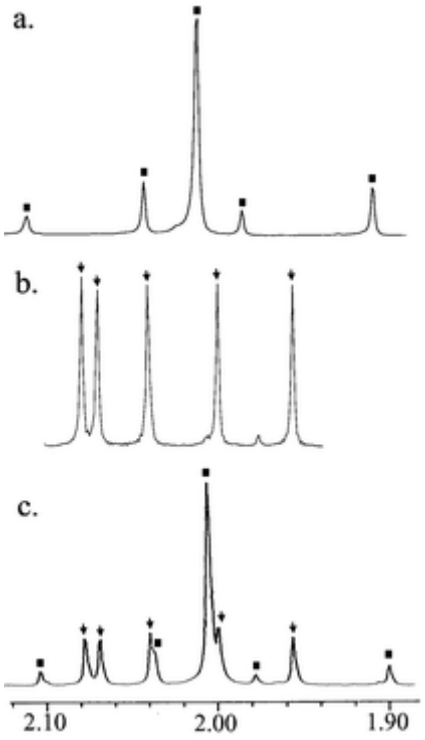

Fig. 5 ^{1}H NMR spectra taken at 300 MHz in solutions of $CDCl_3$(as supplied by the manufacturer). (a) commercial $Pd_3(OAc)_6$, (b) $Pd_3(OAc)_5(NO)_2$, (c) "$Pd_3(OAc)_6$" prepared according to ref. 52a.

X-Ray crystallography. The orange crystals are a new crystalline form of the well-known triangular $Pd_3(OAc)_6$ molecule, crystallized with one CH_2Cl_2 molecule per formula unit as interstitial solvent (Fig. 6). The purple crystals, which have the composition $Pd_3(OAc)_5NO_2$, have the structure shown in Fig. 7. In this compound, the trinuclear motif is preserved but one of the acetate groups is replaced by a nitrite group (NO_2^-) which is bound to the palladium atom by the N atom and one O atom. The substitution of an acetate group breaks the D_{3h} symmetry of **6** causing the remaining acetate groups to be nonequivalent, thus accounting for the five peaks of equal intensity in the ^1H NMR spectrum. The formation of **7** can be attributed to the attack of nitrogen oxides on the $Pd_3(OAc)_6$ molecule. These oxides are generated during the oxidation of Pd powder with HNO_3. To avoid the formation of $Pd_3(OAc)_5NO_2$, the brown nitrogen oxide gases must be eliminated promptly by bubbling N_2 gas through the reaction mixture. In this way, pure $Pd_3(OAc)_6$ forms as the sole product.

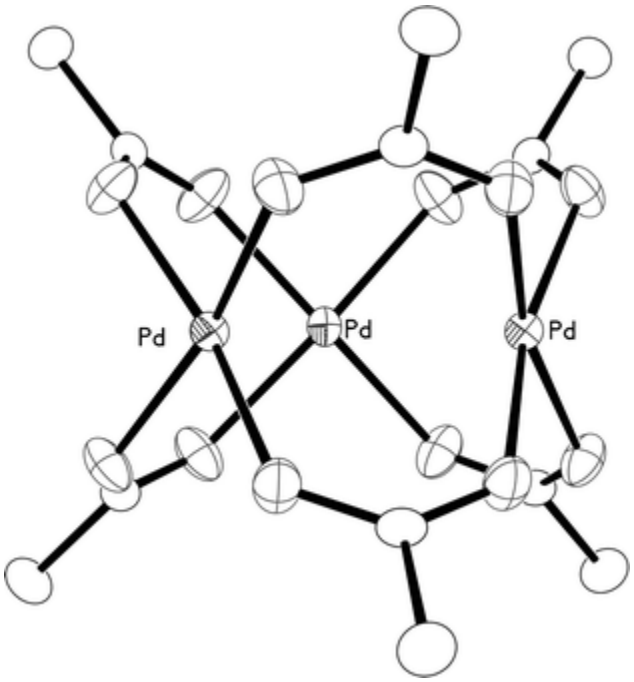

Fig. 6 Molecular structure of $Pd_3(OAc)_6$ with ellipsoids drawn at the 30% probability level and hydrogen atoms removed.

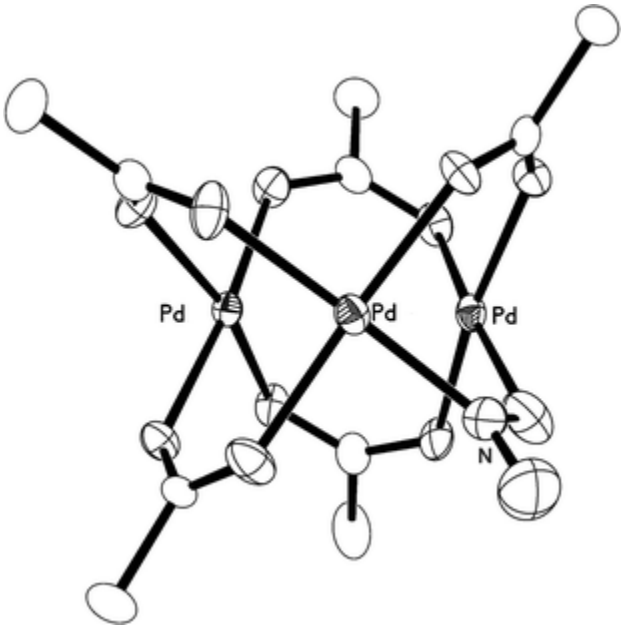

Fig. 7 Molecular structure of $Pd_3(OAc)_5(NO_2)$ with ellipsoids drawn at the 30% probability level and hydrogen atoms removed.

Conclusions. The appearance of various signals in the ^{1}H NMR spectrum of freshly prepared and commercial samples of **6** was puzzling. We studied this issue by examining several ^{1}H NMR spectra of $Pd_3(OAc)_6$ in commercial solvents, such as CD_3OD, $CDCl_3$ and C_6D_6. It was noted that the number and relative intensities of some peaks are extremely sensitive to the nature of the solvent but more importantly the signal for water that was always present in the solvents $CDCl_3$ and C_6D_6 was absent in solutions of **6**. Furthermore, when rigorously dry $CDCl_3$ or C_6D_6 was used to dissolve either freshly synthesized or commercial samples of **6**, each spectrum displayed only one sharp signal. In $CDCl_3$ this signal is at 2.006 ppm and corresponds to the major peak in Fig. 5c. The signal shifts to 1.622 ppm when the spectrum is obtained in C_6D_6.[53] We now believe that these observations are consistent with the occurrence of one or more hydrolysis processes when the nonpolar solvents contain a small amount of water (Scheme 7). Because molecular weight determinations in benzene and dichloromethane solutions indicate that the molecule is trinuclear, it is likely that this trinuclear,[41, 46] core is retained.

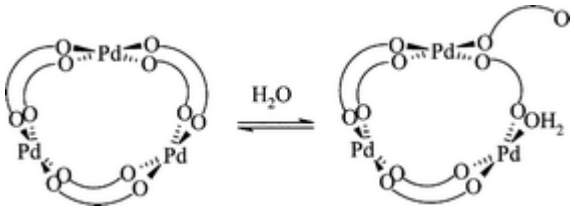

Scheme 7

It is interesting to note that a similar hydrolysis process does not occur in the nitrito compound **7**, since the five expected resonances for the acetate groups all have equal intensity, and no extraneous peaks are present even in the presence of small

amounts of water. A structurally analogous complex having five acetate ligands and one oxazolone ligand around the triangular Pd_3 core also shows only five acetate resonances in its ^{1}H NMR spectrum.[54] Thus, it appears that once one acetate ligand is replaced by a stronger bidentate ligand, the resulting $Pd_3(OAc)_5(L)$ complex is kinetically less labile than the $Pd_3(OAc)_6$ precursor. This would also explain why a more complex mixture of $Pd_3(OAc)_n(NO_2)_{6-n}$ species is not observed in the reaction mixture.

The occurrence of hydrolysis is also consistent with the known reactivity of $Pd_3(OAc)_6$ toward ligands such as amines, phosphines and arsines leading to mononuclear complexes such as *trans*-$[Pd(OAc)_2(PR_3)_2]$, in which the acetate groups are monodentate.[41, 55] The results we report here would seem to provide an explanation for the previously reported "anomalous" behavior of palladium(II) acetate. We note particularly that the hypothesis about various $[Pd(OAc)_2]_n$ species in solution with n other than 3 seems unnecessary.

CHAPTER IV

A STUDY OF Pd_2^{4+} COMPLEXES

INTRODUCTION

Palladium and its complexes are widely used in catalysis,[56] medicine,[57] and many other fields of research such as H_2 storage[58] and thin film deposition.[59] The divalent state is the most common, and the electron configuration produces almost invariably square planar complexes.[60]

This research group has been interested in transition-metal compounds containing metal-metal bonds. Although an enormous variety of dimetal compounds with metal-metal bonds has been described in the literature,[1] dipalladium compounds are very scarce. A generalized molecular orbital diagram for D_{4h} compounds containing bonded pairs of metal atoms is shown on the left of Scheme 1, where it can be seen that, for elements with d^8 configurations of the M_2^{n+} core, both bonding and antibonding orbitals are filled, leading to an M-M bond order of zero. Therefore, it is necessary to look to higher oxidation states to find metal-metal bonds in paddlewheel complexes.

Up to now, there has been only one dipalladium paddlewheel compound known with an unequivocal metal-metal single bond.[50] This $Pd_2(hpp)_4Cl_2$ compound (where hpp is the anion of 1,3,4,6,7,8-hexahydro-2*H*-pyrimido[1,2*a*]pyrimidine) was prepared almost a decade ago. Four hpp ligands are embracing the singly bonded Pd_2^{6+} unit, and the molecule possesses 4-fold symmetry. The two chlorine atoms are located in axial

positions on the 4-fold axis. This molecule was obtained by oxidation of $Pd_2(hpp)_4$ with several oxidizing agents. Two other binuclear dipalladium compounds with presumed bond orders of $^1/_2$ between the palladium atoms have also been described; they have Pd_2^{5+} cores.[51] Oxidation of $Pd_2(DTolF)_4$ (DTolF = *N*,*N*'-di-*p*-tolylformamidinate) with 1.6 equiv of $AgPF_6$[51*b*] gave $Pd_2(DTolF)_4PF_6$. The metal-metal distance in the oxidized compound did not differ significantly from that in the Pd_2^{4+} precursor, which does not have a Pd-Pd bond. Because oxidation is expected to give rise to a bond within the Pd_2^{5+} unit, shortening of the metal-metal distance might have been expected. However, there is also an increase in electrostatic repulsion between the two positively charged metal atoms which may explain the invariance in bond distance, as has been observed before in some dirhenium[61] and ditechnetium[62] compounds. Calculations done for the oxidized species suggest that the unpaired electron resides mainly in a metal-based orbital, but an EPR spectrum of the $Pd_2(DTolF)_4^+$ species showed only one isotropic peak, suggesting that perhaps the unpaired electron is ligand-based rather than metal-based.

Bear and co-workers[51*a*] synthesized and structurally characterized two Pd_2^{4+} isomers containing four DPhBz ligands (DPhBz = the anion of *N*,*N*'-diphenylbenzamidine). One was shown to be the α-isomer where all four ligands bridge the dimetal unit to form a paddlewheel. In the β-isomer, there are two bridging and two chelating ligands. Electrochemical oxidation of the α isomer, followed by an EPR spectrum of the singly oxidized species, revealed anisotropy of the *g*-value and hyperfine splitting of the signal consistent with the nuclear spin of $^5/_2$ of the ^{105}Pd isotope, which suggest that the unpaired electron is in the dimetal unit. It is important to note, however,

that no direct structural evidence for the presence of an α-$Pd_2(DPhBz)_4^+$ species was provided.

As the above summary shows, information about compounds containing palladium-palladium bonds is fragmentary and somewhat contradictory. It is a goal of our research group to explore bond formation (if any) between two palladium atoms in compounds with the general formula $Pd_2L_4^+$ (where L is a bidentate-bridging, singly charged anionic ligand). The strategy that we shall employ, which is similar to that used in previous work,[50, 51] is schematically shown in Scheme 8. Starting with Pd_2L_4 paddlewheel compounds, one electron will be removed from an antibonding molecular orbital by chemical oxidation. This should lead (if oxidation occurs from a mainly metal-based molecular orbital) to the formation of a net one-electron metal-metal bond.[63]

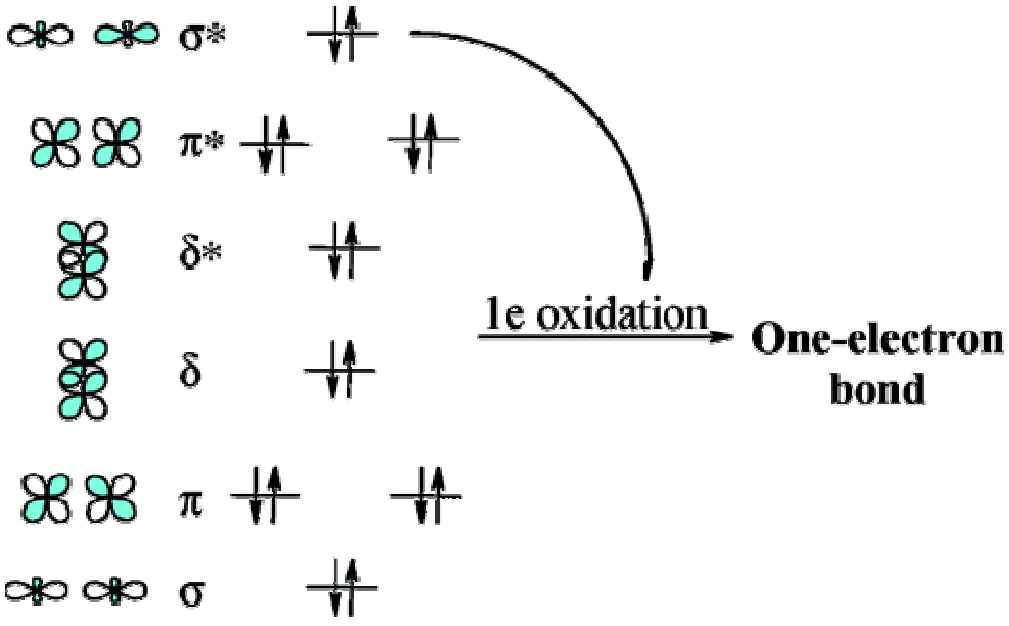

Scheme 8

A first stage in the present work was to identify new precursors to metal-metal bonded dipalladium species, thereby expanding the limited pool for which structures are available (see Table 5).[50, 51, 64, 65, 66, 67, 68] In this report, we describe optimized syntheses for seven Pd_2^{4+} compounds and one mononuclear compound. We have focused our attention on the ligands shown in Scheme 9, where the abbreviations used for the ligands are also defined. We note also that Bear and co-workers[51*a*] have mentioned some species that they made but were not able to characterize unambiguously while preparing $Pd_2(DPhBz)_4$ and $Pd_2(\mu\text{-}DPhBz)_2(\eta^2\text{-}DPhBz)_2$. Therefore, we also re-examined more thoroughly the $Pd^{2+}/DPhBz^-$ system. Numerically, the compounds described here are α-$Pd_2(DAniF)_4$ (**8**), β-$Pd_2(TPG)_2(\eta^2\text{-}TPG)_2$ (**9**), α-$Pd_2(DPhTA)_4$ (**10**), $Pd(DPhBz)_2$ (**11**), β-$Pd_2(\mu\text{-}DPhBz)_2(\eta^2\text{-}DPhBz)_2$ (**12**), $Pd_2(DPhBz)_3(OAc)$ (**13**), α-$Pd_2(DPhBz)_4$ (**14**), and *cis*-$Pd_2[\eta^2\text{-}C_6H_4NC(PH)N(H)Ph]_2(\mu\text{-}OAc)_2$ (**15**). The structures of **10**,[67] **12**,[51*a*] and **14**[51*a*] have been described earlier, and the rest are given here along with electrochemical data for all compounds to help in the evaluation of the best candidates for chemical oxidation, which will be carried out in a separate study.

Table 5 Interpalladium separations in some Pd_2L_4 paddlewheel compounds

Compound	distance (Å)	ref
$Pd_2(DTolF)_4$	2.622(3)	51*b*
$Pd_2(DPhBz)_4$	2.576(1)	51*a*
$Pd_2(hpp)_4$	2.555(1)	50
$Pd_2(dtpa)_4$ (dtpa = $C_6H_5CH_2CS_2^-$)	2.715(3)	64
$Pd_2(dta)_4$ (dta = $CH_3CS_2^-$)	2.738(1)	65
cis-$Pd_2(mhp)_4$ [mhp = (6-methyl-2-oxypyridine)]	2.559(3)	66
trans-$Pd_2(mhp)_4$	2.547(6)	66
$Pd_2(chp)_4$ [chp = (6-chloro-2-oxypyridine)]	2.563(1)	66
$Pd_2(DPhTA)_4$ (DPhTA = 1,3-diphenyltriazene)	2.5626(7)	67
$Pd_2(bttz)_4$ [bttz = tetrakis(μ-1,3-benzothiazole-2-thiolato-*N*,*S*)]	2.745(1)	68

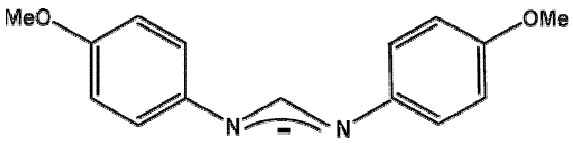

N,N'-di-*p*-anisylformamidinate (DAniF)

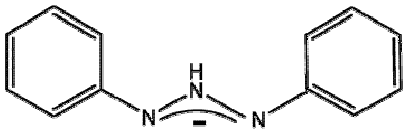

N,N'-diphenyltriazene (DPhTA)

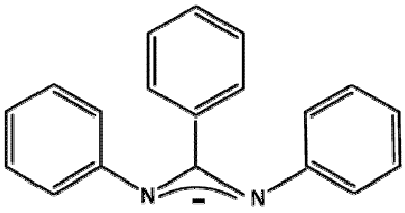

N,N'-diphenylbenzamidinate (DPhBz)

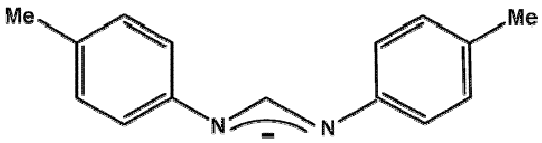

N,N'-di-*p*-tolylformamidinate (DTolF)

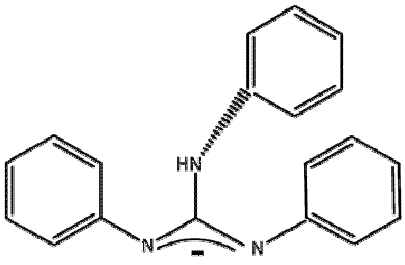

N,N',N''-triphenylguanidinate (TPG)

Scheme 9

EXPERIMENTAL SECTION

General Comments. All manipulations were carried out under an atmosphere of dry nitrogen gas using standard Schlenk techniques, unless otherwise specified. Solvents were either distilled over appropriate drying agents in a nitrogen atmosphere or purified using a Glass Contour solvent system. The organic amines *N,N′,N″*-triphenylguanidine (HTPG) and *N,N*'-diphenyltriazine (HDPhTA) were purchased from TCI and Acros, respectively, and used as received. The formamidine[69] *N,N*'-di-*p*-anisylformamidine (HDAniF) and the benzamidine *N,N*-diphenylbenzamidine[70] (HDPhBz) were synthesized according to published procedures. Palladium acetate was either purchased from Aldrich or was synthesized from $PdCl_2$.[71] A new procedure used for the synthesis of $Pd_2(DPhTA)_4$ is given below.[72]

Physical Measurements. The IR spectra were recorded on a Perkin-Elmer 16PC FTIR spectrometer using KBr pellets. Cyclic voltammograms were measured on a CH Instruments electrochemical analyzer using dichloromethane solutions with 1 M NBu_4PF_6 and 0.1 mM analyte; the electrodes were Pt disk (working), Pt wire (auxiliary), and Ag/AgCl (reference). The redox couple for ferrocene/ferrocenium consistently appeared at +450 mV under these conditions. Elemental analyses were carried out by Canadian Microanalytical Services in British Columbia, Canada. Samples were vacuum-dried prior to elemental analyses to remove the interstitial solvent molecules of the crystals. ^1H and ^{13}C NMR spectra were obtained on VXR-300 and VXR-500 NMR spectrometers. Mass spectrometry data (electrospray ionization) were recorded in the Laboratory for Biological Mass Spectrometry at Texas A&M University, College Station,

Texas, using an MDS Series Qstar Pulsar with a spray voltage of 5 keV. Visible spectra were obtained on either a Shimadzu UV-2501 PC spectrophotometer or a Cary 17D spectrophotometer.

Synthesis of α-$Pd_2(DAniF)_4$, 8. To a solution of $Pd_3(OAc)_6$ (300 mg, 0.446 mmol, 1.34 mmol of Pd^{2+}) in 20 mL of THF was added LiDAniF dissolved in 20 mL of THF. The latter was prepared in situ by deprotonation of HDAniF (686 mg, 2.68 mmol) with a 1.6 M solution of Bu^nLi in *n*-hexane (1.68 mL, 2.7 mmol). The solution was stirred overnight at room temperature. The solvent was then removed under vacuum. The resulting orange solid was washed several times with water and dried under vacuum with a yield of 0.759 g (92%). X-ray quality crystals were grown by dissolving $Pd_2(DAniF)_4$ in 10 mL of CH_2Cl_2 and layering with 45 mL of hexane. Anal. Calcd for $C_{60}H_{60}N_8O_8Pd_2$: C, 58.44; H, 4.87; N, 9.09. Found: C, 58.35; H, 4.85; N, 9.11. ^{1}H NMR ($CDCl_3$, 300 MHz; δ, ppm): 3.767 (s, OCH_3, 6H), 6.674-6.865 (m, aromatic, 8H), 7.035 (s, CH, 1H). IR (KBr, cm^{-1}): 2948 (w), 2832 (w), 1618 (s), 1695 (m), 1499 (vs), 1459 (w), 1438 (w), 1345 (w), 1295 (w), 1243 (s), 1222 (s), 1179 (w), 1108 (w), 1035 (m), 968 (w), 828 (m), 766 (w). ESI+ mass spectrum (*m*/*z*, amu): 1232, M^+. UV-vis (CH_2Cl_2 solution; λ, nm; ε, $M^{-1}cm^{-1}$): 494, 2×10^3.

Synthesis of β-$Pd_2(TPG)_2(\eta^2\text{-}TPG)_2$, 9. To a solution of $Pd_3(OAc)_6$ (300 mg, 0.446 mmol, 1.34 mmol of Pd^{2+}) in 20 mL of THF was added LiTPG dissolved in 20 mL of THF. The latter was prepared in situ by deprotonation of HTPG (769 mg, 2.68 mmol) with a 1.6 M solution of Bu^nLi in *n*-hexane (1.68 mL, 2.7 mmol). After the reaction mixture was stirred overnight at room temperature, the solvent was removed under vacuum. The resulting orange solid was washed several times with water and dried under

vacuum with a yield of 0.799 g (88%). X-ray quality crystals were grown by dissolving $Pd_2(\mu\text{-TPG})_2(\eta^2\text{-TPG})_2$ in 8 mL of CH_2Cl_2 and layering with 47 mL of hexane. Anal. Calcd for $C_{76}H_{66}N_{12}OPd_2$: C, 66.33; H, 4.83; N, 12.21. Found: C, 66.34; H, 4.87; N, 12.06. ^{1}H NMR (C_6D_6, 300 MHz; δ, ppm): 5.461 (s, NH, 1H), 5.638 (d, aromatic, 2H), 5.887 (s, NH, 1H), 6.4-7.1 (m, aromatic, 28H). IR (KBr, cm^{-1}): 3393 (w), 3054 (w), 1602 (m), 1592 (m), 1540 (vs), 1472 (s), 1443 (m), 1423 (s), 1396 (m), 1380 (s), 1307 (m), 1278 (w), 1263 (m), 1247 (w), 1206 (w), 1173 (w), 1074 (w), 1027 (w), 922 (w), 774 (w), 754 (m), 747 (m), 733 (w), 691 (m), 518 (vw), 483 (vw). UV-vis ($CHCl_3$ solution; λ, nm; ε, $M^{-1}cm^{-1}$): 485, 2×10^3; 392, 3×10^3.

Synthesis of α-Pd_2(DPhTA)$_4$, 10. To a solution of $Pd_3(OAc)_6$ (300 mg, 0.446 mmol, 1.34 mmol of Pd^{2+}) in 20 mL of THF was added LiDPhTA dissolved in 20 mL of THF. The latter was prepared in situ by deprotonation of HDPhTA (528 mg, 2.68 mmol) with a 1.6 M solution of Bu^{n}Li in *n*-hexane (1.68 mL, 2.7 mmol). The solution was stirred overnight at room temperature, and the solvent was then removed under vacuum. The reddish-brown residue was washed several times with methanol and had a yield of 0.460 g (69%). ^{1}H NMR ($CDCl_3$, 300 MHz; δ, ppm): 7.051 (t, 1H), 7.154 (t, 2H), 7.572 (d, 2H). IR (KBr, cm^{-1}): 1593 (m), 1483 (m), 1456 (w), 1400 (vs), 1330 (vw), 1292 (vw), 1267 (vw), 1226 (vw), 1211 (m), 1167 (w), 1076 (vw), 1024 (vw), 953 (vw), 902 (vw), 826 (vw), 759 (s), 697 (s), 662 (m), 522 (w), 502 (w). UV-vis ($CHCl_3$ solution; λ, nm; ε, $M^{-1}cm^{-1}$): 574, 5×10^3.

Synthesis of Pd(DPhBz)$_2$, 11. To a solution of HDPhBz (729 mg, 2.67 mmol) in 20 mL of toluene was added a 1.6 M solution of Bu^{n}Li in *n*-hexane (1.68 mL, 2.7 mmol). The mixture was stirred at room temperature for 10 min, and then, it was added to a

solution of $Pd_3(OAc)_6$ (300 mg, 0.446 mmol, 1.34 mmol of Pd^{2+}) in 20 mL of toluene. The mixture was stirred overnight at room temperature, resulting in a dark red solution and a dark red precipitate. After removal of the solvent under vacuum, the residue was washed first with 2 × 25 mL of water and then with 2 × 10 mL of ether, leaving a bright red product that was analytically pure as shown by NMR in a yield of 0.648 g (74%). ^{1}H NMR ($CDCl_3$, 300 MHz; δ, ppm): 6.401 (m, 4H), 6.856 (m, 6H), 6.993 (d, 2H), 7.113 (t, 2H), 7.226 (t, 1H). ^{13}C NMR ($CDCl_3$; δ, ppm): 123.0, 125.1, 128.4, 128.4, 129.3, 129.9, 131.5, 144.4 (all aromatic). IR (KBr, cm^{-1}): 3057 (vw), 1592 (m), 1581 (m), 1494 (vs), 1477 (s), 1433 (s), 1298 (w), 1274 (w), 1211 (w), 1170 (w), 1072 (w), 1025 (w), 958 (w), 794 (w), 777 (w), 706 (m), 693 (m), 499 (w). ESI+ mass spectrum (*m*/*z*): 699 (M^+). UV-vis (λ, nm; ε, $M^{-1}cm^{-1}$): 378 nm, 2 × 10^5; 496 nm, 2 × 10^3.

Synthesis of β-$Pd_2(DPhBz)_2(\eta^2$-DPhBz$)_2$, 12. A solution containing 100 mg of $Pd(DPhBz)_2$ in 50 mL of methanol was heated to reflux for 30 min. The color of the solution darkened, and a small amount of palladium metal was observed. Prolonged heating was avoided to prevent further decomposition. The solvent was removed, and the residue was extracted with 15 mL of CH_2Cl_2. To this extract was added 15 mL of hexanes, and the mixture was separated on a silica gel column using a 1:1 mixture of CH_2Cl_2 and hexanes. The first bright orange band corresponded to β-$Pd_2(DPhBz)_2(\eta^2$-DPhBz$)_2$. Removal of the solvent gave a bright orange powder in a yield of 0.020 g (40%). ^{1}H NMR (22 °C; $CDCl_3$, 300 MHz; δ, ppm): 5.915 (d), 6.138 (d), 6.338 (d), 6.558 (d), 6.629-7.036 (m), 6.729-7.036 (m), 7.141 (t). ^{1}H NMR (-45 °C; $CDCl_3$, 300 MHz; δ, ppm): 5.712 (d), 5.951 (d), 6.048 (d), 6.195 (t), 6.355 (d), 6.474 (t), 6.614-6.949 (t), 7.024 (t), 7.166 (t), 7.522 (t), 7.695 (d), 8.081 (d). ^{13}C NMR ($CDCl_3$; δ, ppm): 122.1,

122.5, 122.6, 123.0, 125.3, 125.9, 126.9, 127.1, 127.3, 128.1, 128.2, 128.4, 129.3, 130.6, 131.2, 131.4, 132.2, 136.027, 146.1, 146.5, 150.1, 152.1, 152.7, 170.0, 174.6. IR (KBr, cm^{-1}): 1655 (vs), 1638 (s), 1561 (s), 1542 (vs), 1508 (m), 1492 (m), 1432 (w), 1263 (w), 1210 (w), 1027 (w), 793 (w), 695 (m). ESI+ mass spectrum (*m*/*z*): 1298 (M+). UV-vis (λ, nm; ε, $M^{-1}cm^{-1}$): 486, 8×10^3.

Synthesis of $Pd_2(DPhBz)_3(OAc)$, 13. To a solution of HDPhBz (729 mg, 2.68 mmol) in 25 mL of CH_2Cl_2 was added a 1.6 M solution of Bu^nLi in *n*-hexane (1.67 mL, 2.68 mmol) at 0 °C, and then the mixture was allowed to reach room temperature. This was added to a solution of $Pd_3(OAc)_6$ (300 mg, 0.450 mmol) in 25 mL of CH_2Cl_2. The mixture was stirred overnight at room temperature, resulting in a dark red solution. The solvent was removed under vacuum, and the dark red residue was washed with 40 mL of MeOH and dried under vacuum with a yield of 0.752 g (75%). ^1H NMR ($CDCl_3$, 300 MHz; δ, ppm): 1.946 (s, OCH_3, 3H), 6.486-7.270 (m, aromatic, 45H). ^{13}C NMR ($CDCl_3$, 300 MHz; δ, ppm): 25.0, 122.8, 123.1, 127.4, 127.7, 127.589, 128.0, 128.4, 131.2, 131.9, 135.6, 135.7, 151.9, 171.8, 172.1, 184.5. IR (KBr, cm^{-1}): 1655 (w), 1580 (vs), 1543 (vw), 1500 (s), 1483 (w), 1440 (m), 1408 (w), 1265 (m), 1215 (m), 1074 (vw), 1026 (vw), 792 (m), 695 (s), 513 (vw). ESI+ mass spectrum (*m*/*z*): 1086 (M+). UV-vis (λ, nm; ε, $M^{-1}cm^{-1}$): 550 (very broad).

Synthesis of α-$Pd_2(DPhBz)_4$, 14. A round-bottomed flask was charged with $Pd_3(OAc)_6$ (100 mg, 0.45 mmol), HDPhBz (607 mg, 2.23 mmol), Et_3N (1 mL), and 40 mL of THF. The mixture was refluxed in air for 3.5 h. After the removal of THF under vacuum, the residue was dissolved in CH_2Cl_2. The mixture was separated by chromatography on a TLC plate. The first bright orange band was collected, and a yield

of 0.035 g (30%) was obtained. ^{1}H NMR (22 °C; $CDCl_3$, 500 MHz; δ, ppm): 6.239 (br, 8H), 6.381 (br, 8H), 6.649-6.752 (m, 20H), 6.786 (br, 16H), 7.046 (br, 8H). ^{1}H NMR (-45 °C; $CDCl_3$, 300 MHz; δ, ppm): 6.215 (br, 8H), 6.456 (br, 8H), 6.685-6.837 (m, 20H), 6.894 (br, 16H), 7.147 (br, 8H). ^{1}H NMR (+45 °C; $CDCl_3$, 300 MHz; δ, ppm): 6.402 (br, 16H), 6.742-6.830 (m, 20H), 6.900 (br, 16H), 7.100 (br, 8H). ESI+ mass spectrum (*m*/*z*): 1086 (M+). UV-vis (λ, nm; ε, $M^{-1}cm^{-1}$): 500, 398, 350.

Synthesis of *cis*-$Pd_2[\eta^2\text{-}C_6H_4NC(Ph)N(H)Ph]_2(\mu\text{-}OAc)_2$, 8. To a solution of HDPhBz (729 mg, 2.68 mmol) in 25 mL of CH_2Cl_2 was added a 1.6 M solution of Bu^{n}Li in *n*-hexane (1.67 mL, 2.68 mmol), and the mixture was allowed to reach room temperature. This was added to a solution of $Pd_3(OAc)_6$ (300 mg, 0.450 mmol) in 25 mL of CH_2Cl_2. The mixture was stirred overnight at room temperature, resulting in a dark red solution. The solvent was removed under vacuum, and the residue was extracted with one 40 mL portion of MeOH. The MeOH solution was transferred into a Petri dish and allowed to evaporate in air. A mixture of pale yellow and dark red crystals formed. The yellow crystals of **15** were separated manually from the red ones of **13**, with a yield of 0.058 g (10%) of yellow crystals. ^{1}H NMR ($CDCl_3$, 300 MHz; δ, ppm): 1.463 (s), 6.442 (d), 6.600 (d), 6.739-7.223 (m), 7.858 (d). ^{13}C NMR ($CDCl_3$, 300 MHz; δ, ppm): 23.5, 114.3, 120.9, 122.4, 124.8, 124.9, 127.1, 127.3, 127.6, 128.1, 128.2, 129.4, 134.1, 134.8, 136.8, 147.4, 153.9, 179.9. IR (KBr, cm^{-1}): 2363 (w), 2344 (w), 1655 (m), 1625 (s), 1583 (vs), 1535 (s), 1509 (m), 1490 (m), 1462 (w), 1414 (w), 1346 (m), 1283 (s), 1265 (w), 1135 (w), 1028 (w), 833 (w), 803 (w), 754 (m), 698 (m), 512 (vw). UV-vis (λ, nm; ε, $M^{-1}cm^{-1}$): 305, 6×10^3.

X-ray Crystallography. Single crystals of each of the compounds **8**, **9**·5C_6H_6, **11**, **13**·$^2/_3$ acetone, and **15**·2CH_3OH were mounted and centered on the goniometer of a Bruker SMART 1000 CCD area detector diffractometer and cooled to -60 °C. Geometric and intensity data were collected using SMART software.[28] The data were processed using SAINT software,[29] and corrections for absorption were applied using the program SADABS.[30]

All structures were solved using the Patterson method available in the SHELX-97 software package.[31] Crystal data are shown in Table 6, and Table 7 lists pertinent bond distances and angles.

Table 6 Crystal data for **8**, **9**·5C_6H_6, **11**, **13**·$^2/_3CH_3C(O)CH_3$, and **15**·2CH_3OH

	8	**9**·5C_6H_6	**11**	**13**·2/3acetone	**15**·2methanol
formula	$C_{60}H_{60}N_8O_8Pd_2$	$C_{106}H_{94}N_{12}P_2d_2$	$C_{38}H_{30}N_4Pd$	$C_{61}H_{52}N_6O_{2.67}Pd_2$	$C_{88}H_{88}N_8O_{12}P_2d_4$
fw	1233.96	1748.73	649.06	1130.55	1875.26
cryst syst	triclinic	triclinic	triclinic	orthorhombic	orthorhombic
space group	$P\bar{1}$	$P\bar{1}$	$P\bar{1}$	$P2_12_12_1$	$Pnn2$
a (Å)	10.306(3)	11.676(2)	11.584(6)	11.527(4)	11.027(1)
b (Å)	10.337(3)	17.172(3)	11.651(6)	22.807(7)	18.183(2)
c (Å)	13.774(5)	22.102(3)	13.222(7)	58.40(2)	10.062(1)
α (deg)	81.103(5)	93.980(3)	105.079(9)	90	90
β (deg)	76.778(5)	100.526(3)	112.883(8)	90	90
γ (deg)	81.146(6)	95.357(3)	96.779(9)	90	90
V (Å^3)	1400.7(8)	4320.7(1)	1538.5(1)	15353(8)	2017.4(4)
Z	1	2	2	12	2
d (calcd) (g cm^{-3})	1.463	1.344	1.401	1.467	1.544
R1,[a] wR2[b] ($I > 2\sigma(I)$)	0.0337, 0.0890	0.0762, 0.1586	0.0509, 0.1353	0.0494, 0.1141	0.0207, 0.0473
R1,[a] wR2[b] (all data)	0.0353, 0.0910	0.1389, 0.1875	0.0590, 0.1445	0.0608, 0.1210	0.0276, 0.0512

[a] $R1 = \sum||F_o| - |F_c||/\sum F_o$. [b] $wR2 = [\sum[w(F_o^2 - F_c^2)^2]/\sum[w(F_o^2)^2]]^{1/2}$ and $w = 1/[\sigma^2(F_o^2) + (aP)^2 + bP]$, where $P = [\max(0 \text{ or } F_o^2) + 2(F_c^2)]/3$.

Table 7 Selected bond distances (Å) and angles (deg) for **8**, **9**·5C_6H_6, **11**, **13**·$^2/_3$ acetone, and **15**·2 methanol[a]

	8	**9**·5C_6H_6	**11**	**13**·$^2/_3$acetone	**15**·2methanol
Pd···Pd	2.6486(8)	2.8971(9)		2.5634[9]	2.9435(4)
Pd-N	2.042[2]		2.045[4]	2.021[5]	2.013(2)
Pd-O				2.070[5]	2.114[2]
Pd-N_{bridge}		2.043[6]			
Pd-$N_{chel.}$		2.054[6]			
Pd-C					1.960(3)
Pd···Pd-N	85.90[6]			85.7[2]	
Pd···Pd-O				86.1[1]	79.02[6]
trans-N-Pd-N	171.75[8]		116.3[1]	171.2[2]	
cis-N-Pd-N	89.71[9]		63.8[1]	90.3[2]	
N-Pd···Pd-N torsion angle	0			14.4	
O-Pd···Pd-O torsion angle				13.5	
Pd···Pd-N_{bridge}		78.5[2]			
Pd···Pd-$N_{chel.}$		107.5[2]			
C-Pd-N					90.7(1)

[a] Values in square brackets are averages.

RESULTS AND DISCUSSION

Synthesis. Reactions of trinuclear palladium(II) acetate with a variety of mononegative N,N-ligands, which include the formamidinate DAniF, the guanidine-type ligand TPG, the triazine DPhTA, and the benzamidine DPhBz, may be complex. Such reactions afford mononuclear or dinuclear species depending on the reaction conditions or the method of isolation. Additionally, the dinuclear species $Pd_2(N,N)_4$ may produce isomeric compounds. In the α isomer, there are four bridging N,N-ligands forming a paddlewheel, and in the β isomer, there are two bridging and two chelating groups. In all cases, however, the palladium atoms are in an essentially square planar environment as shown in Scheme 10.

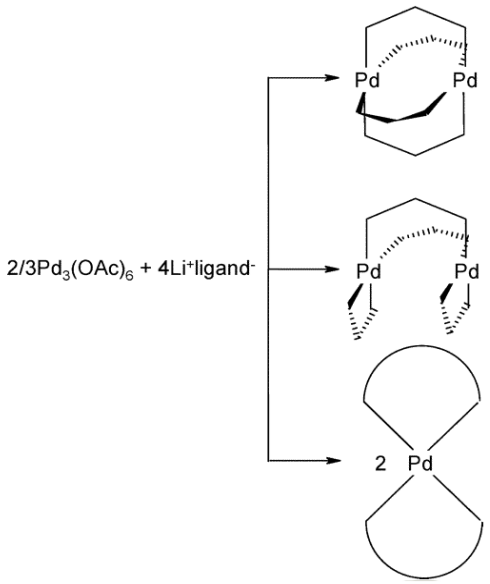

Scheme 10

Whether there were mononuclear and/or dinuclear species in the reaction mixture was easily distinguished by using mass spectrometry, whereas ^{1}H and/or ^{13}C NMR were

useful techniques in distinguishing between the α and the β isomers or their mixtures. Our studies show that with DAniF the only product observed under the experimental conditions reported above is the α form. The presence of a single signal in the methine region of the ^{1}H NMR spectrum at δ of 7.035 ppm, recorded on noncrystalline samples obtained from the reaction mixture, is diagnostic of a single configuration having D_{4h} symmetry because two signals in a 1:1 ratio would be expected for the β isomer. The M^+ peak at 1232 amu in the mass spectrum is consistent with the presence of a dinuclear species, as is the crystal structure which is shown in Fig. 8. The structure is that of a typical tetragonal paddlewheel similar to those of $Pd_2(DTolF)_4$[51b] and $Pd_2(DPhBz)_4$.[51a] One important feature is that the $DAniF^-$ ligands wrap around the dimetal unit so that a fully eclipsed structure is formed with a dihedral angle N-Pd···Pd-N of 0 °. This contrasts with $Pd_2(DTolF)_4$ where the torsion angle is 15.1(6) °[51b] and **13** (vide infra) where the N-Pd···Pd-N and O-Pd···Pd-O torsion angles are 15.4 and 14.5 °, respectively. In the α isomer of $Pd_2(DPhBz)_4$, there is also a considerable torsion angle of 14 °.[51a]

Similarly, results from the reaction of $Pd_3(OAc)_6$ with LiDPhTA show that the only observed product corresponds to the dinuclear α form. A synthesis[72] and structure[67] of $Pd_2(DPhTA)_4$ have been described. The compound was made in unspecified yield in a two-step reaction. First, an unstable diphenyltriazine-palladium species was reported to be obtained by mixing sodium tetrachloropalladate, sodium acetate, and HDPhTA, which then yielded a brown precipitate after standing in a solution of acetone at 50 °C. Our method of preparation using $Pd_3(OAc)_6$ and LiDPhTA gives the pure product straightforwardly in one step and in 69% yield.

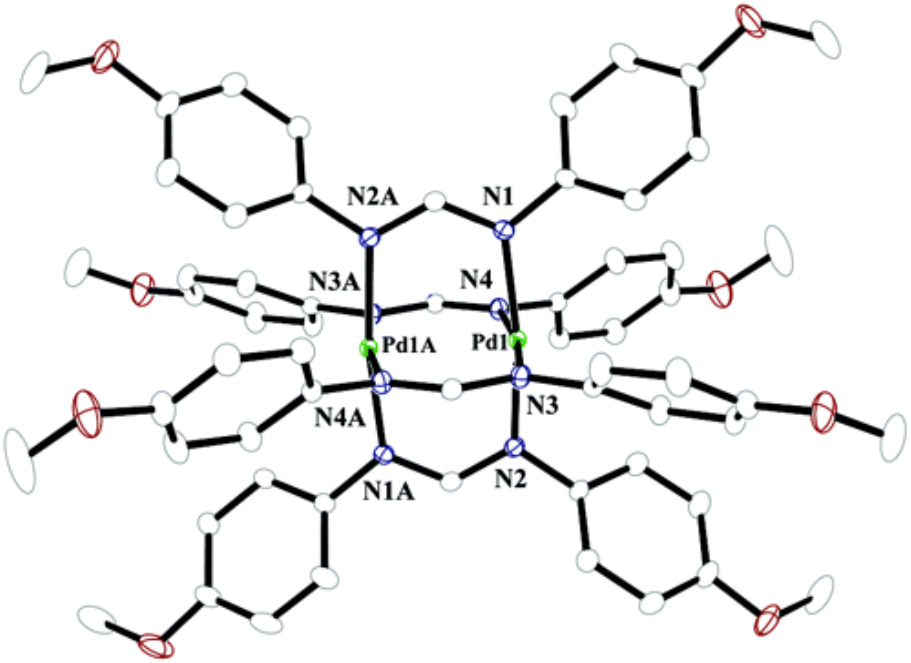

Fig. 8 Paddlewheel **8** having a fully eclipsed configuration. Displacement ellipsoids are drawn at the 30% probability level, and hydrogen atoms have been omitted. Selected bond distances: Pd1-N2 = 2.033(2), Pd1-N3 = 2.040(2), Pd1-N1 = 2.045(2), Pd1-N4 = 2.050(2), Pd1···Pd1A = 2.6486(8) Å.

In contrast to **8** and **10**, reaction with the guanidine-type ligand[73] TPG yields exclusively the *β* isomer **9**. The ^{1}H NMR spectrum is characteristically complex because of the appearance of signals from both the chelating and bridging groups, which when resolved are in a ratio of 1:1. For example, there are two singlets of equal intensities at 5.461 and 5.887 which have been assigned to signals of the -NH hydrogen for the chelating and bridging ligands. The mass spectrum shows the presence of the peak for the dinuclear species, which is also consistent with the solid-state structure shown in Fig. 9.

It should be pointed out that the presence of both *α* and *β* isomers was reported earlier in the Pd/DPhBz system[51*a*] and also in $Pt_2(DArF)_4$ compounds, where DArF is a diarylformamidinate in which Ar is either phenyl or tolyl.[74] These reports indicate that the *α* isomer can sometimes be obtained by heating the *β* isomer in nucleophilic solvents for a short time. However, care must be exercised as prolonged periods in boiling solvents may lead to metal deposition, as we have observed in unpublished results using $Pd_2(hpp)_4$. Another example was found when the guanidine-type compound **9** was heated in MeOH for 1 h; this led to complete decomposition and formation of Pd metal. Also, when heating was attempted using the reaction mixture of $Pd_3(OAc)_6$ and LiTPG, orthometalation of one TPG ligand was observed with formation of $Pd_2(\mu\text{-TPG})(\eta^2\text{-TPG})[\eta^2\text{-}C_6H_4N(CNHPh)N(H)Ph](\mu\text{-OAc})$, as determined by X-ray crystallography.[75]

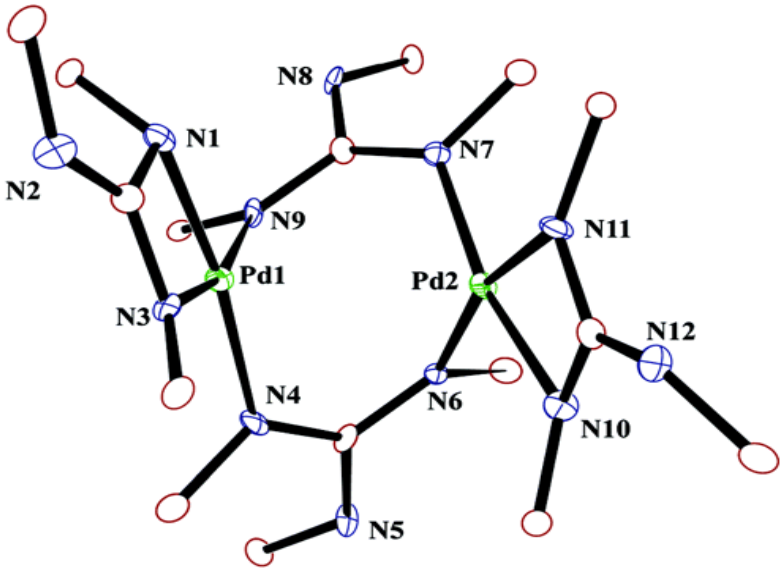

Fig. 9 Core structure of $Pd_2(\mu\text{-TPG})_2(\eta^2\text{-TPG})_2$ with displacement ellipsoids drawn at the 30% probability level. For simplicity, only the attached carbon atom (shown in red) for each of the three phenyl groups of each TPG ligand is shown. The remaining carbon atoms and all hydrogen atoms have been omitted. Selected bond distances: Pd1-N9 = 2.024(6), Pd1-N4 = 2.051(7), Pd1-N3 = 2.059(6), Pd1-N1 = 2.069(7), Pd1···Pd2 = 2.8971(9), Pd2-N6 = 2.037(6), Pd2-N10 = 2.039(6), Pd2-N11 = 2.049(6), Pd2-N7 = 2.058(6) Å.

Palladium/Diphenylbenzamidinate System. The reaction of $Pd_3(OAc)_6$ and Li(DPhBz) was first studied in the Bear group that reported the crystal structures of both the α and β isomers of $Pd_2(DPhBz)_4$ and also the possible existence of a species containing the cation $Pd_2(DPhBz)_4^+$.[51a] Because the latter was of special interest to us, we tried to make the precursor α-$Pd_2(DPhBz)_4$. It was quickly found that this system is far more complex than originally recognized. Furthermore, some of the reported spectroscopic data deviated significantly from what we were finding. A decision was made to reinvestigate this system very carefully to resolve the inconsistencies.

To put the problem in perspective, we begin with a summary of the published report that is relevant to the understanding of our results. The reaction of $Pd_3(OAc)_6$ and Li(DPhBz) was carried out in CH_2Cl_2 at room temperature for 14 h.[51a] The solvent was then removed, and the solid was dissolved in a minimum amount of CH_2Cl_2. Methanol was then added. After the mixture had been stirred overnight, an orange precipitate was isolated. Following "extensive purification" of the solid, it was assigned the formula of the β-form, $Pd_2(\mu\text{-DPhBz})_2(\eta^2\text{-DPhBz})_2$, on the basis of a crystal structure; a 14% yield was reported. The β-isomer was said to give a UV-vis spectrum with two absorption peaks, at 378 and 496 nm, on the edge of a strong band rising into the UV region. The CV (cyclic voltammetry) in CH_2Cl_2 showed two irreversible waves at 1.02 and 1.26 V vs SCE (1.06 and 1.30 V vs Ag/AgCl).

It was further reported that, when a methanol solution of this compound was refluxed for 2 h, a small amount of Pd metal formed and it was removed. Elimination of the solvent from the remaining solution, followed by chromatography, produced another product in a reported yield of 40%. An X-ray study of a crystal showed that it was the

isomer α-$Pd_2(DPhBz)_4$, in which all benzamidinate ligands bridge the Pd_2^{4+} unit. This complex was reported to give a broad absorbance in the visible region centered at 500 nm and a reversible electrochemical wave at 0.695 V from CV or 0.745 V vs Ag/AgCl, as obtained from bulk controlled-potential electrolysis. No additional characterization for any of these compounds, such as elemental analysis[76] or NMR data, was provided. Also, it was stated that other products were observed during chromatography, but they were not identified.

When trying to reproduce the synthesis of $Pd_2(\mu\text{-}DPhBz)_2(\eta^2\text{-}DPhBz)_2$, we noticed that addition of methanol to the reaction mixture, as reported, consistently gave an oily substance instead of the reported solid. This oil prevented the isolation of any crystalline material even when chromatographic separation was attempted. We then decided to modify the synthetic procedure with the hope of overcoming the synthetic difficulties.

A similar reaction of $Pd_3(OAc)_6$ and Li(DPhBz) was carried out in dichloromethane but without methanol. Methanol was used only later to wash the solid obtained after elimination of CH_2Cl_2 from the reaction mixture, and this procedure led to an analytically pure product in high yield that was shown by NMR to contain a ratio of benzamidate to acetate of 3:1. The ratio suggested that the formula is $Pd_2(DPhBz)_3(OAc)$, and this was confirmed by the structure, shown in Fig. 10, where all ligands bridge the dipalladium unit. The CV showed a reversible oxidation at 0.776 V vs Ag/AgCl, a value that is similar to that reported for the α-isomer.[51a]

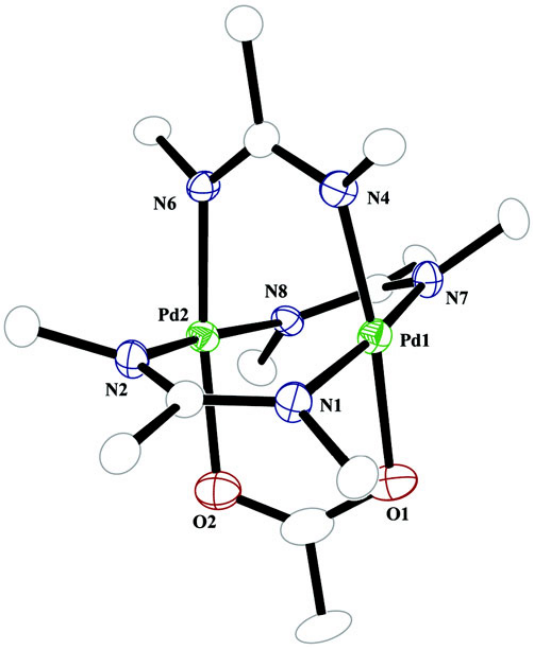

Fig. 10 Core structure of the unsymmetrical compound $Pd_2(DPhBz)_3(OAc)$. Only one of the phenyl carbon atoms for each of the bridging DPhBz ligands is shown. Displacement ellipsoids are drawn at the 30% probability level, and hydrogen atoms have been omitted. Selected bond distances: Pd1-N4 = 2.002(5), Pd1-N1 = 2.027(5), Pd1-N7 = 2.032(5), Pd1-O1 = 2.079(5), Pd1···Pd2 = 2.5678(9), Pd2-N6 = 2.012(5), Pd2-N8 = 2.027(5), Pd2-N2 = 2.036(5), Pd2-O2 = 2.092(5) Å.

By changing the reaction solvent from CH_2Cl_2 to toluene, another product was formed, as shown by NMR and mass spectrometry. The ^1H NMR spectrum is complex; however, it indicates that benzamidinate ligands are present, and there is no acetate. Furthermore, it is consistent with the presence of two types of phenyl rings in a 2:1 ratio. This is consistent with the presence of a highly symmetrical species and only one kind of benzamidinate group. The ^{13}C NMR spectrum, which shows eight sharp peaks in the region between 123 and 145 ppm, is simple and also consistent with equivalent benzamidinate groups. Four of the eight peaks correspond to the unique carbon atoms in the phenyl rings bonded to the nitrogen atoms, and the other four are from the phenyl ring bonded to the bridgehead carbon atom. There are only four unique carbon atoms in each ring because each ring is free to rotate. The signal for the carbon bridgehead was not observed, but this is not unusual as it is bound to two nitrogen atoms, each with a large quadruple moment. The mass spectrum showed only a $[M^+]$ peak consistent with that of a mononuclear molecule of formula $Pd(DPhBz)_2$. This molecular formula is also supported by the crystal structure, shown in Fig. 11, which shows two chelating benzamidinate groups around a single Pd atom in a distorted square planar environment. The CV showed two irreversible oxidation processes at 1.005 and 1.465 V (vs Ag/AgCl). Interestingly, the UV-vis spectrum of $Pd(\eta^2\text{-}DPhBz)_2$ with two bands at 376 and 496 nm is very similar to that reported for the β-isomer.[51a]

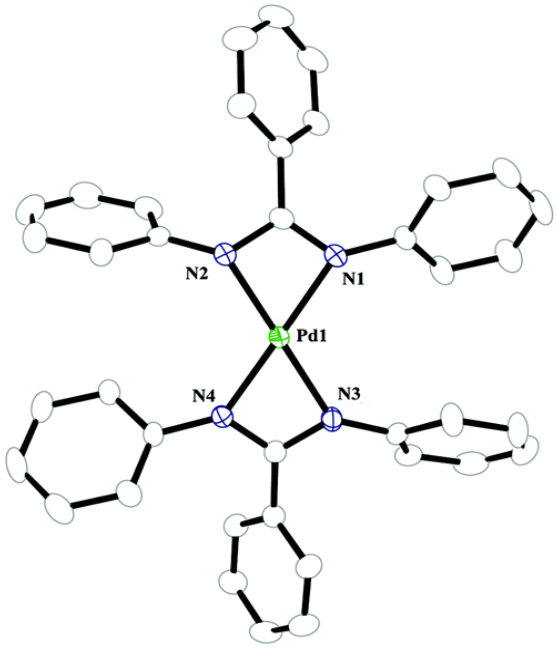

Fig. 11 Structure of the mononuclear compound Pd(η^2-DPhBz)$_2$ showing the distorted square planar arrangement. Displacement ellipsoids are drawn at the 30% probability level, and hydrogen atoms have been omitted. Selected bond distances: Pd1-N1 = 2.037(3), Pd1-N4 = 2.041(3), Pd1-N3 = 2.048(4), Pd1-N2 = 2.053(4) Å.

Boiling of mononuclear $Pd(\eta^2\text{-}DPhBz)_2$ in MeOH followed by chromatographic separation produces an orange product. Its ^1H NMR spectrum is consistent with the existence of only one type of DPhBz group, but it is significantly more complex than that of its precursor. The ^{13}C NMR spectrum is also very complex. Upon slow evaporation of the NMR solvent, all of the solute was recovered as orange crystals. The structure was determined by single-crystal X-ray diffraction, and it is the same as that described earlier for the *β*-isomer, $Pd_2(\mu\text{-}DPhBz)_2(\eta^2\text{-}DPhBz)_2$.[51a] The complexity of the ^1H and ^{13}C NMR spectra may be attributed to restricted rotation of the phenyl groups in each of the benzamidinate ligands, as shown by the changes in the spectra when the temperature is modified. The yield of 40% is significantly higher than that reported earlier (14%). However, there are again some discrepancies in the spectroscopic data. The CV taken by dissolving crystalline samples shows two irreversible processes at 0.927 and 1.291 V (vs Ag/AgCl). These values are somewhat different from those reported earlier (1.065 and 1.305 V vs Ag/AgCl). Also, the electronic spectrum, with only one band at 486 nm, is different from that reported earlier.[51a]

All attempts to prepare the $\alpha\text{-}Pd_2(DPhBz)_4$ from the *β*-isomer by boiling in MeOH were unsuccessful. Once again, a different synthetic approach was sought, and the one used resembled that for the preparation of $Ru_2(DMBz)_4Cl_2$ (DMBz = *N*,*N*'-dimethylbenzamidinate),[77] in which $Ru_2(OAc)_4Cl$ was refluxed with 5 equiv of HDMBz in THF in the presence of an excess of LiCl and Et_3N. By analogy, refluxing of a THF mixture of $Pd_3(OAc)_6$ with 5 equiv of HDMBz in the presence of Et_3N followed by chromatography yielded a dark purple mixture. After separation of a bright orange band by TLC, an ^1H NMR spectrum showed peaks only in the aromatic region, as expected for

a compound with only benzamidinate ligands. The spectrum changed as the temperature was varied, giving a pattern that was significantly simpler at 45 °C than at -45 °C. This is consistent with greater rotational freedom of the phenyl rings at high temperatures. The pattern and integration of these signals are consistent with the presence of a highly symmetrical species in solution. The NMR spectrum, supported by the mass spectrum ([M^+] of 1086 amu), is consistent with a molecule with close to D_{4h} symmetry. Indeed, crystallization of this compound produced crystals in ca. 30% yield, and they have the same structure as that reported earlier for the α-isomer.[78] In this case, the electrochemistry and UV-vis data were the same as those reported.[51a]

We were also interested in the byproducts formed during the synthesis of $Pd_2(DPhBz)_3(OAc)$. Washing the red powder formed after reaction of $Pd_3(OAc)_6$ with Li^+DPhBz^- in CH_2Cl_2 yielded a dark solution. After slow and complete evaporation of MeOH, a mixture of yellow and red crystals was obtained. The dark red crystals were identified as $Pd_2(DPhBz)_3(OAc)$, **13**, and the yellow crystals were identified as *cis*-$Pd_2[\eta^2\text{-}C_6H_4NC(Ph)N(H)Ph]_2(\mu\text{-}OAc)_2$, **15**. In this compound, the two metal atoms are bridged by two cis acetate linkers and there are two chelating orthometalated $DPhBz^-$ ligands which envelop the palladium centers, as shown in Fig. 12. Six-membered rings that consist of three carbon atoms, two nitrogen atoms, and a palladium atom are formed. In these rings, the nitrogen atom not bound to a palladium atom has a hydrogen atom. Its presence is strongly supported by a distance of 2.876 Å between that nitrogen atom and the oxygen atom of an interstitial methanol molecule, a separation that is only consistent with the presence of a hydrogen bond. Thus, the orthometalated groups are mononegative and the dimetal unit has a Pd_2^{4+} core. For this compound, the ^1H NMR

and ^{13}C NMR are very complex. The CV and differential pulse voltammogram show one reversible oxidation wave at 0.930 V (vs Ag/AgCl).

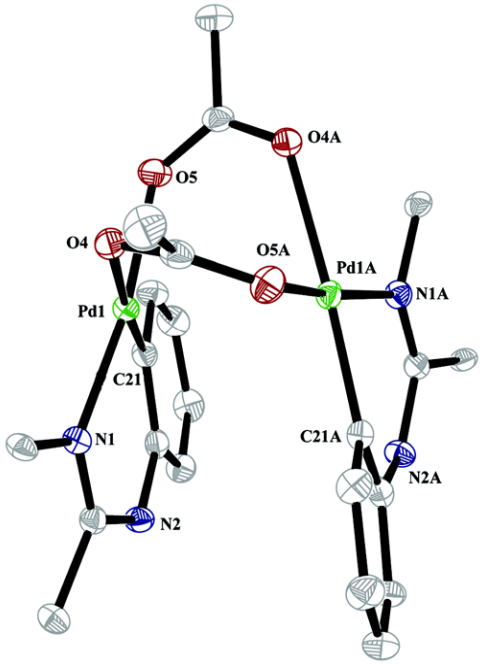

Fig. 12 Core structure of the chiral orthometalated compound *cis*-$Pd_2(\eta^2$-$C_6H_4NC(Ph)NPh)_2(\mu$-$OAc)_2$, **15**. Only one carbon atom of each of the non-orthometalated phenyl groups is shown. Displacement ellipsoids are drawn at the 30% probability level, and all hydrogen atoms have been omitted. Selected bond distances: Pd1-C21 = 1.960(3), Pd1-N1 = 2.013(2), Pd1-O5 = 2.057(2), Pd1-O4 = 2.170(2), Pd1-Pd1 = 2.9435(4) Å.

Conclusions. Because compounds **8**, **13**, **14**, and **15** have reversible oxidation potentials, as shown in Table 8, these compounds appear to be good candidates for chemical oxidation and, thus, good candidates to serve as precursors to metal-metal bonded dipalladium species. This will be done as a second part of this study. It should be noted that the $E_{1/2}$ values in these compounds are dependent on the electron-donating ability of the bridging ligand with the very basic $DAniF^-$ ligand exhibiting the lowest oxidation potential. Interestingly, $Pd_2(DAniF)_4$ can be oxidized reversibly four times, and this will be discussed more thoroughly in a later report where we will explore the electronic structure using DFT calculations.

Table 8 $E_{1/2}$ (V vs Ag/AgCl) Values for Compounds **8-15**

Compound	$E_{1/2}{}^1$	$E_{1/2}{}^2$	$E_{1/2}{}^3$	$E_{1/2}{}^4$
8	0.70	0.97	1.12	1.27
9	0.729 irr	1.031 irr		
10	1.3 irr			
11	1.005 irr	1.465 irr		
12	0.927 irr	1.291 irr		
13	0.776			
14	0.698			
15	0.920			

CHAPTER V

METAL-METAL ATTRACTIONS VERSUS ELECTROSTATIC REPULSIONS IN Pd_2^{5+} COMPLEXES

INTRODUCTION

Species with a bond order less than one are far less abundant than the compounds with a two-electron bond and not as well understood, though these are of great interest from a theoretical standpoint as well as in regard to their physical properties. For example, oxidative doping of polyacetylene gives rise to highly conducting polymers with partial π bonds.[79] It is also well known that partial oxidation of stacked square planar Pt compounds yields materials having a partial σ bond along the Pt axis which gives rise to one dimensional conductivity.[80] Also, "platinum blue" polynuclear complexes which contain only partial delocalized metal-metal bonds have been extensively studied over the years;[81] rhodium and iridium analogs are now known,[82] and the catalytic properties of these species have now been explored.[83]

Recently, the field of molecular electronics has generated a new impetus for the study of chain-like compounds with partial delocalized bonding which could serve as *molecular wires*.[84] Also of interest are systems in which the electron localization/delocalization throughout the molecule can be specifically controlled so that the molecules may behave as *molecular switches*.[85] A fundamental study of bond formation between two nonbonded atoms is therefore of great interest. In previous

chapters on schemes 1 and 8 our approach of obtaining the one-electron bond between two Pd atoms was depicted. As can be seen from the same scheme, these Pd_2^{4+} complexes contain no formal metal-metal bond, because all of the electrons of the two d^8 metal ions completely fill all of the metal-metal bonding and antibonding orbitals.

Removal of one electron should, in principle, yield Pd_2^{5+} containing species with an overall bond order of 0.5, if the oxidation occurs mainly on metal based molecular orbital. Two main methods will be used to study oxidized species – X-ray crystallography, which will tell us the change in metal-metal bond distances along with other structural features and EPR spectroscopy, which will tell us about the existence and properties of the unpaired electrons in these compounds.

As was already discussed in the previous chapter there are only two articles concerning Pd_2^{5+} compounds.[51] Results obtained for $Pd_2(DTolF)_4PF_6$ and $Pd_2(DPhBz)_4^+$ were somewhat confusing. The isotropic EPR signal of $Pd_2(DTolF)_4PF_6$ suggested oxidation of the DTolF ligand rather than the Pd_2 core. However, theoretical predictions for the same compound proposed the presence of an unpaired electron in a mainly metal-based molecular orbital.[51*b*] The slight increase in the Pd···Pd distance (0.02 Å) in the Pd_2^{5+} complex compared to the corresponding Pd_2^{4+} molecule is too small to be used as an argument to support any theory.

On the other hand, EPR results obtained by Bear differed from those obtained in Pd-DTolF. The EPR spectrum of what was claimed to be electrochemically generated $[Pd_2(DPhBz)_4]^+$ cation is axial and clear hyperfine splitting by Pd nuclear spin was observed.

At the same time, as described in the previous chapter, we found out that Pd^{2+}-$DPhBz^{-}$ system is much more complex and contains many other compounds that were not characterized by Bear.[51a] The fact that Bear was not using NMR spectroscopy to characterize his compounds allows to doubt purity of his EPR experiments and obtaining of particularly $Pd_2(DPhBz)_4^+$ cation. It could as well be $\mathbf{13}^+$ or $\mathbf{14}^+$.

In this chapter we present structural characterization of $Pd_2(DAniF)_4PF_6$ along with analysis of $Pd_2(DTolF)_4^+$, $Pd_2(DPhBz)_4^+$ and $Pd_2(DPhBz)_3(OAc)^+$ with high field EPR spectroscopy. Characterization of the above compounds with NMR spectroscopy and knowledge about the position of the first redox wave in the cyclovoltammogram allows us to be confident about the cations formed after performing electrochemical oxidation of amorphous Pd_2^{4+} species.

Advantages of using high field EPR instruments were described in the literature.[86] In their work Cotton and coworkers[86] have shown a drastic difference in the results obtained at low (X-band) and high (W-Band) field. It was shown that while the X-Band EPR spectrum of $Cr_2(DPPC)_4PF_6$ appears as a single, isotropic peak centered at $g = 1.975$, in the W-Band EPR spectrum of $Cr_2(DPPC)_4PF_6$ parallel and perpendicular components of the *g*-tensor are clearly resolved. Since sometimes low-field experiments fail to reveal anisotropy of the *g*-value, which is crucial in our case and can lead to wrong conclusions. If we do not see the anisotropy of *g*-tensor at X-Band (i.e. $Pd_2(DTolF)_4$) it is necessary to obtain a W-Band EPR spectrum of the same compound to make sure that unpaired electron is really located on mainly ligand based orbital.

EXPERIMENTAL SECTION

General Comments. Unless specified otherwise, all manipulations were carried out under an atmosphere of dry nitrogen gas using standard Schlenk techniques. All solvents were either distilled over appropriate drying agents in a nitrogen atmosphere or purified by means of a Glass Contour solvent system. $Pd_2(DAniF)_4$,[87] $Pd_2(DTolF)_4$,[51b] $Pd_2(DPhBz)_4$[51a] and $Pd_2(DPhBz)_3(OAc)$[87] were synthesized according to the published procedures.

Physical Measurements. The IR spectra were taken on a Perkin-Elmer 16PC FTIR spectrometer using KBr pellets. Cyclic voltammograms were taken on a CH Instruments electrochemical analyzer using dichloromethane solutions with 1 M NBu_4PF_6 and 0.1 mM analyte. The electrodes were: Pt disk (working), Pt wire (auxiliary), and Ag/AgCl (reference). The redox couple for ferrocene/ferrocenium consistently appeared at +450 mV under these conditions. Elemental analyses were carried out by Canadian Microanalytical Services in British Columbia, Canada. Samples were vacuum dried prior to elemental analyses in order to remove the interstitial solvent molecules of the crystals. Magnetic susceptibility measurements were made on a Johnson Matthey Magnetic Susceptibility Balance Mark II. Variable temperature magnetic susceptibility measurements were made on crushed crystalline samples from which the interstitial solvents had been removed by vacuum. The samples were carefully weighed and placed in a plastic bag, which was mounted in a drinking straw and then placed inside a Quantum Design SQUID magnetometer MPMS-XL. Data were collected

from temperatures of 2 K to 300 K at a field of 1000 Gauss and the data were corrected empirically for diamagnetism of the sample and the holder. ^{1}H and ^{13}C NMR spectra were obtained on a VXR-300 NMR spectrometer. Mass spectrometry data (electrospray ionization) were recorded at the Laboratory for Biological Mass Spectrometry at Texas A&M University, using an MDS Series Qstar Pulsar with a spray voltage of 5 keV. Visible spectra were obtained on either a Shimadzu UV-2501 PC UV-Vis spectrophotometer or a Cary 17D spectrophotometer. X-Band EPR spectra were recorded at Bruker EMX X-band EPR spectrometer operating in perpendicular mode with an Oxford Instruments EM910 cryostat and high-frequency measurements were conducted with a custom-built variable-frequency EPR spectrometer at the National High Magnetic Field Laboratory in Tallahassee, FL.

Synthesis of $[Pd_2(DAniF)_4]PF_6$, [8]PF_6. To a solution of **8** (350 mg, 0.284 mmol) in 10 mL of CH_2Cl_2 was added $AgPF_6$ (72.0 mg, 0.284 mmol) dissolved in 10 mL of CH_2Cl_2 at –70 °C. An immediate color change from orange to black was observed. The mixture was stirred for 10 minutes at –70 °C, followed by filtration through Celite. A dark-green powder was precipitated by addition of ether and dried under vacuum. Yield: 0.275 g, 70%. X-Ray quality crystals were obtained by dissolving **8** (20 mg, 0.016 mmol) in 4.0 mL of CH_2Cl_2 and layering with 2.0 mL of benzene. The mixture was held at –70 °C until the benzene layer froze. Then on top of the solid benzene was added $AgPF_6$ (7 mg, 0.03 mmol) dissolved in 10 mL of ethyl ether.

The mixture was kept at -10 °C, so that the benzene layer slowly thawed out. In 5 days large black crystals of [**8**]PF_6 were obtained. Anal. Calcd. for $C_{60}H_{62}N_8O_9Pd_2PF_6$: C 51.59, H 4.47, N 8.02%. Found: C 51.15, H 4.34, N 7.90%. IR (KBr, cm^{-1}): 1608 m, 1591 s, 1499 vs, 1464 w, 1438 w, 1423 w, 1325 vw, 1294 m, 1246 vs, 1226 s, 1132 s, 1094 s, 1024 s, 928 m, 844 s, 829 s, 803 w, 787 w, 722 vw, 645 vw, 585 w, 558 w, 540w, 505 w, 406 w. The Vis-NIR spectrum is nearly identical to that of $Pd_2(DTolF)_4PF_6$, which has already been reported. μ_{eff} (298 K): 1.68 μ_B.

X-ray Crystallography

Single crystal of [**8**]PF_6 was mounted and centered on the goniometer of a Bruker SMART 1000 CCD area detector diffractometer and cooled to -60 °C. Geometric and intensity data were collected using SMART software.[29] The data were processed using SAINT software,[30] and corrections for absorption were applied using the program SADABS.[31]

The structure was solved using the Patterson method, routinely available in the SHELX-97 software package.[32] Crystal data are shown in Table 9. Table 10 lists pertinent bond distances and angles for [**8**]PF_6.

Table 9 Crystal data for [**8**]PF_6

Compound	[**8**]PF_6 $[Pd_2(DAniF)_4]PF_6$
Formula	$C_{60}H_{60}F_6N_8O_8PPd_2$
FW	1378.93
Crystal System	Tetragonal
Space Group	*P*4/*n*
a, Å	12.947(1)
b, Å	12.947(1)
c, Å	17.540(4)
α, deg.	90
β, deg.	90
γ, deg.	90
V, Å^3	2940.1(8)
Z	2
d(calc), g cm^{-3}	1.558
R1[a], *w*R2[b] (*I*>2σ(*I*))	0.0617, 0.1759
R1[a], *w*R2[b] (all data)	0.0872, 0.1982

[a] $R1 = \sum||F_o| - |F_c||/\sum|F_o|$, b. $wR2 = [\sum[w(F_o^2 - F_c^2)^2]/ \sum[w(F_o^2)^2]]^{½}$, $w = 1/\sigma^2(F_o^2) + (aP)^2 + bP$, where $P = [\max(0 \text{ or } F_o^2) + 2(F_c^2)]/3$

Table 10 Selected bond distances (Å) and angles (deg) for [**8**]PF_6

	[**8**]PF_6
M–M	2.597(2)
M–N	2.043[6]
M···F	4.782
M–M–N	86.6[2]
trans-N–M–N	173.3[3]
cis-N–M–N	89.80[2]
N–M–M–N torsion angle	1.4

Density Functional Calculations.[a] Density functional theory (DFT) [88] calculations were performed with the hybrid Becke 3-parameter exchange functional[89] and the Lee-Yang-Parr non-local correlation functional[90] (B3LYP) implemented in the Gaussian 98 (Revision A.9) program suite. [91] For feasibility, the dipalladium formamidinate molecules were represented by a model in which the aryl groups of the formamidinate ligands were replaced by hydrogen atoms, namely $Pd_2(HNCHNH)_4$. Geometry optimizations were performed on both neutral and singly-oxidized models without any symmetry constraint in either case. Double- and triple-ζ basis sets were used for two separate $Pd_2(HNCHNH)_4$ calculations. The singly-oxidized model was calculated using the double-ζ basis set. The double-ζ calculations consisted of the correlation-consistent polarized (cc-pVDZ)[92] valence basis set used for non-metal atoms (carbon, nitrogen, and hydrogen), and an effective core potential (ECP) representing the 1s2s2p3s3p3d core was used for the palladium atoms along with the associated double-ζ basis set (LANL2DZ). [93] The triple-ζ calculations utilized the correlation consistent polarized (cc-pVTZ)[92] basis set for non-metal atoms and an ECP representing the 1s2s2p3s3p3d core along with the Stuttgart triple-ζ basis set.[94] The self-consistent-field cycles criterion for convergence on all calculations was increased from the default value to 10^{-8}. All calculations were run on an Origin 3800 64-processor SGI computer located at the Texas A&M Supercomputing facility.

[a] All calculations were performed by Dino Villagrán.

RESULTS AND DISCUSSION

Synthesis. $AgPF_6$ was chosen as an oxidizing agent for **8**. The oxidation occurred immediately as the solution of $AgPF_6$ diffused into CH_2Cl_2 solution of **8**. We tried to oxidize chemically $Pd_2(DPhBz)_3OAc$ and $Pd_2(DPhBz)_4$. Unfortunately the only oxidizing agent that was strong enough for the reaction and not leading to formation of oily products was $NOBF_4$. As described in chapter III nitrogen oxides are good nucleophyles and tend to substitute bridging ligands in palladium systems. Attempts to oxidize $Pd_2(DPhBz)_3OAc$ and $Pd_2(DPhBz)_4$ chemically with $NOBF_4$ lead to formation of loop based on Pd_2^{4+} units with bridging NO_2^- and OH^- anions (Fig. 13). Not being able to study $Pd_2(DPhBz)_3OAc^+$ and $Pd_2(DPhBz)_4^+$ with the use of X-Ray crystallography we obtained these cations in solution by electrochemical oxidation and studied them in-situ using EPR and UV-visible techniques.

X-Ray Crystallography. When $Pd_2(DTolF)_4$ is oxidized to $Pd_2(DTolF)_4^+$ the metal-metal distance becomes 0.015 Å longer,[51b] while in **8**/**8**$^+$ it is 0.0512 Å shorter.[95] Another important issue worth mentioning is that DTolF wraps around the dimetal unit with a considerable N–Pd–Pd–N torsion angle of 15.1(6) and 17(1) Å for the 4+ and 5+ compounds, respectively, while DAniF on the contrary forms eclipsed structures in both the neutral and singly oxidized compounds.

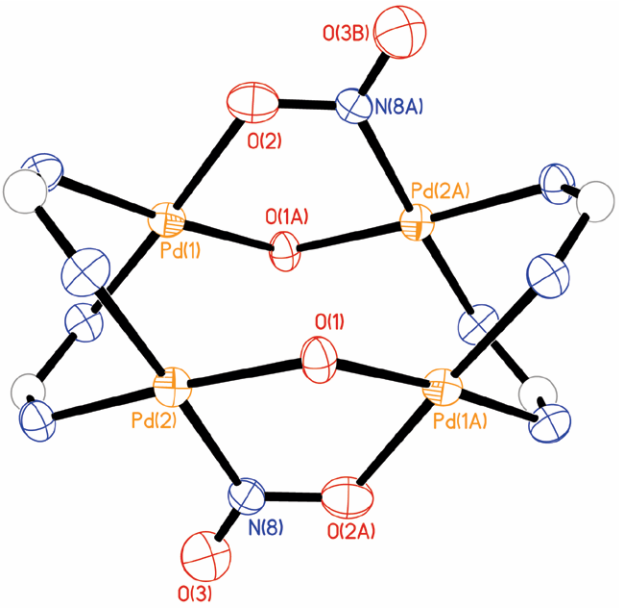

Fig. 13 Core structure of $[Pd_2(DPhBz)_2]_2(NO_2)_2(OH)_2$. Displacement ellipsoids are drawn at the 30% probability level, and all hydrogen atoms have been omitted.

It should be emphasized that the Pd_2^{5+} compound presented here has *isolated* M_2^{5+} units. Although in the structures $Pd_2(DTolF)_4PF_6$ and [**8**]PF_6 the fluoro-anions occupy positions which are collinear with the M–M axes, the closest M···F distances are > 4.5 Å, far too long to be chemically important. The fact that there are essentially no cation-anion bonding interactions is quite significant because this provides a great contrast to the case of many of the mixed-valence "Pt_2^{5+}"[96, 1] complexes reported. For example, diplatinum complexes with bridging pyrophosphite ligands have been extensively studied in the mixed-valence "Pt_2^{5+}" oxidation state, though these species tend to form Pt–Pt···X···Pt–Pt···X chains (X = halide) which give rise to conducting properties. Recent variable temperature Raman spectra have shown that many species are better described as having a charge density wave structure at low temperatures (i.e., $Pt^{2+}\cdots Pt^{2+}\cdots X–Pt^{3+}–Pt^{3+}–X\cdots$).[97] In fact, there is only one compound reported with a truly isolated Pt_2^{5+} unit with which we may compare our Pd_2^{5+} and Ni_2^{5+} results, namely $[Pt_2(DTolF)_4]PF_6$,[98] in which the closest Pt···F–PF_5 distance is > 4 Å, and the Pt–Pt distance of 2.5304(6) Å falls between those of the Pt_2^{4+} compound $Pt_2(DPhF)_4$[98] (2.649(2) Å) and the singly bonded $Pt_2(DPhF)_4Cl_2$ (2.5169(7) Å). In a similar way, the Pd–Pd distance in [**8**]PF_6 of 2.597(2) Å lies between that of the neutral **8** (2.6482(8) Å) and that of the only genuine singly bonded Pd_2^{6+} compound known to date, $Pd_2(hpp)_4Cl_2$ (2.391(2) Å).[50]

EPR Spectroscopy. EPR spectra of $Pd_2(DTolF)_4PF_6$ (Fig. 14) and $Pd_2(DAniF)_4PF_6$ (Fig. 15) were obtained from powder samples. Both show obvious anisotropy of the *g*-value, which is a characteristic feature of systems, where unpaired electron is located on molecular orbitals with mainly metal character. This result also shows us again the importance of using high field EPR instrument for these systems, since same compound $Pd_2(DTolF)_4PF_6$ at low field shows perfectly isotropic signal.

$Pd_2(DPhBz)_3(OAc)^+$ and $Pd_2(DPhBz)_4^+$ cations were obtained by electrochemical oxidation of corresponding Pd_2^{4+} molecules in CH_2Cl_2 solution. EPR spectra of these two Pd_2^{5+} compounds were obtained *in situ* same way as Bear did it.[51*a*]

$Pd_2(DPhBz)_3(OAc)^+$ reveals anisotropy of *g*-value. Also, because the tetragonal symmetry of this molecule is broken by replacement of $DPhBz^-$ for OAc^- separation of $g_\perp$ into g_x and g_y is clearly seen (Fig. 16). Spectra of $Pd_2(DPhBz)_4^+$ is exactly the same, as was obtained by Bear and coworkers and shows anisotropy of *g*-value and hyperfine splitting which is in agreement with 5/2 nuclear moment of Pd.

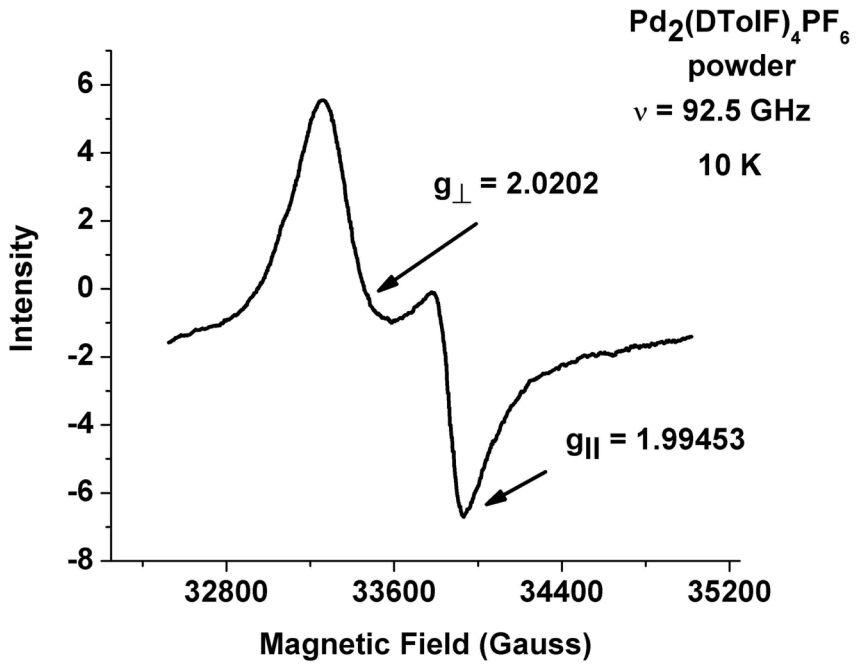

Fig. 14 EPR spectra of $Pd_2(DTolF)_4PF_6$ powder

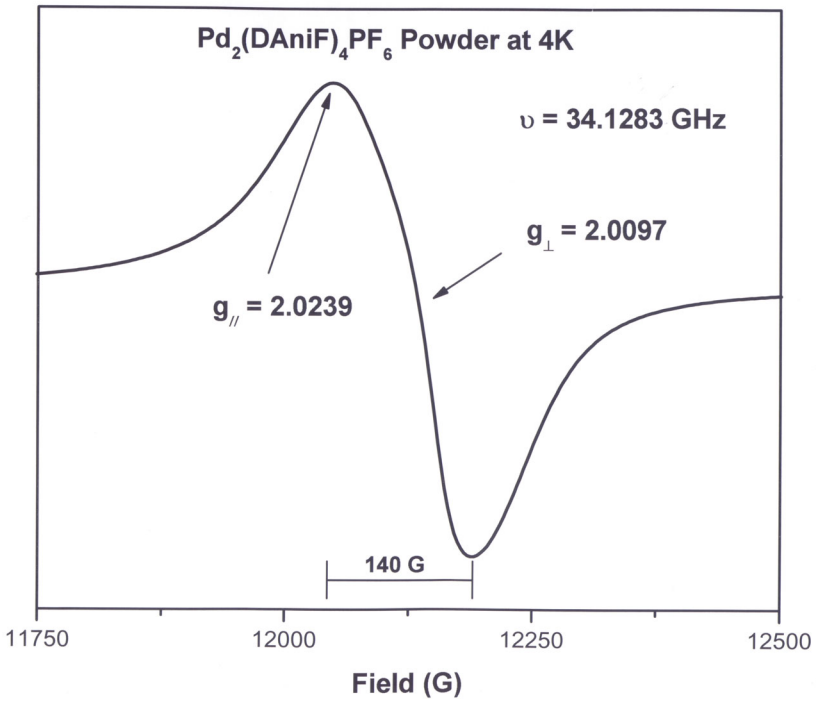

Fig. 15 EPR spectra of $Pd_2(DAniF)_4PF_6$ powder

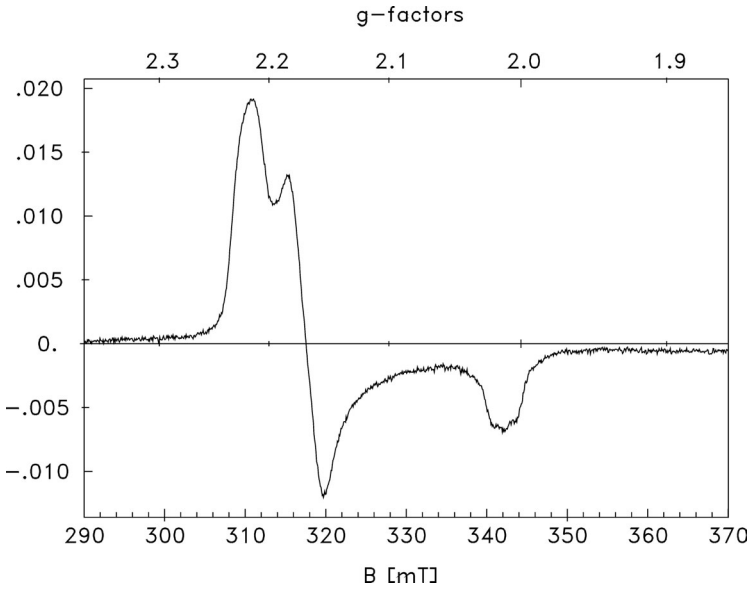

Fig. 16 EPR spectra of $Pd_2(DPhBz)_3(OAc)^+$ cation

Electronic Structure. In previous work on Pd_2 complexes,[51b] SCF-Xα-SW calculations of the electronic structures of the Pd_2^{4+}, and Pd_2^{5+} complexes were done using a model in which the aryl groups of the formamidinate ligands used in the syntheses are replaced by H atoms. These results showed that many of the orbitals of the idealized M–M bonding manifold (i.e., Scheme 1) are perturbed in energy due to interactions with ligand-based orbitals, and that there is significant mixing of the metal and ligand π orbitals. It is interesting to note that calculations of the electronic structure of the analogous dimolybdenum model, $Mo_2(HNCHNH)_4$, showed very little deviation from the orbital ordering given in Scheme 1 and also very little mixing of the Mo *d* orbitals with the ligand π orbitals.[99] This difference between the Pd_2 model and the Mo_2 model can be attributed to the increased effective nuclear charge of the Pd atoms as compared to Mo, which causes the *d* orbitals of the former to contract and have lower energy (due to the increased stabilizing electron-nuclear interactions), and thus the Pd-based orbitals can be considered to be quite close in energy to the energies of the ligand π orbitals.[100]

The Xα calculations[51b] show that many of the orbitals of interest (HOMO, HOMO-1, HOMO-2, etc.) are calculated to be quite close in energy (< 0.1 eV in several cases), and the ordering is very sensitive to subtle effects such as lowering the symmetry from D_{4h} to D_4.[51b] Moreover, the SOMO calculated for $Pd_2(HNCHNH)_4^+$ was a δ^* orbital with significant ligand character which is formed from the two d_{xy} orbitals of the metal atoms and the π orbitals of the formamidinate ligands.[51b] This was interpreted as not being in accord with the experimental data because $Pd_2(DTolF)_4^+$ was believed to contain a ligand-centered radical.[51b]

We have re-examined the problem of the electronic structures $Pd_2^{4+/5+}$ complexes using current levels of theory. For this investigation we employed the B3LYP functional which has been used successfully in our laboratory[101] and elsewhere[102] for analysis of the electronic structures of metal-metal bonded systems. In this case, we optimized the geometry of the model by starting from the atomic coordinates of the crystal structure of $Pd_2(DTolF)_4$ which presents a staggered conformation of D_4 symmetry. For completeness, two different calculations were performed with two different basis sets of double- and triple-ζ quality respectively, as described previously in the computational details section. The calculated relaxed geometry of the dipalladium model results in an eclipsed conformation, D_{4h} symmetry, regardless of both the starting geometry or the basis set. The Pd-Pd distance, nominally with a bond order of zero, was calculated at 2.7394 and 2.731 Å with the double- and triple-ζ respectively.

The results of these calculations can be explained in terms of a perturbation of the idealized M–M manifold (Scheme 1) by interactions with the π orbitals of the HNCHNH

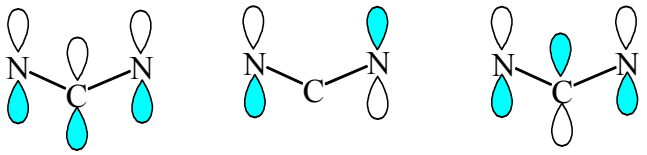

a **b** **c**

Scheme 11

units (shown diagrammatically in Scheme 11 and Fig. 17).

Each formamidinate ligand has a bonding (**a**), nonbonding (**b**), and antibonding (**c**) combination of π orbitals (Scheme 11), which forms 12 molecular orbitals for the $M_2(HNCHNH)_4$ species in D_{4h} symmetry disposed as shown in the right-hand column of Fig. 17.[103] Shown in the left-hand column of Fig. 17 are the orbitals of the idealized M–M bonding manifold.[104]

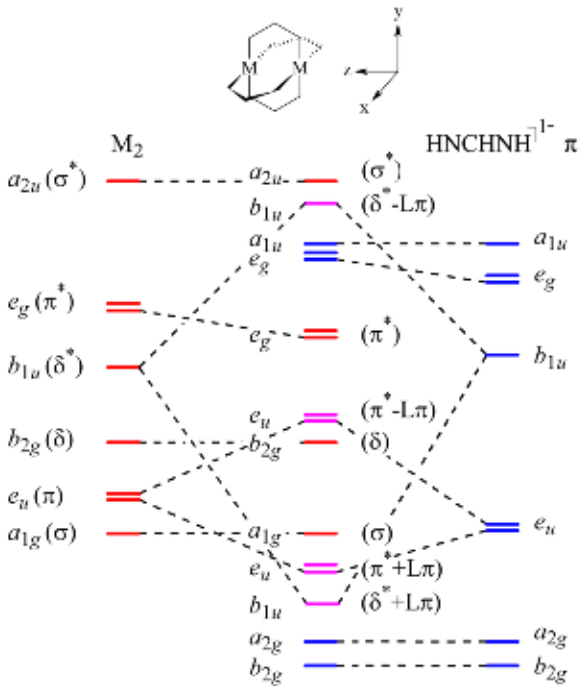

Fig. 17 Schematic molecular orbital diagram showing the interactions of the HNCHNH π orbitals with the metal-metal bonding manifold. The red orbitals are purely metal-based, the blue orbitals are purely ligand-based, and the purple orbitals are highly mixed metal-ligand orbitals.

Analysis of the symmetry-matched interactions between the M_2 orbitals and the formamidinate π orbitals results in the central column of the Fig. 17. Orbitals for which there is no symmetry match (M_2 σ a_{1g}, L π a_{2g}, L π a_{1u}, and M_2 σ^* a_{2u}) are drawn in the central column unchanged in energy from their original positions. Several of the orbitals which could interact (the e_g set and the b_{2g} set) are calculated to be not highly perturbed from their original energies, although the b_{1u} set and the e_u set of orbitals are highly perturbed. The most important of these interactions occurs with the b_{1u} orbitals, which overlap so strongly that their antibonding combination (δ^*-Lπ) is very near in energy to the HOMO (σ^*). Fig. 18 shows contour plots of the frontier molecular orbitals of the $Pd_2(HNCHNH)_4$ model. It should be noted here that the LUMO is an orbital of δ^* symmetry formed by the d_x2_y2 orbitals and which has significant antibonding interactions with the σ orbitals of the HNCHNH ligands.

Also shown in Fig. 17 are qualitative estimates of the metal/ligand contributions to the molecular orbitals. Orbitals shown in red are essentially pure metal orbitals with little or no contributions from the ligands. Orbitals in blue are essentially ligand-based orbitals having very little metal character. The orbitals in purple are *highly mixed* having nearly equal metal and ligand contributions. It should be noted that upon improving the basis set from double-ξ to triple-ξ, the energies of the frontier orbitals are better resolved.

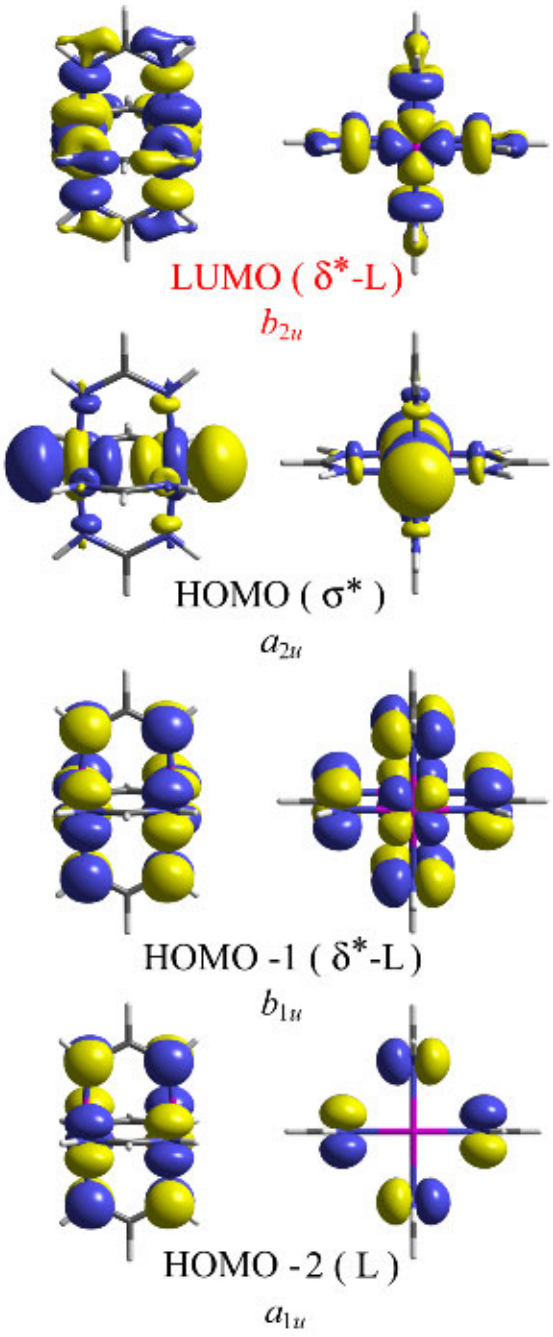

Fig. 18 Surface contour diagrams from DFT (0.04 isodensity) of the three highest occupied and the lowest unoccupied molecular orbitals for the $Pd_2(HNCHNH)_4$ model.

With this orbital diagram available, we can now begin to understand many of the puzzling properties of the compounds. To begin, it is now easy to understand why four reversible oxidations of **8** can be observed electrochemically. The reason is that the HOMO and HOMO-1 are very close in energy (with the double-ζ basis set those values were essentially the same, improving the basis set to triple ζ resolved the difference by 0.2 eV), and thus the four electrons which occupy these two orbitals are easily removed at very similar electrochemical potentials. Also, the absorption spectrum of the Pd_2^{5+} species have a very intense band at rather low energy (ca. 900 nm), which may be due to a HOMO1-SOMO transition which would have some characteristics of a LMCT transition. Secondly, based on the MO diagram in Fig. 17, one-electron oxidation of the Pd_2^{4+} complexes very clearly involves removal an electron from metal-based orbitals producing true Pd_2^{5+} units rather than ligand-centered radicals. Moreover, DFT calculations of the singly oxidized species $M_2(HNCHNH)_4^+$ have been performed using an open shell geometry optimization to a singly-oxidized model using the double-ζ basis set, which also clearly show that the SOMO in each case is the metal-based a_{2u} σ^* orbital. The calculated contraction of the Pd-Pd distance by about 0.026 Å which is consistent with experimental evidence and the formulation of its electronic structure, namely the increase in the bond order by ½.

But there is still one experimental fact which does not appear to fit this picture: If one-electron oxidation involves removing an electron from the σ^* orbital and generation of an M_2^{5+} species with a bond order of 0.5, why does the Pd–Pd distance in $Pd_2(DTolF)_4$ *increase* upon oxidation? In going from **8** to $\mathbf{8}^+$, a *decrease* in the Pd–Pd distance occurs as would be expected. Yet these results are not so incongruous as they at first appear to

be, because one must consider two major changes in the Pd_2 molecule upon oxidation. The first is the shortening of the Pd–Pd distance due to the removal of an antibonding electron. The second is an increase of the positive charge on each Pd atom which will cause a repulsive electrostatic effect between the two Pd atoms, lengthening the distance between them.

We therefore believe that the increase of 0.02 Å in going from $Pd_2(DTolF)_4$ to $Pd_2(DTolF)_4PF_6$ is primarily of electrostatic origin and that any shortening of the Pd–Pd distance is outweighed by the electrostatic effect. In **8**, however, the DAniF ligands are more electron-rich due to the electron-donating properties of the two *p*-OMe groups. This causes the Pd atoms in **8** to be more electron-rich, and therefore the electrostatic repulsions between them are somewhat moderated. Thus the dominating effect of oxidizing **8** to [**8**]PF_6 is the increase of the bond order from 0 to 0.5, which justifies the shortening of the Pd–Pd distance of 0.05 Å. Further support for this view can be obtained by making a comparison to the dinickel compounds, which will be made in next chapter.

Small variations or increases in distances between metal atoms as the bond order and charge of the dimetal units increase have been observed in Re_2^{n+} and $Tc_2^{5+/6+}$ complexes.[105, 106] For example in the species $Re_2Cl_4(PMe_2Ph)_4]^{n+}$, n = 0, 1, and 2[105], in which the Re-Re formal bond orders decrease from 4 to 3.5 to 3, the metal-metal distances are 2.241(1), 2.218(1) and 2.215(2) Å, respectively. The last two distances are essentially the same within experimental error. In the quadruply bonded Tc_2^{6+} molecule $Tc_2(O_2CCH_3)_4Cl_2$,[106*a*] the Tc-Tc bond distance of 2.192(1) Å is actually longer that of 2.1260(5) Å In the Tc_2^{5+} anion $Tc_2(O_2CCH_3)_4Cl_2$ which has a formal bond order of 3.5.[106*b*]

Conclusions. Based on X-Ray crystallography data, EPR results and electronic structure predicted by DFT calculations we propose that in Pd_2^{5+} paddlewheel compounds the unpaired electron is located in a mainly metal based molecular orbital and that a one-electron metal-metal bond is formed. Depending on the electron-donating abilities of bridging ligand, which compensates for increased electrostatic repulsion between two Pd centers metal-metal, the distance can behave differently. In the case of $DAniF^-$, it significantly decreases, whereas in the case of $DTolF^-$ when the ligand is less basic it slightly increases.

CHAPTER VI

METAL-METAL BONDING IN MIXED VALENCE Ni_2^{5+} COMPLEXES AND SPECTROSCOPIC CHARACTERIZATION OF A Ni_2^{6+} SPECIES

INTRODUCTION

Bond formation between transition metal atoms is the main direction of the studies in our research group.[107] Since the description of the quadruple bond in the $[Re_2Cl_8]^{2-}$ anion in 1963,[108] hundreds of compounds with different transition metals and different bond orders have been prepared and characterized,[1] many of which have important uses as catalysts,[109] in biological systems,[110] or as chemical sensors.[111] One transition element for which authentic examples of metal-metal bonding in lantern-type complexes remain scant is nickel,[1] although it should be mentioned that several low-valent organometallic complexes possessing Ni−Ni bonds have been described.[112]

Nickel-to-nickel bonds were first proposed in 1953 to explain the seemingly anomalous insolubility of nickel(II) (bis-dimethylglyoxime) (**I**) as compared to its copper analogue.[113] Also, nickel-nickel bonding has been proposed in the dinuclear oxidation products of certain $Ni(L)_2$ complexes[114] (**II**) which also contain Ni^{II} (the oxidation having been shown to be ligand based[115]). In both of the above situations, the Ni···Ni separations are quite long (≥ 3.0 Å) and no MO description of the supposed "bonding" between the two d^8 Ni^{II} ions has yet been given.[116] There is also a report of dinuclear nickel(II) monothiocarboxylates which suggests the possibility of Ni−Ni bonds based upon a

magnetic study.[117] The dithioacetate complex $Ni_2(S_2CCH_3)_4$ which has a long nickel-nickel separation (2.564(1) Å) has been oxidized by reaction with iodine.[118] The structure shows linear chains of ··I ··$[Ni_2S_8]$ ··I ··$[Ni_2S_8]$ ·· with a Ni−Ni distance of 2.514(3) Å. Because the compound is reported to be EPR silent, assignment of a metal−metal bond to this compound is ambiguous. It was not until our first investigation of Ni_2^{4+} and Ni_2^{5+} species (and their corresponding dipalladium analogues) with the lantern-type structure (**III**) that the ground rules for Ni−Ni bond formation were laid out and demonstrated experimentally and theoretically.[51b] Until our present work, this was the only unambiguous report of a lantern-type compound with a Ni−Ni bond.

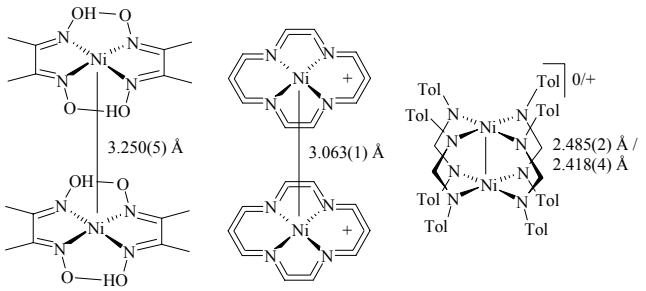

I **II** **III**

Interactions between the *d* orbitals of two metal atoms brought close enough to each other to allow overlap would be expected to give rise to a manifold of bonding and antibonding orbital combinations, as shown in Scheme 1 in which D_{4h} symmetry is assumed.[1] Two d^8 Ni^{2+} ions provide 16 electrons with which to fill these 8 molecular orbitals, resulting in the configuration $\sigma^2\pi^4\delta^2\delta^{*2}\pi^{*4}\sigma^{*2}$. With all of the bonding and antibonding levels filled, no net bonding would result. Removal of one electron from the system would change this picture, since the electron removed would be taken from an antibonding orbital. This would be expected to result in a species with a net bond order of ½ and an unpaired electron in the σ* orbital. However, the precise order of the MOs in

Scheme 1 may vary depending on the metal[119] and the nature of the bridging ligands[120] and the unpaired electron may occupy a different antibonding orbital. Among the factors lacking in the simple picture shown in Scheme 1 are the placement of ligand orbitals, and possible mixing of the ligand π orbitals with the orbitals of the *d* manifold, which can cause ambiguity in the assignment of the electronic structure of Ni_2^{5+} species.

For nickel, this question is particularly pertinent since it is known from X-ray spectroscopy that the *d* orbital manifold becomes significantly lower in energy towards the right side of the transition series.[121] When the *d* orbitals are lower in energy and thus closer to the energy levels of the filled ligand orbitals, it is more likely that mixing with ligand orbitals can occur.[122] It is even possible that the *d* orbitals might fall lower in energy than the filled ligand orbitals, and in such a situation it might be difficult to discern whether oxidations are metal-centered or ligand-centered.

Our recent interest in the formation of nickel-nickel bonds from precursors that lack such bonds stems from our study of polynuclear complexes containing extended metal atom chains (EMACs),[1, 123] where we discovered that linear Ni_3^{6+} complexes, which have been considered not to have Ni−Ni bonds,[124] can be oxidized to Ni_3^{7+} species with short Ni−Ni contacts very suggestive of Ni−Ni bond formation.[125] Extension of this concept to polynickel species having linear chains of five, seven, and nine Ni atoms has been achieved,[126] though one electron oxidation products of only the pentanickel species have been studied in detail.[127] Recent DFT computational studies on these trinickel complexes have quite accurately reproduced the geometrical change in Ni···Ni separations between the neutral and one-electron oxidized trinickel species, but suggested that there is no net change in the Ni–Ni bond order of the two forms.[128] Instead, it was

argued that both Ni_3^{6+} and Ni_3^{7+} complexes have a net bond order of ½ and that the major change in Ni−Ni distances is due primarily to the concomitant removal of axial ligands upon one electron oxidation. A study of polynuclear Ni^{II} and Ni^{II}/Ni^{III} mixed valence complexes during which there is no change in axial ligation is therefore quite desirable. We feel that understanding the simple dinuclear complexes is useful to provide some guidelines for the longer chain species.

With these considerations in mind, we have begun an investigation of nickel complexes of type **III** with formamidinates and guanidinates in order to provide a more detailed picture of what happens upon oxidation of $Ni_2(ligand)_4$ complexes to $[Ni_2(ligand)_4]^+$ ions. The new complexes presented in this chapter are: $Ni_2(DAniF)_4$ (**16**), $[Ni_2(DAniF)_4]BF_4$ (**16**-BF_4), $Ni_2(TPG)_4$ (**17**), and $[Ni_2(TPG)_4]BF_4$ (**17**-BF_4). Comparisons will also be made with other known Ni_2 paddlewheel complexes with N-donor ligands: $Ni_2(DPhF)_4$, [129] **18**; $Ni_2(Ph_2N_3)_4$,[67] **19**; $Ni_2(DTolF)_4$,[51*b*] **20**; $Ni_2(DCl_2PhF)_4$,[130] $Ni_2(MyBz)_4$,[131] and $Ni_2(hpp)_4$.[132] The ligands employed are shown in Scheme 12, and the abbreviation MyBz refers to *N*-myrtanylbenzamidinate.

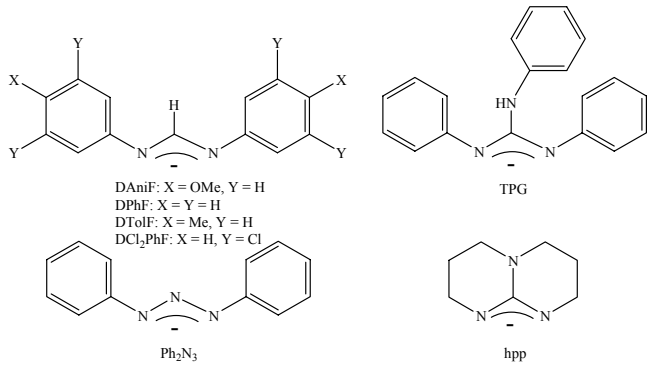

Scheme 12

EXPERIMENTAL SECTION

General Comments. Unless specified otherwise, all manipulations were carried out under an atmosphere of dry nitrogen gas using standard Schlenk techniques. All solvents were either distilled over appropriate drying agents in a nitrogen atmosphere or purified by means of a Glass Contour solvent system. *N,N′,N″*-triphenylguanidine (HTPG) was purchased from TCI and used as received. Nickel acetate was synthesized by dissolving Ni powder in glacial acetic acid followed by crystallization. The dinuclear complex $Ni_2(DAniF)_4$ (2) was synthesized according to the method of Ren.[130]

Physical Measurements. The IR spectra were taken on a Perkin-Elmer 16PC FTIR spectrometer using KBr pellets. Cyclic voltammograms were taken on a CH Instruments electrochemical analyzer using dichloromethane solutions with 1 M NBu_4PF_6 and 0.1 mM analyte. The electrodes were: Pt disk (working), Pt wire (auxiliary), and Ag/AgCl (reference). The redox couple for ferrocene/ferrocenium consistently appeared at +450 mV under these conditions. Spectroelectrochemistry was performed at –25 °C using an EG&G potentiostat/galvanostat with 0.1 M NBu_4PF_6 with a Pt net working electrode, a Pt net auxiliary electrode, and an $Ag/AgNO_3$ reference electrode or alternatively in a thermostated optically transparent thin layer electrode (OTTLE) cell with CaF_2 windows. During coulometry, electronic spectra were monitored using an HP 8453 spectrophotometer (range: 190 – 1100 nm). Elemental analyses were carried out by Canadian Microanalytical Services in British Columbia, Canada. Samples were vacuum dried prior to elemental analyses in order to remove the

interstitial solvent molecules of the crystals. Samples of **16**-BF4 and **17**-BF4 sent for elemental analysis did not analyze well. We believe this is due to their thermal instability, and that the samples decomposed during shipment. Magnetic susceptibility measurements were made on a Johnson Matthey Magnetic Susceptibility Balance Mark II. ^{1}H NMR spectra were obtained on a VXR-300 NMR spectrometer. Mass spectrometry data (electrospray ionization) were recorded at the Laboratory for Biological Mass Spectrometry at Texas A&M University, using an MDS Series Qstar Pulsar with a spray voltage of 5 keV. Visible spectra were obtained on either a Shimadzu UV-2501 PC UV-vis spectrophotometer or a Cary 17D spectrophotometer.

Synthesis of $[Ni_2(DAniF)_4]BF_4$, 16-BF_4. To a mixture of $Ni_2(DAniF)_4$ (200 mg, 0.176 mmol) and $AgBF_4$ (38 mg, 0.19 mmol) was added 20 mL of dichloromethane. The resulting black mixture was stirred for 1.5 h, and then filtered through Celite. The black solution was cooled to 0 °C and layered with cold hexanes. Crystals of $[Ni_2(DAniF)_4]BF_4 \cdot 2CH_2Cl_2$ grew within a week. Yield: 136 mg, 63%. IR (KBr, cm^{-1}): 3301 w, 1688 m, 1604 m, 1500 s, 1460 w, 1343 w, 1293 m, 1252 s, 1183 w, 1083 m, 1026 s, 830 m, 585 w, 523 w. μ_{eff} (298 K) = 1.88 μ_B.

Synthesis of $Ni_2(TPG)_4$, 17. A flask was charged with $Ni(OAc)_2 \cdot 4H_2O$ (130 mg, 0.522 mmol) and 1.50 g (5.22 mmol) of HTPG. The solids were mixed at room temperature and then heated to 120 °C for 1 h while the flask was open to air. The mixture became brown. The residues were then cooled to room temperature and dichloromethane was used to extract the product. The extracts were concentrated, and chromatographed on silica gel using dichloromethane as the eluent. The brown band which was the first to clear the column contained the product, and no other bands were

collected. The crude product was then recrystallized several times in a mixture of CH_2Cl_2/hexanes producing brown crystals. Yield: 118 mg, 50%. X-ray quality crystals were grown by slow evaporation of a $CDCl_3$ solution of **17** in an NMR tube (after an NMR spectrum had been taken). Anal. Calcd. for $C_{76}H_{64}N_{12}Ni_2$: C 72.30, H 5.07, N 13.32%. Found: C 72.11, H 4.88, N 12.94%. ^{1}H NMR ($CDCl_3$, 300 MHz, δ, ppm): 4.862 (s), 5.921 (d, J = 8.1 Hz), 6.485 (m), 6.572 (m), 6.695 (br s), 6.856 (br s), 6.978 (m), 7.441 (br s), 7.924 (br s). ESI + mass spectrum (m/z, amu): 1262, M^+. IR (KBr, cm^{-1}): 3402 w, 3055 w, 1604 m, 1560 vs, 1525 w, 1475 s, 1421 s, 1374 m, 1302 w, 1264 m, 1210 w, 1176 w, 1073 w, 1027 w, 926 w, 837 w, 777 w, 749 m, 730 w, 693 m, 521 w, 485 w, 451 w. UV-vis, CH_2Cl_2 solution (λ_{max}, ε): 496, 5×10^3; 393, 8×10^3; 272, 2×10^5.

Synthesis of $[Ni_2(TPG)_4]BF_4$, 17-BF_4. To a solution of $Ni_2(TPG)_4$ (200 mg, 0.223 mmol) in 30 mL of Et_2O was added an Et_2O solution of $AgBF_4$ (43 mg, 0.22 mmol). A brown precipitate formed immediately. The mixture was filtered and the brown solid was then treated with CH_2Cl_2 to give a black slurry. This was filtered through Celite to give a clear black solution, which was cooled to 0 °C, layered with cold hexanes, and kept in the freezer.

Crystals grew within a week. Yield: 120 mg, 56%. IR (KBr, cm^{-1}): 3398 m, 3057 m, 1638 m, 1600 s, 1560 vs, 1482 vs, 1424 vs, 1375 m, 1304 m, 1265 m, 1208 w, 1175 w, 1061 m, 1056 m, 1023 m, 926 w, 833 w, 778 w, 752 s, 693 s, 515 w, 448 w. μ_{eff} (298 K) = 1.95 μ_B.

X-Ray Crystallography

Suitable crystals of **16**-$BF_4 \cdot 2CH_2Cl_2$, **17**$\cdot 4CDCl_3$ and **17**-$BF_4 \cdot 2CH_2Cl_2$ were mounted and centered in the goniometer of a Bruker SMART 1000 CCD area detector diffractometer and cooled to –60 °C. Geometric and intensity data were collected using SMART software.[29] The data were processed using SAINT software,[30] and corrections for absorption were applied using the program SADABS.[31] A suitable crystal of $1 \cdot 1.5CH_2Cl_2$ was mounted and centered on the goniometer of a Nonius FAST area detector system. Data were collected using the program MADNES and processed using the program PROCOR.[27] An absorption correction was applied using the program SORTAV.[28] All structures were solved and refined using the SHELXTL program package.[32] Crystal data are shown in Table 11, and Table 12 lists pertinent bond distances and angles.

Table 11 Crystal data for **16**-BF_4·$2CH_2Cl_2$, **17**·$4CDCl_3$ and **17**-BF_4·$2CH_2Cl_2$

	16-BF_4·$2CH_2Cl_2$	**17**·$4CDCl_3$	**17**-BF_4·$2CH_2Cl_2$
formula	$C_{62}H_{64}BCl_4F_4N_8Ni_2O_8$	$C_{80}H_{64}Cl_{12}D_4N_{12}Ni_2$	$C_{78}H_{68}BCl_4F_4N_{12}Ni_2$
fw	1395.24	1744.31	1519.47
cryst syst	Triclinic	Monoclinic	Orthorhombic
space group	*P*-1 (№ 2)	*P*2/n (№ 14)	*Aba*2 (№ 41)
a (Å)	13.1601(8)	17.715(1)	17.592(1)
b (Å)	13.7494(9)	11.818(7)	18.815(2)
c (Å)	18.450(1)	18.648(1)	21.662(2)
α (deg)	99.574(1)	90	90
β (deg)	93.743(1)	90.039(1)	90
γ (deg)	92.096(1)	90	90
V (Å^3)	3281.2(4)	3904.2(4)	7170.0(1)
Z	2	2	4
d (calcd) (g cm^{-3})	1.412	1.484	1.408
R1,[a] wR2[b] (*I* > 2σ(*I*))	0.0433, 0.1205	0.0390, 0.1047	0.0539, 0.1452
R1,[a] wR2[b] (all data)	0.0506, 0.1255	0.0477, 0.1133	0.0705, 0.1589

[a] $R1 = \sum F_o - |F_c| / \sum |F_o|$. [b] $wR2 = [\sum[w(F_o^2 - F_c^2)^2] / \sum[w(F_o^2)^2]]^{1/2}$ and $w = 1/[\sigma^2(F_o^2) + (aP)^2 + bP]$, where $P = [\max(0 \text{ or } F_o^2) + 2(F_c^2)]/3$.

Table 12 Selected interatomic distances and angles for **16**·$1.5CH_2Cl_2$, **16-**BF_4·$2CH_2Cl_2$, **17**·$4CDCl_3$, and **17-**BF_4·$2CH_2Cl_2$[a]

Compound	**16**·$1.5CH_2Cl_2$	**16-BF_4**·$2CH_2Cl_2$	**17**·$4CDCl_3$	**17-BF_4**·$2CH_2Cl_2$
Ni–Ni	2.476(1)	2.3703(4)	2.4280(5)	2.3298(6)
Ni–N	1.910[6]	1.909[2]	1.929[2]	1.921[2]
Ni–Ni–N	86.9[2]	88.46[6]	87.09[5]	88.90[5]
N–Ni–Ni–N torsion	15.6	14.1	19.9	15.7

[a] Distances are given in Å, angles in °. Numbers in brackets correspond to average values.

Density Functional Calculations. DFT[88] calculations were performed with the hybrid Becke 3-parameter exchange functional[89] and the Lee-Yang-Parr non-local correlation functional[90] (B3LYP) implemented in the Gaussian 03 (Revision C.02) program suite.[91] For feasibility, the dinickel formamidinate molecules were represented by a model in which the aryl groups of the formamidinate ligands were replaced by hydrogen atoms, namely $Ni_2(HNCHNH)_4$. Double-ζ basis sets were used for the geometry optimization calculations of the neutral, singly oxidized, doubly oxidized, and excited state models of $Ni_2(HNCHNH)_4$, and triple-ζ basis sets were used in the neutral and singly-oxidized models as described in the discussion section. The double-ζ calculations consisted of the correlation-consistent polarized (cc-pVDZ)[92] valence basis set applied to the non-metal atoms (carbon, nitrogen, and hydrogen), and an effective core potential (ECP) representing the 1s2s2p core was used for the nickel atoms along with the associated double-ζ basis set (LANL2DZ).[93] The triple-ζ calculations utilized the correlation consistent polarized (cc-pVTZ)[92] basis set for non-metal atoms and an EPC representing the 1s2s2p core along with the corresponding Stuttgart triple-ζ basis set[94] for nickel. For the all-atom single-point calculation of the $Ni_2(DAniF)_4$ molecule, the positions of all the non-hydrogen atoms were obtained from the crystal structure geometry. The hydrogen atoms were placed at positions calculated with the universal force field[133] (UFF) as implemented in the program Cerius.[134] Time-dependent DFT calculations[135] were performed by calculating the seven lowest excited states in all the neutral and singly-oxidized calculations, and the ground state of the doubly oxidized calculations, in order to predict their electronic spectra. The self-consistent-field cycle convergence criterion on all calculations was increased from the default value to 10^{-8}.

All calculations were run on an Origin 3800 64-processor SGI computer located at the Texas A&M Supercomputing facility.

RESULTS AND DISCUSSION

Synthesis. The Ni_2^{4+} complex **16** was synthesized as previously reported,[130] while the guanidinato complex **17** was synthesized in good yields via a new route by reaction of $Ni(OAc)_2$ and molten HTPG at high temperature in a process that also liberates acetic acid, eq 1. Because **17** is stable to air, it is straightforwardly purified by column chromatography.

$$2Ni(OAc)_2 + 4HTPG \rightarrow Ni_2(TPG)_4 + 4HOAc \quad (1)$$

Oxidation of **16** and **17** to their respective monocations (**16**-BF_4 and **17**-BF_4) is easily accomplished by the oxidant $AgBF_4$, according to eq 2. The silver metal byproduct was observed as a mirror which coated the bottom of the flask. For the oxidation of **17**, a brown precipitate was observed upon addition of $AgBF_4$ to an ether solution of **17**. However, it was not until this brown solid was dissolved in CH_2Cl_2 that silver metal precipitated from the reaction mixture. The brown intermediate is probably a silver complex in which the Ag^+ ions are coordinated by the free amine *N* atoms of the triphenylguanidinate ligand (eq 3). A similar silver intermediate has been reported in the process of oxidizing 1,1'-diacetylferrocene to the corresponding ferrocenium salt.[136]

$$Ni_2(DAniF)_4 + AgBF_4 \rightarrow [(Ni_2(DAniF)_4]BF_4 + Ag^0 \quad (2)$$

$$Ni_2(TPG)_4 + AgBF_4 \rightarrow \text{“}[AgNi_2(TPG)_4]BF_4\text{”} \rightarrow [Ni_2(TPG)_4]BF_4 + Ag^0 \quad (3)$$

It should be noted that solutions of **16**-BF_4 and **17**-BF_4 are not stable at room temperature and these compounds were crystallized at low temperatures. Oxidation of two additional dinickel complexes was also attempted during this work. The compounds $Ni_2(DPhF)_4$ (**18**) and $Ni_2(Ph_2N_3)_4$ (**19**) (DPhF = *N*,*N*′-diphenylformamidinate, and Ph_2N_3 = 1,3-diphenyltriazinate) both show reversible oxidation waves in their cyclic voltammograms at scan speeds of 100 mV sec^{-1}, but the oxidized species which were generated either by Ag^+ or nitrosonium oxidation at –78 °C were too short lived to be isolated. Nevertheless, since the crystal structures of **18** and **19** have been reported,[129, 67] it is useful to include them in our discussion, as well as $Ni_2(DTolF)_4$ (**20**, DTolF = *N*,*N*′-di-*p*-tolylformamidinate), and the corresponding oxidized species (**20**-BF_4) which is also known.[51*b*] The compounds $Ni_2(DCl_2PhF)_4$,[130] and $Ni_2(hpp)_4$[132] have also been structurally characterized, though a reproducible synthetic procedure of the latter is not yet available.

Crystal Structures. The neutral Ni_2^{4+} complexes **16** and **17** crystallize as the halocarbon solvates **16**·1.5CH_2Cl_2 and **17**·4$CDCl_3$ (the latter having been crystallized after an NMR experiment), and both complexes show the typical lantern-type structure with the two nickel atoms being four coordinate (essentially square planar) and held together face-to-face by the four bridging ligands (see Fig. 19 and Fig. 20). Geometrical parameters for the complexes are given in Table 11. Molecules of **16** reside on a crystallographic inversion center in the space group *Pccn* and **17** contains a crystallographic two-fold axis normal to the Ni···Ni vector in the space group *P*2/*n*. The Ni−N bond distances of 1.910[6] Å and 1.929[2] Å for **16** and **17**, respectively, are comparable to those in similar dinickel compounds,[51*b*, 128, 67, 130] and the two nonbonded

Ni atoms are held together at distances of 2.476(1) Å in **16** and 2.4280(5) in **17**, and both are within the range of distances observed in other Ni_2^{4+} complexes. [51*b*, 128, 67, 130]

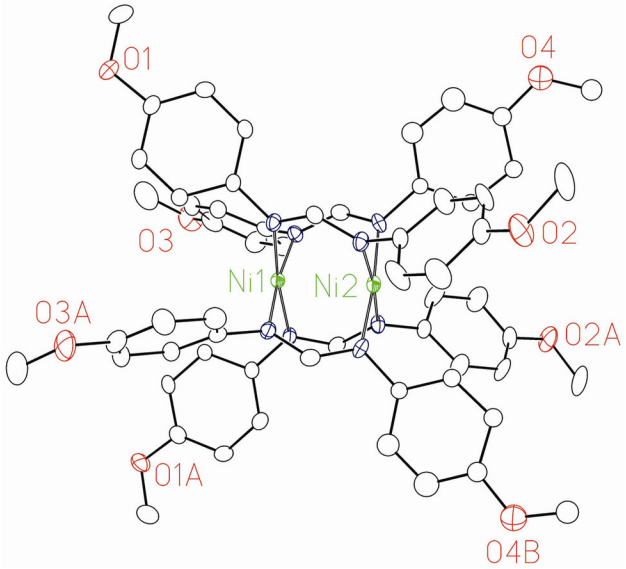

Fig. 19 The molecule of **16** from **16**·1.3CH_2Cl_2 with displacement ellipsoids drawn at the 30% probability level and hydrogen atoms removed.

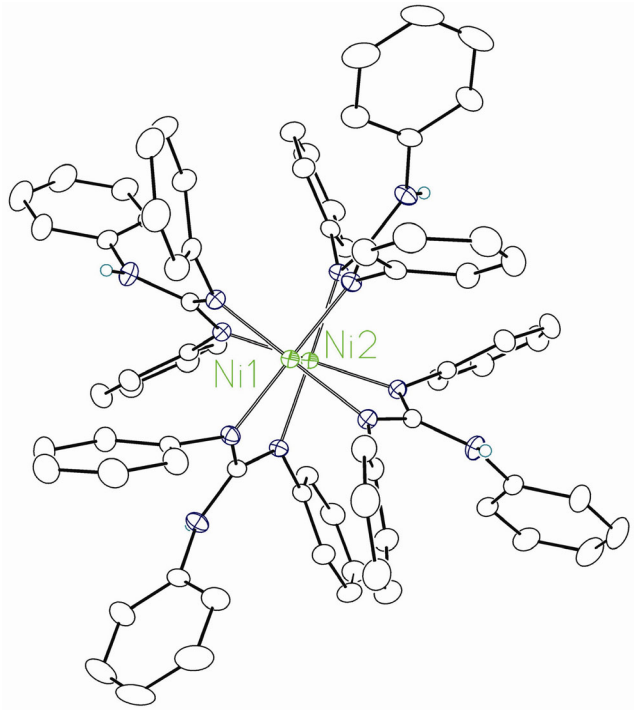

Fig. 20 The molecule of **17** from **17**·4$CDCl_3$ with displacement ellipsoids drawn at the 30% probability level. Hydrogen atoms have removed, except for the amino hydrogen atoms.

The Ni atoms lie away from the center of the molecule and out of the square planes formed by the nitrogen atoms of the coordinated ligands by 0.103 Å and 0.098 Å in **16** and **17**, respectively, indicating a repulsive interaction between the nickel ions. This is in contrast to the dichromium tetraformamidinates[137] and -tetraguanidinates,[138] in which a supershort Cr−Cr quadruple bond is formed. In these Cr_2^{4+} species the two Cr atoms are also pulled out of the N_4 plane of the coordinated ligands, but towards the centers of the molecules. This results in obtuse Cr−Cr−N angles of ~ 95° in dichromium tetraguanidinates[138] and tetraformamidinates,[137] whereas the Ni···Ni−N angles are acute (86.9[2]° and 87.09[5]° in **16** and **17**, respectively). Another important difference between the dinickel complexes **16** and **17** and their dichromium, dimolybdenum, or ditungsten analogues is that there is a significant twisting of the ligands resulting in large torsion angles (N−Ni···Ni−N) of 15.6° in **16** and 19.9° in **17**. Quadruply bonded Cr_2^{4+}, Mo_2^{4+}, and W_2^{4+} species do not have large torsion angles due to the stabilizing effect of the δ bond which is highly sensitive to the torsion angle.[139]

The main features of the cationic species in the one electron oxidized complexes **16**-BF_4·$2CH_2Cl_2$ and **17**-BF_4·$2CH_2Cl_2$ (Fig. 21 and Fig. 22) are similar to those in the neutral complexes in that the lantern-type dinickel core is retained. Similar to $[Ni_2(DTolF)_4]BF_4$,[51b] the Ni−Ni distances in the oxidized complexes **16**-BF_4 and **17**-BF_4 of 2.3703(4) Å and 2.3298(6) Å, respectively, are significantly shorter than the Ni···Ni distances in the neutral species.[140] These changes are consistent with the removal of an electron from a Ni−Ni antibonding orbital, as will be described in more detail below. Interestingly, the shortening of the Ni−Ni distances upon oxidation (which we shall call Δd_{Ni-Ni}) for **16**/**16**$^+$ and **17**/**17**$^+$ (0.106(1) Å and 0.0982(6) Å, respectively) are significantly larger than Δd_{Ni-Ni} for **20**/**20**$^+$ (0.069(4) Å).[51b] Other changes in the structures upon oxidation are to be noted: The Ni−N distances of 1.909[2] Å in **16**-BF_4 are statistically the same as those of 1.910[6] Å found in **16**. In contrast, the Ni−N distances in **17**-BF_4 of 1.921[2] Å are shorter than those of 1.929[2] Å in **17** by 0.008 Å, which is just above $3\sigma = 0.006$ Å and therefore significant. A decrease in M−N distances is expected if the dimetal core is oxidized since the charge of the dinuclear unit changes from 4+ to 5+, although these changes are often difficult to observe since the extra charge is spread over two metal atoms. As in their neutral counterparts, there are large torsion angles of 14.1° and 15.7° in **16**-BF_4 and **17**-BF_4, respectively. Table 12 summarizes the bond distances and angles for **16**, **17**, **16**-BF_4, and **17**-BF_4.

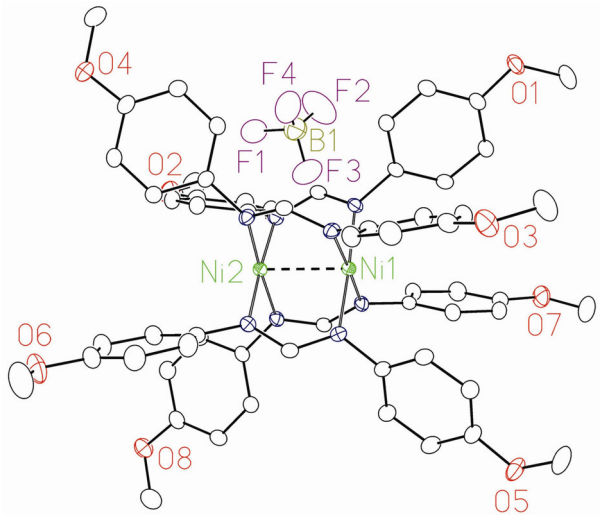

Fig. 21 Thermal ellipsoid plot of **16**-BF_4 from **16**-$BF_4 \cdot 2CH_2Cl_2$ with ellipsoids drawn at the 30% probability level and hydrogen atoms removed.

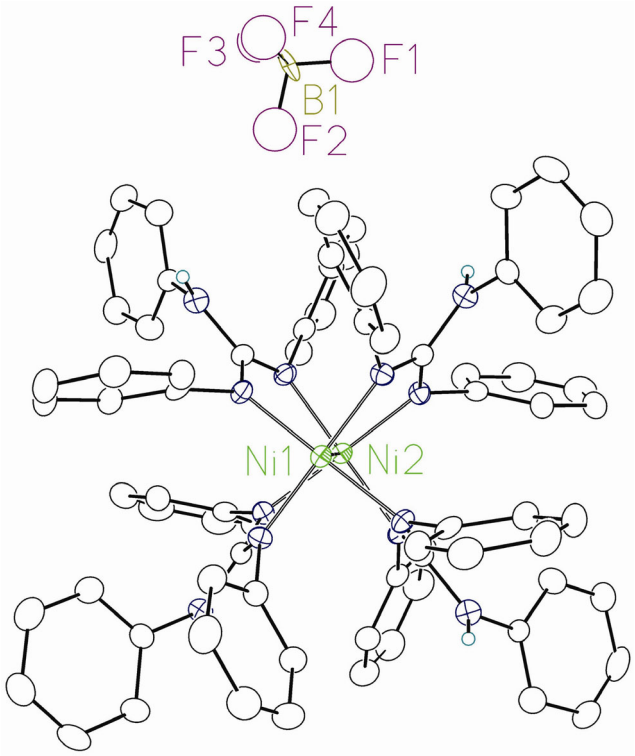

Fig. 22 Thermal ellipsoid plot of **17**-BF_4 from **17**-BF_4·1.25CH_2Cl_2 with ellipsoids drawn at the 30% probability level and only amino hydrogen atoms shown.

Electrochemistry. There have been few reports of electrochemical data for lantern-type Ni_2^{4+} compounds with N-donor ligands. In the initial investigation of **20**,[51b] a reversible one-electron oxidation wave was seen at 0.24 V (all potentials in this paper are reported vs ferrocene/ferrocenium). An irreversible wave at ca. 0.75 V was also noted. A more thorough electrochemical study of nine Ni_2(formamidinate)$_4$ compounds by Ren et al.[130] showed that the first oxidation potentials of these compounds are very sensitive to the nature of the ligands and that there is a strong correlation of the $E_{½}$ with the Hammet constant of the substituent in the diarylformamidinate ligands. The $E_{½}$ values changed from 0.207 V for the electron donating *p*-anisyl derivative, compound **16**, to 0.867 V for the electron withdrawing *m*-$CF_3C_6H_4$ derivative. For two compounds with ligands with even more electron withdrawing capacity than the *m*-CF_3 derivative, namely, the *p*-CF_3 and the 3,5-Cl_2 derivatives, irreversible oxidation processes were observed. In no case, was there a mention of any additional redox processes.

A reinvestigation of the redox behavior of **16** yielded a pleasant surprise. The cyclic voltammogram (shown in Fig. 23) shows not one but *four* waves with the characteristic profiles shown by reversible waves. The first wave at +0.205 V can be assigned to the $Ni_2^{4+/5+}$ process and it is in essentially the same position as reported by Ren.[130] The additional waves at +0.528 V, +0.680 V, and +0.842 V must correspond to further oxidation processes not documented before.

Compound **17** shows a more typical behavior in that its cyclic voltammogram consists of a single reversible oxidation wave at 0.084 V.

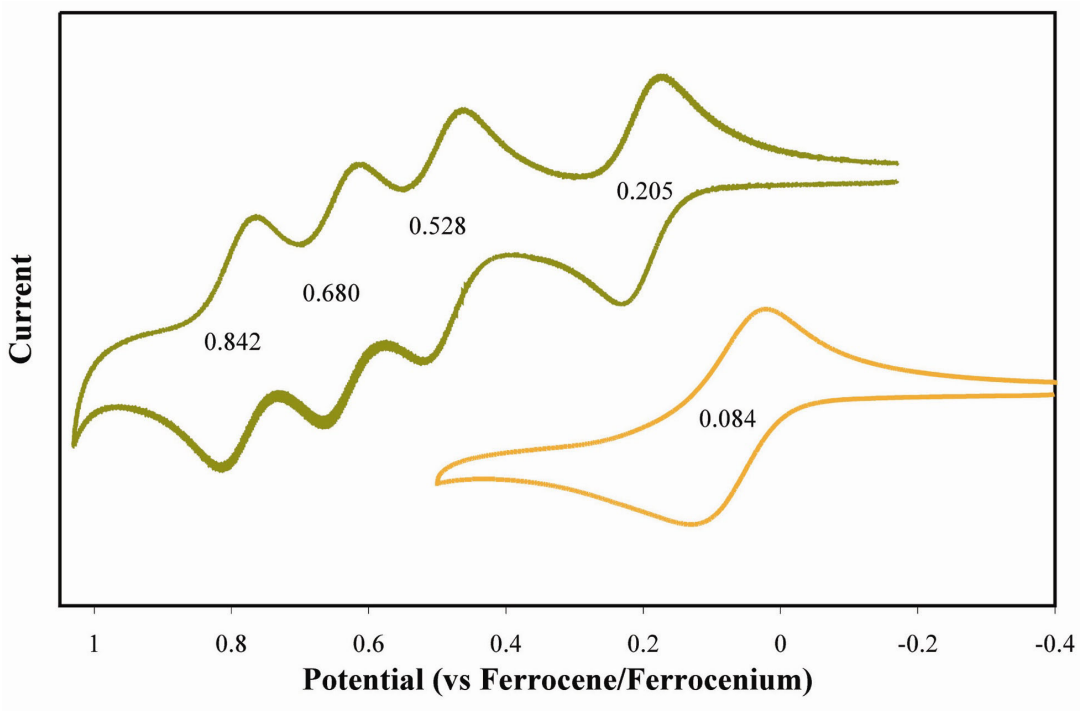

Fig. 23 Cyclic voltammograms of **16** and **17** at a scan rate of 100 mV/s. $E_{1/2}$ values are given near the appropriate wave

However, this oxidation process is significantly more accessible than the corresponding $Ni_2^{4+/5+}$ couple in **16**. This is in agreement with the known ability of guanidinate ligands to stabilize dimetal complexes in higher than usual oxidation states.[141, 142] But whereas the dimolybdenum complex of triphenylguanidinate can be oxidized twice (first from Mo_2^{4+} to Mo_2^{5+} and then to Mo_2^{6+}),[142] there is no evidence for a second reversible oxidation in the dinickel complex **17**.

The first oxidation potentials of all of the known structurally characterized Ni_2^{4+} complexes, along with selected structural information, are given in Table 13. Because no electrochemical data had been reported for the triazinato complex **19**, its cyclic voltammogram was measured and it showed an oxidation process at 0.653 V. It is interesting to note that this potential is about 0.23 V higher than that of the formamidate analog (0.423 V). Even though **19** exhibits one of the shortest non-bonded Ni···Ni distances known (2.395(3) Å) chemical oxidation did not provide any isolable product, possibly because of high reactivity of the oxidized product.

Table 13 Structural and Electrochemical Information for Structurally Characterized Ni_2^{n+} (n = 4 and 5) Complexes.

Compound	$E_{1/2}$, V vs Fc/Fc^+	Ni_2^{4+} Ni···Ni, Å	Ni_2^{5+} Ni–Ni, Å	Δd_{Ni-Ni}, Å	Ref.
$Ni_2(Ph_2N_3)_4$	0.653	2.395(3)	—	—	67, this work
$Ni_2(DCl_2PhF)_4$	—[a]	2.462(1)	—	—	69
$Ni_2(DPhF)_4$	0.423	2.490(3)	—	—	129, 69
$Ni_2(DTolF)_4$	0.279	2.487[3]	2.418(4)	0.069(4)	51*b*
$Ni_2(DAniF)_4$	0.207	2.476(1)	2.3703(4)	0.106(1)	69, this work
$Ni_2(MyBz)_4$	—	2.448(1)	—	—	131
$Ni_2(TPG)_4$	0.084	2.4280(5)	2.3298(6)	0.0982(6)	this work
$Ni_2(hpp)_4$	—	2.3764(9)	—	—	132

[a] Irreversible oxidation

Electronic and EPR Spectroscopy. Spectroelectrochemistry is an excellent method for studying metal-metal bonded complexes in various oxidation states,[143] thereby enabling a wealth of knowledge about the electronic structure of such species to be obtained because electronic spectra can be monitored during electrochemical oxidation or reduction. This technique was used to study the multiple redox processes (vide supra) in **16**. Only the first and second oxidation products (i.e., $\mathbf{16}^{+}$ and $\mathbf{16}^{2+}$) were stable enough in CH_2Cl_2 solution at –25 °C for their electronic spectra to be recorded (Fig. 24). Attempts to generate the triply oxidized species showed non-isosbestic behavior in the monitored electronic spectra due to rapid decomposition of the species being generated.

The greenish-brown compound **16** shows three absorption maxima at 635, 485, and 400 nm in its electronic spectrum in the visible region. These all have molar absorptivities (ε) lower than 5000 M^{-1} cm^{-1}, though oxidation to $\mathbf{16}^{+}$ produces a black solution which shows maxima at 887, 690, and 500 nm all of which have ε values larger than 5000 M^{-1} cm^{-1}, similar to the result reported for oxidation of **20**.[51*b*] The most startling result, however, appears in the absorption spectrum of the doubly oxidized species, $\mathbf{16}^{2+}$, where a very intense band (ε ~ 30,000 M^{-1} cm^{-1}) in the near-IR is observed at 960 nm, as well as an intense transition at 415 nm (ε ~ 22,000 M^{-1} cm^{-1}). Thus, upon oxidation there is an increase in intensity of the absorption spectrum as well as a bathochromic shift of the lowest energy bands. Because of the intensity of the bands in the electronic spectrum of $\mathbf{16}^{2+}$, it is reasonable to assign them to charge transfer transitions.

The electronic spectra of **17** and **17**-BF_4 were also measured in CH_2Cl_2 solution (Fig. 25).

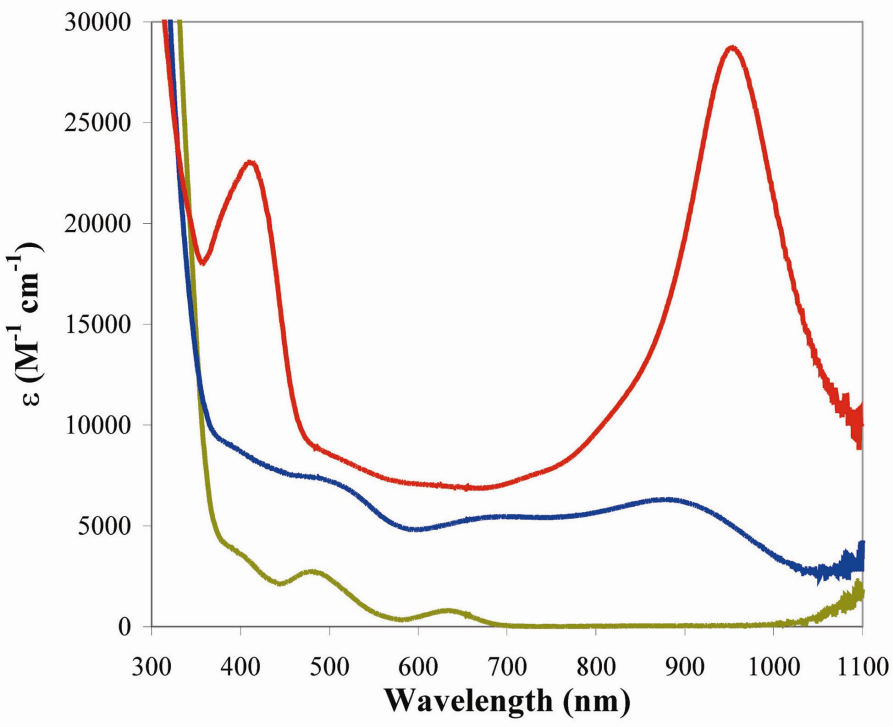

Fig. 24 Electronic spectra of **16** (lower trace), **16**-BF_4 (middle trace), and the Ni_2^{6+} species in CH_2Cl_2 solution at –25 °C. The latter two species were generated electrochemically.

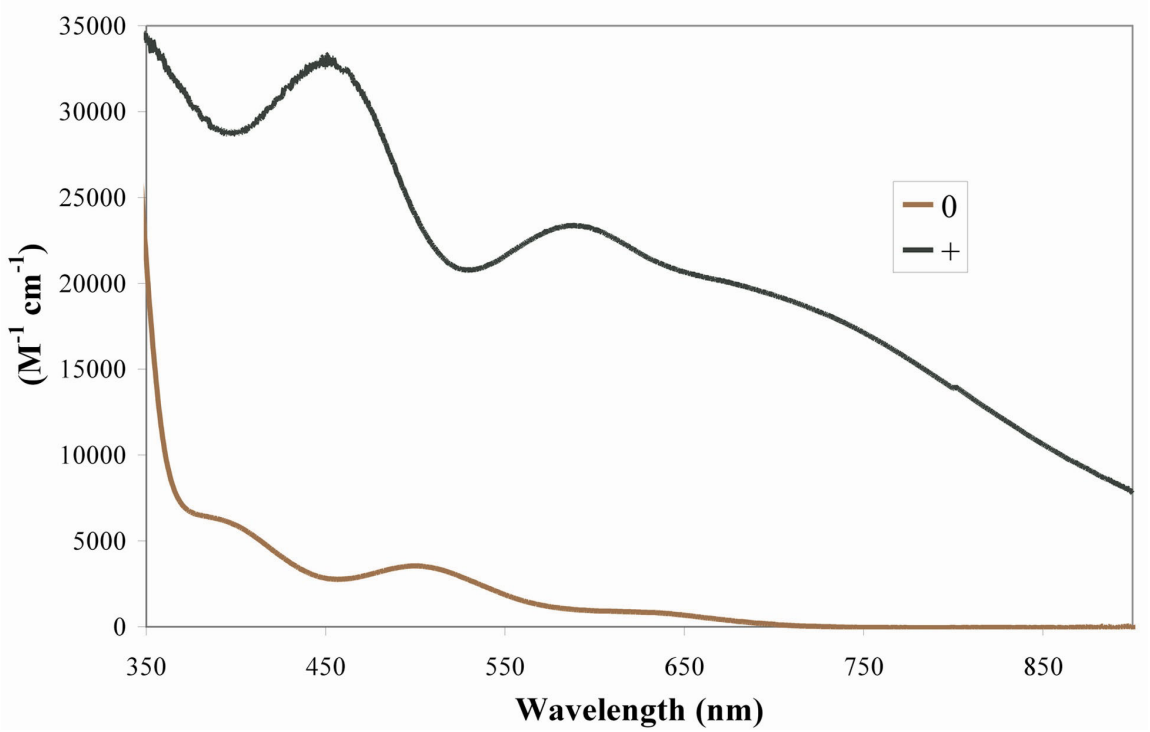

Fig. 25 UV-Visible spectra of **17** (upper trace) and **17**-BF_4 (lower trace) in CH_2Cl_2 solution.

While **17** is brown and exhibits maxima at 496 and 393 nm (both with ε ~ 5000 M^{-1} cm^{-1}), **17**-BF_4 is greenish-black and shows very intense bands at 711, 587, and 453 nm, all having ε values above 10,000 M^{-1} cm^{-1}, which identifies them as charge transfer transitions. Interestingly, the electronic spectrum of **17**-BF_4 is quite different from the spectrum of the corresponding formamidinato complex, **16**-BF_4. This difference is probably caused by the much higher basicity[144] of the guanidinate ligands relative to the formamidate ligands.

The EPR spectrum of **16**-BF_4 at 10 K, shown in Fig. 26, has two components. The $g\perp$ component appears at 2.234 and the g_{II} component at 2.045. The latter is partly overlapped by a somewhat broad, structureless signal at about g = 2.0 which may be due to contamination by an organic radical whose signal is broadened by interaction with a metal atom. The nature of this spectrum clearly establishes the presence of one unpaired electron on a Ni_2^{5+} core with, of course, partial delocalization into ligand orbitals. The triplet structure on the g_{II} signal was simulated using a molecule with an axially coordinated nitrogen atom of an acetonitrile molecule which is almost certainly carried over from the electrochemistry work that was performed in CH_3CN. The spectrum of **16**-BF_4 is similar to that of **20**-BF_4 where g values are $g\perp$ = 2.210 and g_{II} = 2.038.[51b] The isotropic g value obtained at room temperature for **19**-BF_4, 2.16, is just about that expected for the average of $g\perp$ and g_{II} for **16**-BF_4: $(2 \times 2.23 + 2.04)/3 = 2.16$, which again supports the assertion that in these Ni_2^{5+} species the unpaired electron is mainly in metal-based orbitals.

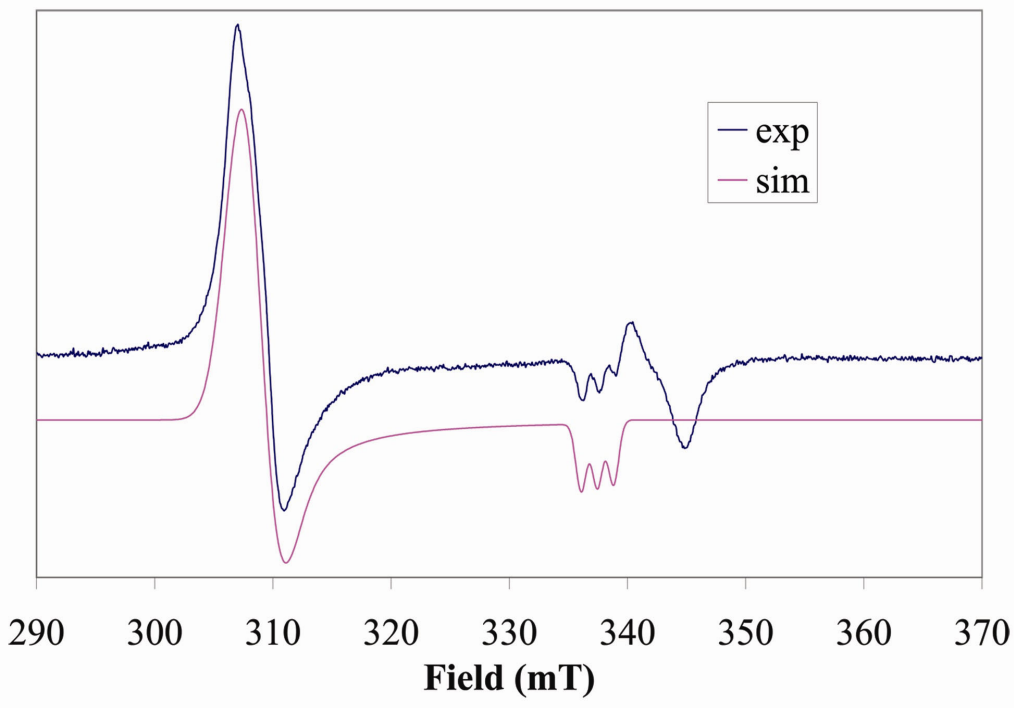

Fig. 26 X-band EPR spectrum of **16**-BF_4 in CH_2Cl_2 solution at 10 K. The upper trace corresponds to the experimental spectrum while the lower trace is a simulation for the compound with an axial acetonitrile molecule (see text). The A value is 13 gauss. The signal with a *g* value of ca. 2.00 corresponds to an impurity.

Molecular Orbital Considerations. To better understand the quantitative calculations presented below, we must first make a qualitative survey of the molecular orbitals (MOs) involved. Those of the nickel atoms have already been presented in Scheme 1. It should be noted that the $d_x2_{-y}2$ orbitals interact strongly with the σ orbitals of the ligands and they are not used in metal−metal bonding. Since ligand π orbitals may interact with the dimetal unit, they must also be considered in order to obtain an overall MO picture as they are bound to cause changes in the total MO diagram. The atoms of the N−C−N bridge form a π system which can be described in terms of N−C−N bonding, nonbonding, and antibonding interactions as shown in Scheme 13.

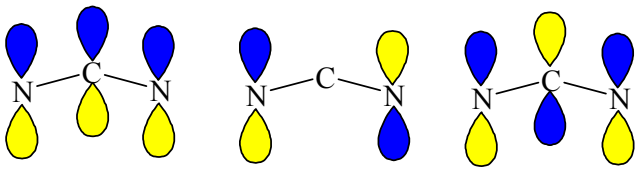

Scheme 13

Since the $[N−C−N]^-$ formamidinate unit is a 4 π electron system, the antibonding combination on each ligand will be empty. These empty orbitals are presumably sufficiently high in energy that they can be disregarded. The filled bonding and nonbonding combinations, however, may fall within the energy range of the Ni_2 *d* manifold and interactions between combinations of these orbitals and the Ni_2 *d* orbitals should be considered. To do this, a model $Ni_2(ligand)_4$ molecule of full D_{4h} symmetry in the coordinate system shown in Scheme 14 will be used. In this coordinate system, the ligand π bonding orbitals form combinations of a_{2g}, b_{2g}, and e_u symmetry and the nonbonding orbitals form combinations of a_{1u}, b_{1u}, and e_g symmetry.

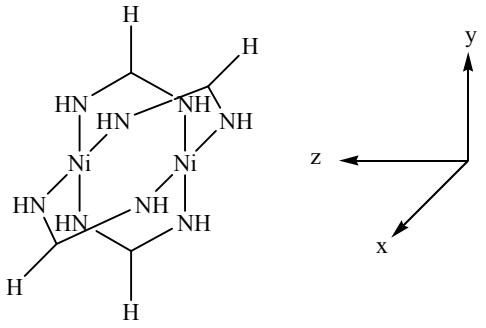

Scheme 14

The orbitals of the *d* manifold (Scheme 1) have the following symmetries in this coordinate system: σ, a_{1g}; π, e_u; δ, b_{2g}; δ*, b_{1u}; π*, e_g; and σ*, a_{2u}. It can be envisioned that some of the metal-based orbitals may have significant interactions governed by symmetry with the π system of the coordinated formamidinate ligands. Such interactions may change the relative energies of the metal-based orbitals. When the symmetry is lowered from D_{4h} to D_4 (which results from non-zero torsion angles) the interactions will remain similar but the symmetry labels lose their *gerade* and *ungerade* subscripts.

Changes in the relative energies of the orbitals may also have important consequences for the electronic configuration of the oxidized species. Such variations in relative energy of the various orbitals may even generate oxidized species in which the oxidation is either metal-based or ligand-based. To differentiate between a ligand-based and a metal-based oxidation, DFT calculations were carried out. The theoretical results are compared to the experimental data below.

DFT Calculations. The first calculations were done on a simplified model of the neutral molecule, $Ni_2(HNCHNH)_4$. This model was used for both geometry and energy calculations at the B3LYP level using basis sets of double- and triple-ζ quality (see Experimental Section). In each case the initial geometry was taken from the crystal structure coordinates, and the final geometry converged to a structure with D_{4h} symmetry. The calculated geometrical parameters are given in Table 14. The calculated Ni–N bond distances (1.930 Å from double-ζ, 1.922 Å from triple-ζ) reproduce very well the average value from the crystal structure of **16** (1.910[6]). However, the calculated Ni···Ni distances (2.569 Å from double-ζ and 2.547 Å from triple-ζ) are 0.07–0.09 Å longer than the experimental value (2.476(1) Å), in what appears to be a systematic overestimation.

Table 14 Calculated geometries using the model $[Ni_2(HNCHNH)_4]^{0/+/2+}$

	Ni_2^{4+}		Ni_2^{5+}			Ni_2^{6+}	
	$^1A_{1g}$ 2-ζ	$^1A_{1g}$ 3-ζ	$^2A_{1u}$ 2-ζ	$^2A_{1u}$ 3-ζ	$^2A_{2u}$ 2-ζ	$^1A_{1g}$ (ligand oxidation)	$^1A_{1g}$ (nickel oxidation)
Ni–Ni, Å	2.569	2.547	2.565	2.547	2.445	2.554	2.327
Ni–N, Å	1.930	1.922	1.912	1.905	1.913	1.901	1.907
C–N, Å	1.321	1.314	1.324	1.377	1.318	1.328	1.315
C–H, Å	1.104	1.093	1.100	1.089	1.101	1.099	1.101
N–H, Å	1.016	1.008	1.020	1.011	1.017	1.025	1.021
Relative energy (eV)	—	—	0	—	+0.30	0	+2.61

The MO diagram in Fig. 27 is based on the electronic structure calculated using the triple-ζ basis set and contains several features worth mentioning. To the left of the diagram, the orbitals of the *d* manifold (including the antibonding combination from the $d_x2_{-y}2$ used in metal−ligand σ bonding) are listed, and the ligand π orbitals are shown to the right. Interactions between these sets of orbitals produce the MOs shown in the central section of the diagram. The σ and σ^* orbitals both appear to be substantially raised in energy through antibonding interactions (shown in Fig. 27 with dotted red lines) with the σ orbitals of the bridging ligands (not shown in the picture). It is possible that these interactions may occur via overlap with the torus of the d_z2 orbitals. Strong π interactions (shown in green) also occur between the δ and δ^* orbitals of the Ni_2 manifold. The two highest occupied orbitals, a_{1u} and a_{2u} are illustrated in Fig. 28 to facilitate the discussion below.

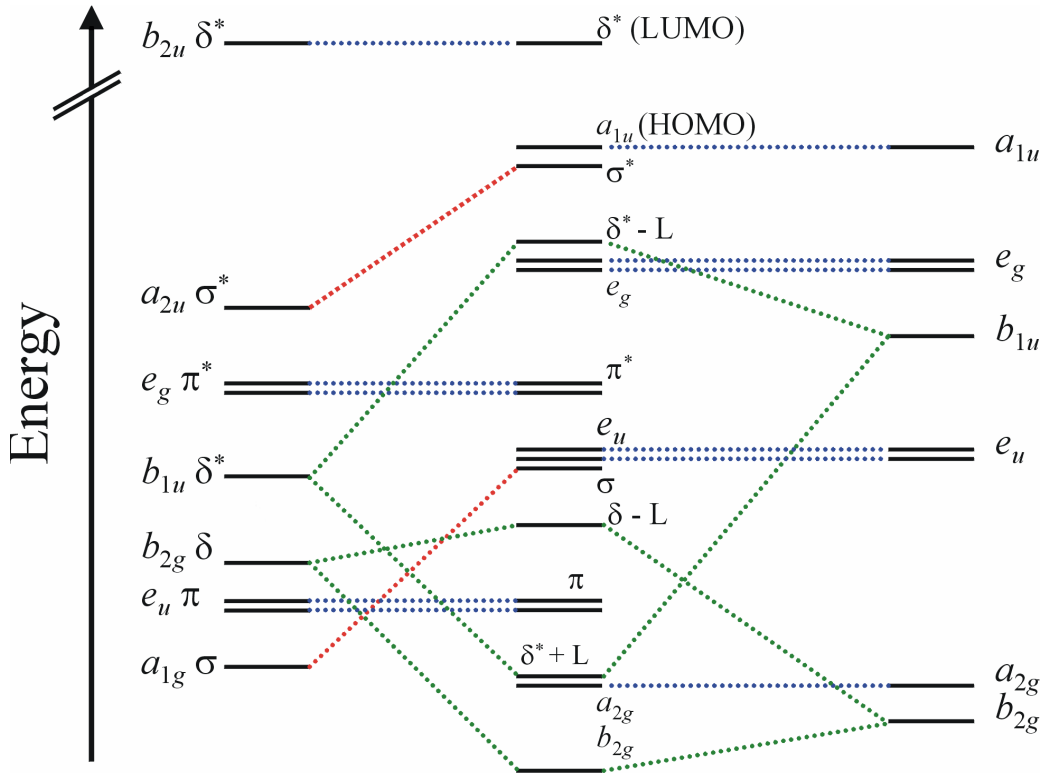

Fig. 27 Molecular orbital diagram of $Ni_2(HNCHNH)_4$ species in D_{4h} symmetry showing interactions between the Ni_2 orbitals (far left) and the filled π orbitals of the ligand (far right). In the neutral dinickel complexes, all of the orbitals are filled except the top one (LUMO). Blue dotted lines indicate no interaction, red dotted lines indicate only a σ interaction, and green dotted lines indicate the π interactions.

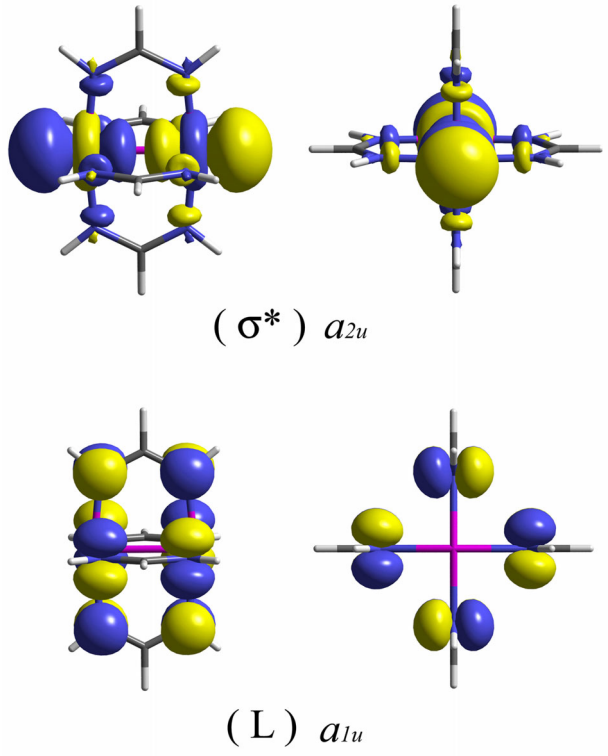

Fig. 28 Depiction of the a_{1u} ligand orbital (bottom) and a_{2u} Ni_2 σ^* orbital (top) both viewed either from the side (left) or along the Ni–Ni vector (right).

The most striking result is that the HOMO is mainly ligand based. This would seem to imply that removal of one electron from the model species should give rise to a cation having one electron missing from the π orbitals of the ligand ($^2A_{1u}$). The geometry of this doublet state using the model cation $[Ni_2(HNCHNH)_4]^+$ has also been calculated from B3LYP using double- and triple-ζ basis sets (Table 14). Importantly, the Ni···Ni and Ni–N distances are essentially the same as those calculated for the analogous neutral model (Table 14). Thus, it might seem that this simplified model does not reproduce the experimental data for **16**/**16**$^+$ where the Ni–Ni distance becomes shorter by 0.1 Å upon oxidation and where there is an EPR signal consistent with a metal-centered radical. However, the HOMO−1 of the neutral model is only 0.19 eV lower than the HOMO (for the 3- ζcalculation). This difference is within the uncertainties of the calculation. Moreover, even if the calculated order is correct, with such a small difference between the HOMO and HOMO−1, Koopmans' theorem is not to be trusted.[145]

The non-Koopmans $^2A_{2u}$ excited state, which represents the nickel-centered oxidation, was then calculated and its geometry was optimized.[146] The $^2A_{2u}$ state lies 0.3 eV (~ 2,400 cm^{-1}) in energy above the ground doublet state, but the geometry of this state reproduces remarkably well the magnitude of the shortening of the Ni–Ni distances from **16** to **16**-BF_4 (0.105 Å). The calculated Ni–Ni distance of 2.445 Å is shorter than that calculated for the neutral complex by 0.13 Å.

It is therefore natural to ask why DFT did not straightforwardly predict the correct ground state for the $[Ni_2(HNCHNH)_4]^+$ model. An obvious part of the answer is that the ligand has been oversimplified and that by using the HNCHNH model ligand the $^2A_{2u}$ state has been disfavored.[147] To test this hypothesis, a computationally expensive single

point calculation employing the entire $Ni_2(DAniF)_4$ molecule as a model was made using the geometry observed in the crystal structure.[148] The ligand based orbital (a_{1u}, shown in black) is greatly affected by both changing of the basis set from double-ζ to triple-ζ, as well as inclusion of the *p*-anisyl groups. The Ni_2 σ^* orbital, on the other hand, is only slightly raised in energy by changing the basis set from double-ζ to triple-ζ, and in the calculation of the full molecule, its energy is lowered again (since this calculation uses a double-ζ basis). The calculated HOMO/HOMO–1 energy difference becomes much smaller as a function of the basis set as well as upon inclusion of the *p*-anisyl groups into the model. Furthermore, when the anisyl groups are included, there is a crossing of the energy of these two orbitals. The σ^* orbital becomes the HOMO and the HOMO–1 is the a_{1u} ligand π orbital.[149] It should be mentioned that the very small energy difference (ΔE = 0.02 eV for the calculation of the full molecule) between the HOMO and HOMO–1 is consistent with the observation of four sequential reversible waves in the cyclic voltammogram of **16**. Because calculating the full $[Ni_2(DAniF)_4]^+$ cation as an open shell system will be even more computationally expensive than for the neutral analogue, such a calculation was not attempted. However, results from the neutral compound suggest that if the full $[Ni_2(DAniF)_4]^+$ cation were to be calculated in a similar way, the resulting electronic state would correctly be assigned as the one in which one electron is removed from the Ni_2 σ^* orbital.

Additional support for the assignment of the $^2A_{2u}$ state as the ground state of the cation $[Ni_2(DAniF)_4]^+$, is provided by time-dependent DFT (TD-DFT). Calculations were performed to determine whether the features of the electronic spectrum of $\mathbf{16}^+$ could be modeled using either the $^2A_{2u}$ state or the $^2A_{1u}$ state. The lowest energy-allowed

transition calculated for the $^2A_{1u}$ state is at 1205 nm (oscillator strength f = 0.04) and corresponds to excitations from the ligand π orbitals of e_g symmetry to the singly occupied a_{1u} ligand orbital, a process which can be essentially described as a ligand-to-ligand intervalence transition. For the $^2A_{2u}$ state, the lowest energy band is calculated to be a Ni_2 π* → σ* transition at 874 nm (f = 0.0002). This value of 874 nm compares very well to the experimental value observed in **16**-BF_4, in which the lowest energy band is at 887 nm with ε = 7500 M^{-1} cm^{-1}. The observed transition is too high in energy to be ascribed to an intervalence transition, as these bands typically appear in the NIR for ligand-based processes.[150] Thus the band at 887 nm in **16**-BF_4 should be attributed to a Laporte allowed Ni_2 π* → σ* transition and this assignment is consistent with a species that contains a Ni_2^{5+} unit and a bond order of ½.

One of the advantages of DFT is that it can provide useful information about hypothetical compounds or those which are known to exist but cannot or have not been isolated. A good example is the doubly oxidized species generated from **16**, i.e. $[Ni_2(DAniF)_4]^{2+}$, which we have been unable to isolate in crystalline form, though its electronic spectrum in solution has been measured. Geometry optimization of the model complex $[Ni_2(HNCHNH)_4]^{2+}$ leads to a situation similar to that observed for $[Ni_2(HNCHNH)_4]^{+}$, and shows that the lowest energy state is essentially the result of ligand oxidation (removal of two electrons from the a_{1u} orbital). Thus the calculated geometrical values (Table 14) are similar to those for $Ni_2(HNCHNH)_4$ itself. In accord with all the preceding discussion, we suggest that here again the use of a simplified model does not reproduce experimental results, and it is likely that there is actually a metal-based oxidation in **16**-BF_4. Support for this suggestion comes from a calculation of

the geometry of the excited state of $[Ni_2(HNCHNH)_4]^{2+}$ which corresponds to the Ni_2^{6+} state having an empty σ^* orbital was used. The main difference in the geometry afforded by this calculation is that the Ni–Ni distance in such a Ni_2^{6+} state is 0.24 Å shorter than that in the neutral compound, a difference which is similar to that observed upon oxidation of $Pd_2(hpp)_4$ to $Pd_2(hpp)_4Cl_2$ (0.164 Å).[50] It should be noted, however, that the Ni_2^{6+} state is an excited state and is over 2 eV higher in energy than the ground state. For this reason, no TD-DFT calculations were attempted on it. For simplicity, we have not taken into account states in which one electron is removed from the metal and another is removed from the ligands due to the complexities involved in such states (they would necessarily be multideterminantal in nature). Therefore, at this time it is not possible to determine unambiguously the precise nature of the $[Ni_2(DAniF)_4]^{2+}$ cation. Nevertheless, by analogy to the singly oxidized compound it may well contain a Ni_2^{6+} unit and it may have an Ni–Ni distance ~ 0.2 Å shorter than that in $Ni_2(DAniF)_4$. Thus, we could postulate a Ni–Ni single bond distance of ~ 2.25 Å.

Conclusions. New dinickel compounds with formamidinato and guanidinato ligands have been synthesized and their one-electron oxidation products, **16**-BF_4 and **17**-BF_4, have been isolated and crystallographically characterized. Each complex shows a shortening of the Ni–Ni separation of about 0.1 Å upon oxidation, which is consistent with a metal-centered oxidation and formation of a Ni_2^{5+} species with a bond order of ½. Further evidence of this formulation is provided by EPR spectra of both species, for which isotropic *g* values of 2.171 and 2.160 are observed. The EPR spectrum of **16**-BF_4 at 10 K shows distinct axial anisotropy, consistent with the presence of the unpaired electron in the Ni_2 σ^* orbital. A species with an Ni_2^{6+} core, observed by spectroelectrochemistry at −25 °C, is postulated to be the first lantern-type compound with a Ni−Ni bond order of one.

DFT calculations on the model complex $Ni_2(HNCHNH)_4$ reveal that the HOMO (a_{1u}, a ligand π orbital) and HOMO–1 (a_{2u}, the Ni_2 σ^* orbital) are close in energy, and the splitting between the two orbitals is basis set dependent. A single point calculation of the full $Ni_2(DAniF)_4$ molecule results in an energy reversal of these two orbitals, suggesting that the HOMO of **16** is the Ni_2 σ* orbital. This shows that results obtained using simplified models in DFT calculations should be treated with caution. Unfortunately, for large molecules such models are the only practical approach.

CHAPTER VII

OBTAINING COMPOUNDS CONTAINING METAL-METAL BONDS BASED ON Ti(III)

INTRODUCTION

Compounds containing metal-metal bonds are relatively rare for elements of the first transition metal series compared to those of the second and third transition series.[1] There are for example no iron analogues of the many ruthenium and osmium compounds, nor any manganese analogue of the various technetium and rhenium compounds having strong, multiple M-M bonds. Therefore synthesizing compounds containing Ti-Ti bond is a challenge.

Dinuclear Ti(III) complexes are usually paramagnetic [151] with intermetallic distances longer than 3 Å. Several molecules with a proposed Ti-Ti bond in them have been prepared in various research groups. S. Gambarotta and coworkers[152] prepared and characterized a dinuclear titanium(III) formamidinate complex $Ti_2(\mu\text{-}CyNC(H)NCy)_2(\eta\text{-}CyNC(H)NCy)_2(\mu\text{-}Cl)_2$ (Cy = C_6H_{11}). In this compound which has two formamidinate and two Cl ligands bridging Ti^{3+} ions, the metal-metal distance was 2.942 (2) Å. The diamagnetism of this molecule and calculations led the authors to suggest the presence of Ti-Ti bond in this compound, even though the Ti-Ti distance is very long.

P. Sobota et. al[153] studied reactions of $Ti_4(OMe)_{14}Cl_2$ with $AlMe_3$ and of $TiCl_4$ and $Ti(OEt)_4$ with $Al/AlMe_3$. Three molecules ($[Ti_2(\mu\text{-}OMe)_2(\mu\text{-}Cl)Cl_3(thf)_3]$, $[Ti_2(\mu\text{-}$

$OMe)_3Cl_3(thf)_3]$ and $[Ti_2(\mu\text{-}OEt)_2(\mu\text{-}Cl)Cl_3(thf)_3]$) based on Ti_2^{6+} units with bridging OMe, OEt and Cl and Ti-Ti distances varying from 2.543 (1) to 2.599 (1) Å were obtained. The diamagnetism of these molecules, reasonable metal-metal distances and topological analysis of the Electron Localization Function (ELF), revealing the presence of ELF maximum between two Ti atoms led the authors to suggest an intermetallic bond.

Two other substances based on Ti_2^{6+} dimetal unit were prepared in our research group. [154] Ti-Ti distances (2.8990 (8) Å in $Ti_2[H_5C_6NC(H)NC_6H_5]_2(\mu\text{-}Cl_2)[\mu\text{-}H_5C_6NC(H)NC_6H_5]_2$ and 2.916 (3) Å in $Ti_2[H_5C_6NC(H)NC_6H_5]_2(\mu\text{-}Cl_2)[\mu\text{-}H_5C_6NC(H)NC_6H_5]_2$) define the upper limit of the formamidinate bridging distance range. Both compounds are also diamagnetic. Based on these data an intermetallic bond for both of these compounds was proposed. One can find some other examples of compounds containing Ti-Ti bond.[155]

Among all these compounds in the literature none was of the paddlewheel type. It was our goal to prepare a dititanium (III) paddlewheel based on hpp.

Recently M. P. Coles et. al[156] prepared various Ti(IV) complexes based on hpp and its derivatives ligands. By reacting the hpp^- ligand and its derivatives with commercially available Ti(IV) chloride complexes several mononuclear complexes and one binuclear Ti^{4+} complex were obtained.

Our synthetic strategy is the following. Starting with one of these Ti(IV) complexes, $Ti(hpp)_2Cl_2$, we shall try to perform a one-electron chemical reduction hoping to obtain dititanium (III) paddlewheel $Ti_2(hpp)_4Cl_2$.

EXPERIMENTAL SECTION

General Comments. Unless specified otherwise, all manipulations were carried out under an atmosphere of dry nitrogen gas using standard Schlenk techniques. All solvents were either distilled over appropriate drying agents in a nitrogen atmosphere or purified by means of a Glass Contour solvent system. ^{1}H NMR spectra were obtained on a VXR-300 NMR spectrometer. $TiCl_4(THF)_2$ and Hhpp were purchased from Aldrich. Hhpp was sublimed prior to being used. $Ti(hpp)_2Cl_2$ was prepared based on the published procedure.[156]

Synthesis of $[Ti_2(hpp)_4]Cl_2$, 18. To a solid mixture of $Ti(hpp)_2Cl_2$ (150 mg, 0.380 mmol) and KC_8 (56 mg, 0.418 mmol) 15 mL of THF were added. The color of the solution changed from red to dark green within several minutes. It was stirred at room temperature for 30 min. Solvent was then removed under vacuum, and the green solid was extracted with 10 mL of CH_2Cl_2, filtered through Celite, and then precipitated with 80 mL of hexanes.

A green powder was collected. Yield: 107 mg, 78%. ^{1}H NMR ($CDCl_3$, δ): 2.011 (q, $CH_2CH_2CH_2$, 1H), 3.315 (t, CH_2CH_2, 1H), 3.334 (t, CH_2CH_2, 1H). Crystals of **18**·$2CH_2Cl_2$ were obtained by extracting the green solid with 13 mL of CH_2Cl_2, filtering it through Celite and layering the solution with 45 ml of hexanes. The solution was kept at -10 °C, and dark-green crystals, suitable for X-ray single crystal diffraction, formed within 3 weeks, when the diffusion was complete.

X-Ray Crystallography

Suitable crystals of **18**·$2CH_2Cl_2$ was mounted and centered in the goniometer of a Bruker SMART 1000 CCD area detector diffractometer and cooled to –60 °C. Geometric and intensity data were collected using SMART software.[29] The data were processed using SAINT software,[30] and corrections for absorption were applied using the program SADABS.[31] The structure was solved and refined using the SHELXTL program package.[32] Crystal data are shown in Table 15, and Table 16 lists pertinent bond distances and angles.

Table 15 Crystal data for **18**·$2CH_2Cl_2$

	18·$2CH_2Cl_2$
Formula	$C_{30}H_{52}Cl_6N_{12}Ti_2$
FW	889.34
Crystal System	Triclinic
Space Group	*P*-1
a, Å	9.230(2)
b, Å	9.433(2)
c, Å	11.687(2)
α, deg.	85.889(3)
β, deg.	84.348(4)
γ, deg.	77.300(4)
V, Å^3	986.5(3)
Z	1
d(calc), g cm^{-3}	1.497
R1[a], *w*R2[b] (I>2σ(*I*))	0.0366, 0.0910
R1[a], *w*R2[b] (all data)	0.0472, 0.0982

[a] $R1 = \sum||F_o| - |F_c||/\sum|F_o|$, [b] $wR2 = [\sum[w(F_o^2 - F_c^2)^2]/ \sum[w(F_o^2)^2]]^{½}$, $w = 1/\sigma^2(F_o^2) + (aP)^2 + bP$, where $P = [\max(0 \text{ or } F_o^2) + 2(F_c^2)]/3$

Table 16 Selected interatomic distances and angles for **18**·$2CH_2Cl_2$[a]

Ti1–Cl2	2.4650 (9)
Ti1–Ti1A	2.5944 (9)
Ti1–$N_{chel.}$	2.159 [2]
Ti1–$N_{bridg.}$	2.191 [2]
Ti1–N4–Ti1A	72.16 (6)
Ti1–N5–Ti1A	71.58 (6)

[a] Distances are given in Å, angles in °. Numbers in brackets correspond to average values.

RESULTS AND DISCUSSION

Synthesis. Reaction of $Ti(hpp)_2Cl_2$ with KC_8 involves complex equilibria and we don't completely understand it yet. The NMR spectra of crystals as well as that of amorphous powders have only one type of hpp^- ligand (one quintet and two triplets integrated as 1:1:1). The spectrum does not change between -50 °C and 40 °C. The crystal structure of the compound though is not consistent with the NMR spectra. It shows a dimetal unit with two bridging and two chelating hpp^- ligands which should yield different sets of signals (structure of **18** will be described in more detail later). We recrystallized crystals of **18** and studied its structure and NMR again. Again crystal structure and NMR spectrum of **18** were the same. There are two hypotheses which can explain these experimental results. One is that hpp^- ligands in chelating and bridging positions switch places very fast, thus giving rise to the simple NMR spectrum. If this explanation is correct, we should have seen a more complex spectrum at low temperature. Since the spectrum remained the same, this assumption is probably wrong. It is also possible that the compound with empirical formula $Ti_2(hpp)_4Cl_2$ has different forms in solution and in solid state and that in solution **18** is more symmetrical than in the solid state thus yielding a simpler NMR spectrum. A possible equilibrium is shown in Scheme 15.

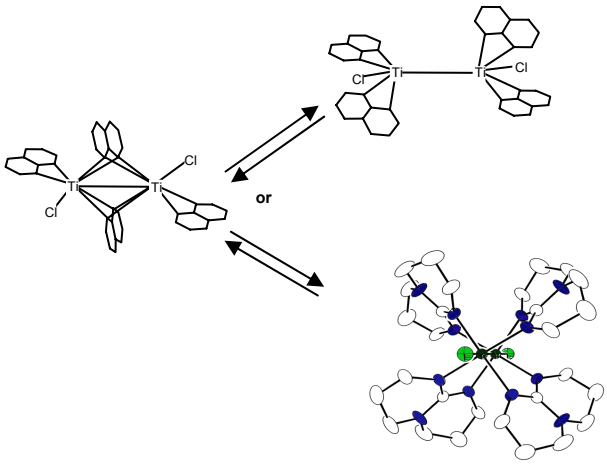

Scheme 15

As one can see if $Ti_2(hpp)_4Cl_2$ takes in solution either one of two forms shown on the right of scheme 15 the additional mirror plane perpendicular to Ti-Ti bond along with a free rotation in solution around the same bond, makes this compound more symmetrical, which is consistent with all NMR spectra.

Crystal structure. In $(\eta\text{-hpp})_2Ti_2(\mu\text{-hpp})_2Cl_2$ two Ti^{3+} atoms are held together by two bridging hpp^- ligands. A unique feature of this structure is that the bridging hpp^- linkers are located in a plane perpendicular to Ti-Ti bond (Fig. 29). This has never been observed before. The other hpp^- ions chelate Ti atoms. Each of those Ti atoms are also coordinated by a Cl^- ion. The molecule resides on a special position in the P_1^- space group. The idealized point group symmetry of this molecule is D_{2h}.

The metal-metal distance of 2.5944(9) Å is the shortest among all the Ti_2^{6+} compounds known. The compound is diamagnetic which suggests the presence of a single σ bond in this molecule.

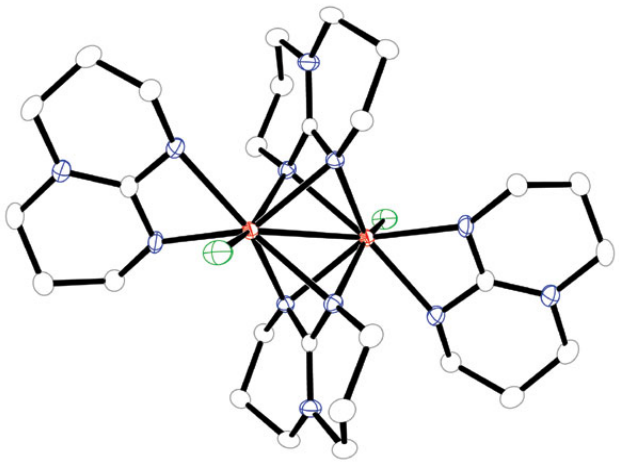

Fig. 29 Thermal ellipsoid plot of $Ti_2(hpp)_4Cl_2$ with ellipsoids drawn at the 30% probability level and no hydrogen atoms shown.

Conclusions. A Ti_2^{6+} compound with the shortest known metal-metal distance of 2.5944(9) Å was obtained. A new type of linking of two metal atoms was first observed in this molecule. Noncorresponding results of the analysis of this compound in solution and in solid state suggests that it has different structures in solution and in the crystalline form. For a better understanding of these phenomena crystallization from solvents of different polarity as well as replacement of the terminal Cl by other ligands should be performed. Such work is currently in progress.

CHAPTER VIII

CONCLUSIONS

The highlights of this dissertation concern understanding of the chemistry of chiral supramolecules with dimetal units and formation of metal-metal bond.

Reactions of *ortho*-, *metha*-, and *para*- chiral, enantiomericaly pure dicarboxilate linker with $Mo_2(DAniF)_2^{2+}$ building block were studied in Chapter II. It was shown that the structure of final product strongly depends on the geometry of the dicarboxylate. While *para*- isomer yields loops, *metha*- isomer favors the chelated product and *orhto*- produces mixture of both chelated and loop products. First crystal structure of enantiomerically pure molecular loop based on chiral dicarboxilate linker and dimolibdenum unit - *R, R, R, R*-$Mo_2(DAniF)_2$(*p*-$O_2CCH(CH_3)O$-C_6H_4-$OCH(CH_3)CO_2$) - was obtained. It was shown, that when crystallized, these molecules stack on top of each other forming channels with chiral environment, large enough to host guest molecules (in our case it was solvent molecules CH_2Cl_2). Observed property makes this work interesting for stereoselective catalysis.

$Pd_3(OAc)_6$ is widely used as a precursor for synthesis of Pd_2^{4+} complexes. Since our interest in preparation of such complexes we were seeking for a good preparation procedure of $Pd_3(OAc)_6$ from $PdCl_2$. We were also curious about behavior of $Pd_3(OAc)_6$ in solution since literature data about it were controversial. We found out that to obtain a pure $Pd_3(OAc)_6$ by reaction of $PdCl_2$ with HOAc and catalytic amounts of HNO_3 constant removal of nitrogen oxides from the reaction mixture must be performed. Otherwise one

of the acetate groups is easily replaced by NO_2^- forming $Pd_3(OAc)_5(NO_2)$ molecule, which structure was solved. It was also shown, that when using dry organic solvents such as dichloromethane and benzene $Pd_3(OAc)_6$ preserves its triangular structure in solution.

Preparation of various Pd (II) complexes is described in chapter IV. Depending on the ligand and reaction conditions interaction between palladium acetate and a ligand can lead to different products. Preparation of 8 compounds, 5 of which were new was presented. Their electrochemical properties were studied. Reversible oxidation waves in the cyclic voltammograms were observed for **8**, **13**, **14** and **15**. Therefore these 4 substances were selected for further studying.

In chapters V and VI synthesis and study of Pd_2^{5+} and Ni_2^{5+} paddlewheel complexes respectively are discussed. EPR spectra of both Pd_2^{5+} and Ni_2^{5+} paddlewheels clearly reveal the anisotropy of *g*-value, which shows that the unpaired electron is located on mainly metal-based molecular orbital. Theoretical calculations propose the same thing for both Ni and Pd systems. Behavior of metal-metal bond distance is greatly dependent on electron donating abilities of the bridging ligand. When ligand is strongly electron donating, like DAniF or TPG metal-metal distance shrinks significantly, when it is not so basic as DTolF, it even can remain the same as in $Pd_2(DTolF)_4$. All these experimental data allowed us to assume the formation of one-electron metal-metal bond upon one-electron oxidation of Ni_2^{4+} and Pd_2^{4+} paddlewheels.

In chapter VII synthesis and crystallographic characterization of Ti_2^{6+} molecule is described. Upon one-electron reduction of $Ti(hpp)_2Cl_2$ with KC_8 $Ti_2(hpp)_4Cl_2$ compound was obtained. It has shortest Ti(III)-Ti(III) distance yet known (2.5944(9) Å). A new type of linking of two metal atoms was first observed in this molecule. Two Cl atoms are

located in an axial position, two hpp ligands are chelating and two are bridging and are perpendicular to Ti-Ti single bond. It is suggested, that this compound has different structures in solution and in the crystalline form.

REFERENCES

[1] *Multiple Bonds Between Metal Atoms*; Cotton, F. A., Murillo, C. A., Walton, R. A., Eds.; Springer Science and Business Media, Inc.: New York 2005.

[2] (*a*) Cotton, F. A.; Lin, C.; Murillo, C. A. *Acc. Chem. Res.*, **2001**, *34*, 759; (*b*) Cotton, F. A.; Lin, C.; Murillo, C. A. *Proc. Natl. Acad. Sci. USA*, **2002**, *99*, 4810.

[3] (*a*) Doyle, M. P.; Ren, T. *Prog. Inorg. Chem.*, **2001**, *49*, 113; (*b*) *Catalysis by Di- and Polynuclear Metal Cluster Complexes*; Adams, R. D., Cotton, F. A., Eds.; Wiley-VCH: New York, 1998; (*c*) Matsumoto, K. *Cisplatin: Chemistry and Biochemistry of a Leading Anticancer Drug*; In Ed. B. Lippert, Ed.; Wiley-VCH: New York, 1999, p. 455; (*d*) Saeki, N.; Nakamura, N.; Ishibashi, T.; Arime, M.; Sekiya, H.; Ishihara K.; Matsumoto, K. *J. Am. Chem. Soc.*, **2003**, *125*, 3605; (*e*) Pillinger, M.; Goncalves, I. S.; Ferreira, P.; Rocha, J.; Schafer, M.; Schon, D.; Nuyken, O.; Kühn F. E. *Macromol. Rapid Commun.*, **2001**, *22*, 1302; (*f*) Whelan, E.; Devereux, M.; McCann, M.; McKee, V. *Chem. Commun.*, **1997**, 427.

[4] (*a*) Asara, J. M.; Hess, J. S.; Lozada, E.; Dunbar K. R.; Allion, J. *J. Am. Chem. Soc.*, **2000**, *122*, 8; (*b*) Catalan, K. V.; Hess, J. S.; Maloney, M. M.; Mindiola, D. J.; Ward, D. L.; Dunbar, K. R. *Inorg. Chem.*, **1999**, *38*, 3904; (*c*) Dale, L. D.; Dyson, T. M.; Tocher, D. A.; Tocher, J. H.; Edwards, D. I. *Anti-Cancer Drug Des.*, **1989**, *4*, 295; (*d*) Aoki, K.; Yamazaki, H. *J. Chem. Soc.*, *Chem. Commun.*, **1980**, 186; (*e*) Howard, R. A.; Kimball, A. P.; Bear, J. L. *Cancer Res.*, **1979**, *39*, 2568; (*f*) Fu, P.; Bradley P. M.; Turro, C. *Inorg. Chem.*, **2001**, *40*, 2476; (*g*) Aoki, K.; Salam, M. A. *Inorg. Chim. Acta*, **2001**, *316*, 50; (*h*) Lippert, B. *Prog. Inorg. Chem.*, **1989**, *37*, 1; (*i*) Micklitz, W.; Müller, G.; Huber, B.; Riede, J.; Rashwan, F.; Heinze J.; Lippert, B. *J. Am. Chem. Soc.*, **1988**, *110*, 7084.

[5] (*a*) Pérez-Prieto, J.; Stiriba, S.-E.; Moreno E.; Lahuerta, P. *Tetrahedron*: *Asymmetry*, **2003**, *14*, 787; (*b*) Barberis, M.; Pérez-Prieto, J.; Herbst K.; Lahuerta, P. *Organometallics*, **2002**, *21*, 1667; (*c*) Barberis, M.; Pérez-Prieto, J.; Lahuerta, P.; Sanaú, M. *Chem. Comm.*, **2001**, 439; (*d*) Estevan, F.; Krueger, P.; Lahuerta, P.; Moreno, E.; Pérez-Prieto, J.; Sanaú, M.; Werner, H. *Eur. J. Inorg. Chem.*, **2001**, 105; (*e*) Doyle, M. P.; Forbes, D. C. *Chem. Rev*., **1998**, *98*, 911; (*f*) Doyle, M. P. *Catalytic Asymmetric Synthesis*; In Ed. I. Ojima, Ed.; Wiley-VCH: New York, 2nd ed., 2000.

[6] See, for example: (*a*) Scapin, G.; Reddy, S. G.; Blanchard, J. S. *Biochemistry*, **1996**, *35*, 13540 and references therein; (*b*) Koyama, T.; Ogura, K.; Seto, S. *J. Am. Chem. Soc*., **1997**, *99*, 1999.

[7] Habereder, T.; Warchhold, M.; Nöth, H.; Severin, K. *Angew. Chem., Int. Ed.*, **1999**, *38*, 3225.

[8] (*a*) Jiang, H.; Lin, W. *J. Am. Chem. Soc.*, **2003**, *125*, 8084; (*b*) Lee, S. J.; Hu, A.; Lin, W. *J. Am. Chem. Soc.*, **2002**, *124*, 12948; (*c*) Ali, M. M.; MacDonnell, F. M. *J. Am. Chem. Soc.*, **2000**, *122*, 11527. (*d*) Lee, S. J.; Lin, W. *J. Am. Chem. Soc.*, **2002**, *124*, 4554; (*e*) Lee, S. J.; Lumman, C. R.; Castellano, F. N.; Lin, W. *Chem. Commun*., **2003**, 2124.

[9] Süss-Fink, G.; Wolfender, J.-L.; Neumann, F.; Stoeckli-Evans, H. *Angew. Chem., Int. Ed. Engl.*, **1990**, *29*, 429.

[10] Cotton, F. A.; Donahue, J. P.; Murillo, C. A. *Inorg. Chem. Commun.*, **2002**, *5*, 59.

[11] Cotton, F. A.; Lin, C.; Murillo, C. A. *Inorg. Chem.*, **2001**, *40*, 5886.

[12] (*a*) Cotton, F. A.; Lin, C.; Murillo, C. A. *Inorg. Chem.*, **2001**, *40*, 478; (*b*) Cotton, F. A.; Daniels, L. M.; Lin, C.; Murillo, C. A. *J. Chem. Soc., Dalton Trans.*, **2001**, 502; (*c*) Angaridis, P.; Berry, J. F.; Cotton, F. A.; Murillo, C. A.; Wang, X. *J. Am. Chem. Soc.*, **2003**, *125*, 10327.

[13] (*a*) Cotton, F. A.; Lin, C.; Murillo, C. A. *Inorg. Chem.*, **2001**, *40*, 575; (*b*) Cotton, F. A.; Lin, C.; Murillo, C. A. *J. Am. Chem. Soc*., **1999**, *121*, 4538.

[14] Cotton, F. A.; Lin, C.; Murillo, C. A. *Inorg. Chem.*, **2001**, *40*, 472.

[15] Shiu, K.-B.; Lee, H.-C. *Organometallics*, **2002**, *21*, 4013.

[16] Bonar-Law, R. P.; McGrath, T. D.; Singh, N.; Bickeley, J. F.; Steiner, A. *Chem. Commun.,* **1999**, 2457.

[17] (*a*) Gallagher, J. F.; Ferguson, G.; McAlees, A. J. *Acta Cryst.*, *Sect. C*, **1997**, *53*, 567; (*b*) Taber, D. F.; Meagley, R. P.; Louey, J. P.; Rheingold, A. L. *Inorg. Chim. Acta*, **1995**, *239*, 25.

[18] Bickley, J. F.; Bonar-Law, R. P.; Femoni, C.; MacLean, E. J.; Steiner, A.; Teat, S. J. *J. Chem. Soc.*, *Dalton Trans.*, **2000**, 4025.

[19] Bonar-Law, R. P.; McGrath, T. D.; Singh, N.; Bickley, J. F.; Femoni C.; Steiner, A. *J. Chem. Soc.*, *Dalton Trans.*, **2000**, 4343.

[20] Bonar-Law, R. P.; McGrath, T. D.; Bickley, J. F.; Femoni, C.; Steiner, A. *Inorg. Chem. Commun.*, **2001**, *4*, 16.

[21] Bonar-Law, R. P.; Bickley, J. F.; Femoni, C.; Steiner, A. *J. Chem. Soc.*, *Dalton Trans.*, **2000**, 4224.

[22] Effenberg, F.; Burkard, U.; Willfahrt, J. *Liebegs Ann. Chem*., **1986**, 314.

[23] Burkard, U.; Effenberg, F. *Chem. Ber.*, **1986**, *119*, 1594.

[24] Chisholm, M. H.; Cotton, F. A.; Daniels, L. M.; Folting, K.; Huffman, J.; Iyer, S.; Lin, C.; MacIntosh, A. M.; Murillo, C. A. *J. Chem. Soc.*, *Dalton Trans.*, **1999**, 1387.

[25] Wenfa, Y.; Zixiu, D. *Huaxue Shiji*, **2002**, *24*, 363.

[26] Pflugrath, J. W.; Messerschmidt, A. *J. Appl. Crystallogr.*, **1987**, *20*, 306.

[27] (*a*) Kabsch, W. *J. Appl. Crystallogr.*, **1988**, *21*, 67. (*b*) Kabsch, W. *J. Appl. Crystallogr.*, **1988**, *21*, 916.

[28] R. H. Blessing, *Acta Crystallogr.*, *Sect. A*, **1995**, *51*, 33.

[29] *SMART*, *Software for the CCD Detector System, version 5.625*; Bruker Analytical X-ray Systems, Inc.: Madison, WI, 2001.

[30] *SAINT*. *Data Reduction Software*. V*ersion 6.33B*; Bruker Analytical X-ray Systems, Inc.: Madison, WI, 2001.

[31] *SADABS. Bruker/Siemens Area Detector Absorption and Other Corrections*. *V2.03*; Bruker Analytical X-ray Systems, Inc.: Madison, WI, 2001.

[32] Sheldrick, G. M., *SHELXTL. Version 6.10*; Bruker Analytical X-ray Systems, Inc.: Madison, WI, 2000.

[33] Wenfa, Y.; Zixiu, D. *Huaxue Shiji*, **2002**, *24*, 363.

[34] For a recent 3D network with channels in a chiral environment, see: Zhang, Y.; Saha, M. K.; Bernal, I. *Cryst. Eng. Commun.*, **2003**, *5*, 34.

[35] (*a*) Leadbeater, N. E.; Marco, M. *J. Org. Chem.*, **2003**, *68*, 888; (*b*) Zhao, F. Y.; Shirai, M.; Arai, M. *J. Mol. Catal. A: Chem.*, **2000**, *154*, 39; (*c*) Jia, C. G.; Lu, W. J.; Kitamura, T.; Fujiwara, Y. *Org. Lett.*, **1999**, *1*, 2097; (*d*) Bedford, R. B.; Blake, M. E.; Butts, C. P.; Holder, D. *Chem. Commun.*, **2003**, 466; (*e*) Yao, Q. W.; Kinney E. P.; Yang, Z. *J. Org. Chem.*, **2003**, *68*, 7528; (*f*) Lee, H. M.; Nolan, S. P. *Org. Lett.*, **2000**, *2*, 2053; (*g*) Wolfe, J. P.; Singer, R. A.; Yang, B. H.; Buchwald, S. L. *J. Am. Chem. Soc.*, **1999**, *121*, 9550.

[36] (*a*) Zhang, J. Y.; Boyd, I. W. *Appl. Phys. A: Mater. Sci. Process.*, **1997**, *65*, 379; (*b*) Esrom, H.; Zhang, J. Y.; Kogelschatz, U.; Pedraza, A. J. *Appl. Surf. Sci.*, **1995**, *86*, 202.

[37] Morooka, C. S.; Yan, S. C.; Yokoyama, S.; Kusakabe, K. *Sep. Sci. Technol.*, **1995**, *30*, 2877.

[38] (*a*) Mayer, A. B. R; Mark, J. E. *Colloid Polym. Sci.*, **1997**, *275*, 333; (*b*) Dhas, N. A.; Gedanken, A. *J. Mater. Chem.*, **1998**, *8*, 445.

[39] Cheng, C. D.; Gonela, R. K.; Gu, Q.; Haynie, D. T. *Nano Lett.*, **2005**, *5*, 175.

[40] (*a*) Henry, P. M. *Adv. Organomet. Chem.*, **1975**, *13*, 363; (*b*) Weissman, S. A.; Zewge, D.; Cheng, C. *J. Org. Chem.*, **2005**, *70*, 1508; (*c*) Kamiya, I.; Nishinaka, E.; Ogawa, A. *J. Org. Chem.*, **2005**, *70*, 696; (*d*) Matteoli, U.; Scrivanti, A.; Beghetto, V. *J. Mol. Catal. A: Chem.*, **2004**, *213*, 183 (*e*) Darses, S.; Pucheault, M.; Genet, J.-P. *Eur. J. Org. Chem.*, **2001**, 1121; (*f*) Hirabayashi, K.; Ando, J.-I.; Yasushi, N.; Mori, A.; Hiyama, T. *Synlett.*, **1999**, 99; (*g*) Contento, M.; Da Col, M.; Galletti, P.; Sandri, S.; Umani-Ronchi, A. *Tetrahedron Lett.*, **1998**, *39*, 8743.

[41] Stephenson, T. A.; Morehouse, S. M.; Powell, A. R.; Heffer, J. P.; Wilkinson, G. *J. Chem. Soc.*, **1965**, 3632.

[42] Albéniz, A. C.; Espinet, P. *Encyclopedia of Inorganic Compounds*; In Ed. R. B. King, Ed., John Wiley & Sons: New York, USA, 1994, vol. 6, p. 3010.

[43] (*a*) Skapski, A. C.; Smart, M. L. *J. Chem. Soc., Chem. Commun.*, **1970**, 658; (*b*) Cotton, F. A.; Han, S. *Rev. Chim. Miner.*, **1983**, *20*, 496; (*c*) Cotton, F. A.; Han, S. *Rev. Chim. Miner.*, **1985**, *22*, 277; (*d*) Lyalina, N. N.; Dargina, S. V.; Sobolev, A. N.; Buslaeva, T. M. Romm, I. P. *Koord. Khim.*, **1993**, *19*, 57.

[44] Clérac, R.; Cotton, F. A.; Dunbar, K. R.; Hillard, E. A.; Pretrukhina, M. A.; Smucker, B. W. *C. R. Acad. Sci. Paris, Chim.*, **2001**, *4*, 315.

[45] Kirik, S. D.; Mulagaleev, R. F.; Blokhin, A. I. *Acta Crystallogr., Sect. C: Cryst. Struct. Commun.*, **2004**, *C60*, 449.

[46] Romm, I. P.; Buslaeva, T. M.; Lyalina, N. N.; Shifrina, R. R.; Simitsyn, N. M. *Koord. Khim.*, **1992**, *18*, 165.

[47] See for example: Stoyanov, E. S. *J. Struct. Chem.*, **2000**, *41*, 440.

[48] Marson, A.; van Oort, A. B.; Mul, W. P. *Eur. J. Inorg. Chem.*, **2002**, 3028.

[49] Bianchini, C.; Meli, A.; Oberhauser, W. *Organometallics*, **2003**, *22*, 4281.

[50] Cotton, F. A.; Gu, J.; Murillo, C. A.; Timmons, D. J. *J. Am. Chem. Soc.*, **1998**, *120*, 13280.

[51] (*a*) Yao, C.-L.; He, L.-P.; Korp, J. D.; Bear, J. L. *Inorg. Chem.*, **1988**, *27*, 4389; (*b*) Cotton, F. A.; Matusz, M.; Poli, R.; Feng, X. *J. Am. Chem. Soc.*, **1988**, *110*, 1144.

[52] (*a*) Zhang, R.; Ma, C.; Yin, H. *Huaxue Shiji*, **1994**, *16*, 383; (*b*) Romm, I. P.; Noskov, Yu. G.; Perepelkova, T. I.; Kravtsova, S. V.; Buslaeva, T. M. *Russ. J. Gen. Chem.*, **1998**, *68*, 681; (*c*) Jiang, D.; Wang, J.; Tang, B.; Wang, W. *Guijinshu*, **1997**, *18*, 16.

[53] When untreated CD_3OD was used, several signals were also observed in the region where the acetate signal was expected. We tried to minimize the amount of water in

methanol (which is notoriously difficult to dry) by leaving it over freshly regenerated molecular sieves and then by adding a small amount of sodium metal. This procedure was followed by vacuum distillation. The ^{1}H NMR spectrum of **1** was recorded at each drying stage. There were small changes in the spectra depending on the amount of water present but we never observed only one signal in the acetate region. Furthermore, whenever the samples were allowed to stand overnight in the NMR tubes, a dark solid formed at the bottom of each tube, and this solid behaved chemically like Pd metal (insoluble in concentrated HCl but soluble in *aqua regia*.) It is not clear if some of the additional signals observed in CD_3OD are due to hydrolysis or methanolysis of $Pd_3(OAc)_6$. However, it is clear that there is a chemical reaction that deposits the solid.

[54] Bauer, W.; Prem, M.; Polborn, K.; Sünkel, K.; Steglich, W.; Beck, W. *Eur. J. Inorg. Chem.*, **1998**, 485.

[55] J. F. Knifton, *J. Catal.*, **1979**, *60*, 27.

[56] (*a*) Raminelli, C.; Prechtl, M. H.; Santos, L. S.; Eberlin, M. N.; Comasseto, J. V. *Organometallics* **2004**, *23*, 3990; (*b*) Nishimura, T.; Nishiguchi, Y.; Maeda, Y.; Uemura, S. *J. Org. Chem.* **2004**, *69*, 5342; (*c*) Stahl, S. S. *Angew. Chem.* **2004**, *43*, 3400; (*d*) Mueller, J. A.; Goller, C. P.; Sigman, M. S. *J. Am. Chem. Soc.* **2004**, *126*, 9724; (*e*) Goj, L. A.; Cisneros, G. A.; Yang, W.; Widenhoefer, R. A. *J. Organomet. Chem.* **2004**, *689*, 2845.

[57] See, for example: (*a*) Phillips, A. D.; Gonsalvi, L.; Romerosa, A.; Vizza, F.; Peruzzini, M. *Coord. Chem. Rev.* **2004**, *248*, 955; (*b*) Bincoletto, C.; Tersariol, L. S.; Oliveira, C. R.; Dreher, S.; Fausto, D. M.; Soufen, M. A.; Nascimento, F. D.; Caires, C. F. *Bioorg. Med. Chem.* **2005**, *13*, 3047; (*c*) Jackson, A.; Davis, J.; Pither, R. J.; Rodger, A.; Hannon, M. J. *Inorg. Chem.* **2001**, *40*, 3964.

[58] (*a*) Kishore, S.; Nelson, J. A.; Adair, J. H.; Eklund, P. C. *J. Alloys Compd.* **2005**, *389*, 234; (*b*) Sun, Y.; Tao, Z.; Chen, J.; Herricks, T.; Xia, Y. *J. Am. Chem. Soc.* **2004**, *126*, 5940; (*c*) Souza, E. C.; Ticianelli, E. A. *J. Braz. Chem. Soc.* **2003**, *14*, 544; (*d*) Higuchi, K.; Yamamoto, K.; Kajioka, H.; Toiyama, K.; Honda, M.; Orimo, S.; Fujii, H. *J. Alloys Compd.* **2002**, *330*, 526; (*e*) Fujii, H.; Orimo, S. *J. Phys. B* **2003**, *328*, 77; (*f*) Watari, N.; Ohnishi, S.; Ishii, Y. *J. Phys. C* **2000**, *12*, 6799.

[59] (*a*) Love, J. C.; Wolfe, D. B.; Haasch, R.; Chabinyc, M. L.; Paul, K. E.; Whitesides, G. M.; Nuzzo, R. G. *J. Am. Chem. Soc.* **2003**, *125*, 2597; (*b*) Yurakov, Yu. A.; Kashkarov, V. M.; Kushchev, S. B.; Balashova, V. Yu. *Poverkhnost* **2003**, *6*, 10.

[60] *Advanced Inorganic Chemistry*, Cotton, F. A.; Wilkinson, G.; Murillo, C. A.; Bochmann, M. 6th Ed.; Wiley-Interscience: New York, 1999.

[61] Cotton, F. A.; Dunbar, K. R.; Falvello, L. R.; Tomas, M.; Walton, R. A. *J. Am. Chem. Soc*. **1983**, *105*, 4950.

[62] (*a*) Nefedov, V. I.; Koz'min *Inorg. Chim. Acta* **1982**, *64*, L177; (*b*) Cotton, F. A.; Gage, L. D. *Nouv. J. Chim*. **1977**, *1*, 441; (*c*) See also: Sattelberger, A. P. Chapter 7. In *Multiple Bonds Between Metal Atoms*; Cotton, F. A., Murillo, C. A., Walton, R. A., Eds.; Springer Science and Business Media, Inc.: New York, 2005.

[63] It should be noted that with N,N-ligands other than hpp a one-electron oxidation is far more likely to occur than a two-electron oxidation. For a discussion of the extraordinary ability of the guanidinate ligand hpp to stabilize high-oxidation states in dimetal complexes, see, for example: (*a*) Cotton, F. A.; Gruhn, N. E.; Gu, J.; Huang, P.; Lichtenberger, D. L.; Murillo, C. A.; Van Dorn, L. O.; Wilkinson, C. C. *Science* **2002**, *298*, 1971; (*b*) Cotton, F. A.; Daniels, L. M.; Murillo, C. A.; Timmons, D. J.; Wilkinson, C. C. *J. Am. Chem. Soc.* **2002**, *124*, 9249; (*c*) Berry, J. F.; Cotton, F. A.; Huang, P.; Murillo, C. A. *J. Chem. Soc., Dalton Trans*. **2003**, 1218.

[64] Bonamico, M.; Dessy, G.; Fares, V. *J. Chem. Soc., Dalton Trans.* **1977**, 2315.

[65] Piovesana, O.; Bellitto, C.; Flamini, A.; Zanazzi, P. F. *Inorg. Chem.* **1979**, *18*, 2258.

[66] Bancroft, D. P.; Cotton, F. A.; Falvello, L. R.; Schwotzer, W. *Inorg. Chem.* **1986**, *25*, 1015.

[67] Corbett, M.; Hoskins, B. F.; McLeod, N. J.; O'Day, B. P. *Aust. J. Chem.* **1975**, *28*, 2377.

[68] Kubiak, M. *Acta Crystallogr., Sect. C* **1985**, 41, 1288.

[69] Lin, C.; Protasiewicz, J. D.; Smith, E. T.; Ren, T. *Inorg. Chem.* **1996**, *35*, 6422.

[70] Kakimoto, M.; Ogata, S.-I.; Mochizuki, A.; Imai, Y. *Chem. Lett*. **1984**, 821.

[71] Bakhmutov, V. I.; Berry, J. F.; Cotton, F. A.; Ibragimov, S.; Murillo, C. A. *J. Chem. Soc., Dalton Trans*. **2005**, 1989.

[72] A synthesis for this compound was reported earlier. See: Dwyer, F. P. *J. Am. Chem. Soc.* **1941**, *63*, 78.

[73] For a review on guanidine-type ligands see: Bailey, P. J.; Pace, S. *Coord. Chem. Rev*. **2001**, *214*, 91.

[74] Cotton, F. A.; Matonic, J. H.; Murillo, C. A. *Inorg. Chem*. **1996**, *35*, 498.

[75] Crystallographic data for $Pd_2(\mu\text{-TPG})(\eta^2\text{-TPG})[\eta^2\text{-}C_6H_4N(CNHPh)N(H)Ph](\mu\text{-OAc})\cdot 2CD_3CN$: triclinic; *P*; $a = 11.209(1)$ Å, $b = 12.0459(1)$ Å, $c = 23.011(3)$ Å; $\alpha = 74.877(2)$, $\beta = 89.529(2)$, $\gamma = 71.256(2)$; $V = 2830.3(5)$ Å^3; R (all data) = 0.0410; Pd···Pd = 2.9202(4) Å, average Pd-N = 2.037[2] Å, Pd-C = 2.483(3) Å, Pd-O = 2.105[2] Å.

[76] It should be mentioned that we have had serious difficulties obtaining elemental analyses for all compounds having benzamidinate ligands. In all cases, the experimental percentage of C was well below the calculated value. It is our belief that this is due to the formation of carbides that could form upon heating of the samples because orthometalation to form Pd-C bonds occurs, for example, in compound **8**.

[77] Xu, G.; Campana, C.; Ren, T. *Inorg. Chem.* **2002**, *41*, 3521.

[78] Another way to synthesize the α-isomer in low yield is by reaction in THF of $Pd_2(DPhBz)_3(OAc)$ and one equivalent of a DPhBz anion.

[79] (*a*) Heeger, A. J. *Rev. Mod. Phys.* **2001**, *73*, 681. (*b*) MacDiarmid, A. G. *Rev. Mod. Phys.* **2001**, *73*, 701. (*c*) Shirakawa, H. *Rev. Mod. Phys.* **2001**, *73*, 713.

[80] (*a*) K. Krogmann and P. Dodel, *Chem. Ber.* **1966**, *99*, 3402. (*b*) K. Krogmann and P. Dodel, *Chem. Ber.* **1966**, *99*, 3408. (*c*) K. Krogmann, *Z. Anorg. Allg. Chem.* **1968**, *358*, 97. (*d*) K. Krogmann, *Angew. Chem., Int. Ed. Engl.* **1969**, *8*, 35. (*e*) *Extended Linear Chain Compounds* Miller, J. S., Ed. Vol. 1, Plenum Press: New York, 1982. (*f*) *Extended Linear Chain Compounds* Miller, J. S., Ed. Vol. 2, Plenum Press: New York, 1982. (*g*) *Extended Linear Chain Compounds* Miller, J. S., Ed. Vol. 3, Plenum Press: New York, 1983.

[81] (*a*) Barton, J. K.; Rabinowitz, H. N.; Szalda, D. J.; Lippard, S. J. *J. Am. Chem. Soc.* **1977**, *99*, 2827. (*b*) Lippard, S. J. *Science* **1982**, *218*, 1075. (*c*) Ginsberg, A. P.; O'Halloran, T. V.; Fanwick, P. E.; Hollis, L. S.; Lippard, S. J. *J. Am. Chem. Soc.* **1984**, *106*, 5430. (*d*) Arrizabalaga, P.; Castan, P.; Geoffroy, M.; Laurent, J. P. *Inorg. Chem.* **1985**, *24*, 3656. (*e*) Lippert, B.; Schoellhorn, H.; Thewalt, U. *Inorg. Chem.* **1987**, *26*, 1736. (*f*) Sakai, K.; Matsumoto, K. *J. Am. Chem. Soc.* **1989**, *111*, 3074. (*g*) Sakai, K.; Matsumoto, K.; Nishio, K. *Chem. Lett.* **1991**, 1081. (*h*) Matsumoto, K.; Sakai, K.; Nishio, K.; Tokisue, Y.; Ito, R.; Nishide, T.; Shichi, Y. *J. Am. Chem. Soc.* **1992**, *114*, 8110. (*i*) Matsunami, J.; Urata, H.; Matsumoto, K. *Inorg. Chem.* **1995**, *34*, 202. (*j*) Mitewa, M. *Coord. Chem. Rev.* **1995**, *140*, 1.

[82] Tejel, C.; Ciriano, M. A.; Oro, L. A. *Chem. Eur. J.* **1999**, *5*, 1131.

[83] (*a*) Matsumoto, K.; Sakai, K. *Adv. Inorg. Chem.* **2000**, *49*, 375. (*b*) Matsumoto, K.; Ochiai, M. *Coord. Chem. Rev.* **2002**, *231*, 229. (*c*) Ochiai, M.; Lin, Y.-S.; Yamada, J.; Misawa, H.; Arai, S.; Matsumoto, K. *J. Am. Chem. Soc.* **2004**, *126*, 2536.

[84] (*a*) Bera, J. K.; Dunbar, K. R. *Angew. Chem., Int. Ed.* **2002**, *41*, 4453. (*b*) Finniss, G. M.; Canadell, E.; Campana, C.; Dunbar, K. R. *Angew. Chem., Int. Ed.* **1997**, *35*, 2772. (*c*) Prater, M. E.; Pence, L. E.; Clérac, R.; Finniss, G. M.; Campana, C.; Auban-Senzier, P.; Jerome, D.; Canadell, E.; Dunbar, K. R.. *J. Am. Chem. Soc.* **1999**, *121*, 8005. (*d*) Tejel, C.; Ciriano, M. A.; Villarroya, B. E.; López, J. A.; Lahoz, F. J.; Oro, L. A.. *Angew. Chem., Int. Ed.* **2003**, *42*, 529. (*e*) Berry, J. F.; Cotton, F. A.; Murillo, C. A.; Roberts, B. K. *Inorg. Chem.* **2004**, *43*, 2277. (*f*) Berry, J. F.; Cotton, F. A.; Murillo, C. A.

Organometallics, **2004**, *23*, 2503. (g) Kiehl, P.; Rohmer, M.-M.; Bénard, M. *Inorg. Chem.* **2004**, *43*, 3151.

[85] (*a*) Berry, J. F.; Cotton, F. A.; Daniels, L. M.; Murillo, C. A. *J. Am. Chem. Soc.* **2002**, *124*, 3212. (*b*) Berry, J. F.; Cotton, F. A.; Lu, T.; Murillo, C. A.; Wang, X. *Inorg. Chem.* **2003**, 3595. (*c*) Berry, J. F.; Cotton, F. A.; Lei, P.; Lu, T.; Murillo, C. A. *Inorg. Chem.* **2003**, *42*, 3534. (*d*) Berry, J. F.; Cotton, F. A.; Daniels, L. M.; Murillo, C. A.; Wang, X. *J. Am. Chem. Soc.* **2003**, *42*, 2418.

[86] Cotton, F. A.; Dalal, N. S.; Hillard, E. A.; Huang, P.; Murillo, C. A.; Ramsey, C. M. *Inorg. Chem.Commun.*, 2003, **42**, 1388

[87] Berry, J. F.; Cotton, F. A.; Ibragimov, S. A.; Murillo, C. A.; Wang, Xiaoping *Inorg. Chem.*, **2005**, *44*, 6129.

[88] (*a*) Hohenberg, P.; Kohn, W. *Phys. Rev*. **1964**, *136*, B864. (*b*) Parr, R. G.; Yang, W. *Density-Functional Theory of Atoms and Molecules*; Ed.; Oxford University Press: Oxford, 1989.

[89] (*a*) Becke, A. D. *Phys. Rev. A.* **1988**, *38*, 3098. (*b*) Becke, A. D. *J. Chem. Phys.* **1993**, *98*, 1372. (*c*) Becke, A. D. *J. Chem. Phys.* **1993**, *98*, 5648.

[90] Lee, C. T.; Yang, W. T.; Parr, R. G. *Phys. Rev. B*. **1998**, *37*, 785.

[91] Frisch, M. J.; Trucks, G. W.; Schlegel, H. B.; Scuseria, G. E.; Robb, M. A.; Cheeseman, J. R.; Zakrzewski, V. G.; Montgomery, J. A.; Stratmann, R. E.; Burant, J. C.; Dapprich, S.; Millam, J. M.; Daniels, A. D.; Kudin, K. N.; Strain, M. C.; Farkas, O.; Tomasi, J.; Barone, V.; Cossi, M.; Cammi, R.; Mennucci, B.; Pomelli, C.; Adamo, C.; Clifford, S.; Ochterski, J.; Petersson, G. A.; Ayala, P. Y.; Cui, Q.; Morokuma, K.; Malick, D. K.; Rabuck, A. D.; Raghavachari, K.; Foresman, J. B.; Cioslowski, J.; Ortiz, J. V.; Stefanov, B. B.; Liu, G.; Liashenko, A.; Piskorz, P.; Komaromi, I.; Gomperts, R.; Martin, R. L.; Fox, D. J.; Keith, T.; Al-Laham, M. A.; Peng, C. Y.; Nanayakkara, A.; Gonzalez, C.; Challacombe, M.; Gill, P. M. W.; Johnson, B. G.; Chen, W.; Wong, M. W.; Andres, J. L.; Head-Gordon, M.; Replogle, E. S.; Pople, J. A. *Gaussian 98*, revision A.9; Gaussian, Inc.: Pittsburgh, PA, 1998.

[92] Dunning, T. H., Jr. *J. Chem. Phys.* **1989**, *90*, 1007.

[93] (*a*) Wadt, W. R.; Hay, P. J. *J. Chem. Phys*. **1985**, *82*, 284. (*b*) Wadt, W. R.; Hay, P. J. *J. Chem. Phys.* **1985**, *82*, 299.

[94] Andrae, D.; Haussermann, U.; Dolg, M.; Stoll, H.; Preuss, H. *Theor. Chim. Acta* **1990**, *77*, 123.

[95] Because of this unusual behavior, we checked the structural data reported in ref by solving the structure of new crystals of [**4**]PF_6. All cell dimensions, bond distances, and angles are the same as those in ref. 51*b* within their standard deviations.

[96] Roundhill, D. M.; Gray, H. B.; Che, C.-M. *Acc. Chem. Res.* **1989**, *22*, 55.

[97] Yamashita, M.; Miya, S.; Kawashima, T.; Manabe, T.; Sonoyama, T.; Kitagawa, H.; Mitani, T.; Okamoto, H.; Ikeda, R. *J. Am. Chem. Soc.* **1999**, *121*, 2321.

[98] See for example ref. 74

[99] Cotton, F. A.; Feng, X.; Matusz, M. *Inorg. Chem.* **1989**, *28*, 594.

[100] This effect has been noted in the gas-phase UV photoelectron spectra of dimolybdenum and dipalladium formamidinate complexes. D. L. Lichtenberger, personal communication.

[101] (*a*) Cotton, F. A.; Donahue, J. P.; Murillo, C. A.; Pérez, L. M. *J. Am. Chem. Soc.* **2003**, *125*, 5486. (*b*) Cotton, F. A.; Donahue, J. P.; Murillo, C. A.; Villagrán, D. *J. Am. Chem. Soc.* Submitted. (*c*) Cotton, F. A.; Liu, C. Y.; Murillo, C. A.; Villagrán, D.; Wang, X. *J. Am. Chem. Soc.* **2003**, *125*, 13564.

[102] See for example: (*a*) Chisholm, M. H.; Click, D. R.; Galluci, J. C.; Hadad, C. M.; Wilson, P. J. *Organometallics*, **2003**, *22*, 4725. (*b*) Chisholm, M. H.; Davidson, E. R.; Quinlan, K. B. *J. Am. Chem. Soc.* **2002**, *124*, 15351. (*c*) Lichtenberger, D. L.; Lynn, M. A.; Chisholm, M. H. *J. Am. Chem. Soc.* **1999**, *121*, 12167.

[103] Only the first 8 of these orbitals are shown, since the other four (a_{2g}^*, e_u^*, and b_{2g}^*) are vacant and strognly antibonding, and thus too high in energy to be of importance to this discussion.

[104] The set of δ and δ* orbitals arising from the overlap of the $d_x2_{-y}2$ functions are not shown as these orbitals are vacant and high in energy and thus not relevant to our discussion.

[105] See for example: (*a*) Cotton, F. A.; Dunbar, K. R.; Falvello, L. R.; Tomas, M.; Walton, R. A. *J. Am. Chem. Soc*. **1983**, *105*, 4950 and references therein. (*b*) Bursten, B. E.; Cotton, F. A.; Fanwick, P. E.; Stanley, G. G.; Walton, R. A. *J. Am. Chem. Soc*. **1983**, *105*, 2606.

[106] See for example: (*a*) Koz'min, P. A.; Larina, T. B.; Surazhskaya, M. D. *Sov. J. Coord. Chem*. **1982**, *8*, 451. (*b*) Cotton, F. A.; Gage, L. D. *Nouv. J. Chim*. **1977**, *1*, 441.

[107] Cotton, F. A. *Inorg. Chem.* **1998**, *37*, 5710.

[108] (a) Robinson, W. T.; Fergusson, J. E.; Penfold, B. R. *Proc. Chem. Soc. London* **1963**, 116. (c) Bertrand, J. A.; Dollase, W. A.; Cotton, F. A. *J. Am. Chem. Soc.* **1963**, *85*, 1349.

[109] See for example: Doyle, M. P.; Ren, T. *Prog. Inorg. Chem.* **2001**, *49*, 113.

[110] Chifotides, H. T.; Dunbar, K. R. *Acc. Chem. Res.* **2005**, *38*, 146.

[111] Hilderbrand, S. A.; Lim, M. H.; Lippard, S. J. *J. Am. Chem. Soc.* **2004**, *126*, 4972.

[112] Denninger, U.; Schneider, J. J.; Wilke, G.; Goddard, R.; Kruger, C. *Inorg. Chim. Acta* **1993**, *213*, 129.

[113] (*a*) Godycki, L. E.; Rundle, R. E. *Acta Crystallographica* **1953**, *6*, 487. (*b*) Banks, C. V.; Anderson, S. *J. Am. Chem. Soc.* **1962**, *84*, 1486.

[114] (*a*) Peng, S. M.; Ibers, J. A.; Millar, M.; Holm, R. H. *J. Am. Chem. Soc.* **1976**, *98*, 8037. (*b*) Peng, S. M.; Goedken, V. L. *J. Am. Chem. Soc.* **1976**, *98*, 8500.

[115] (*a*) Millar, M.; Holm, R. H. *J. Am. Chem. Soc.* **1975**, *97*, 6052. (*b*) Herebian, D.; Bothe, E.; Neese, F.; Weyhermüller, T.; Wieghardt, K. *J. Am. Chem. Soc.* **2003**, *125*, 9116.

[116] In the latter case, DFT calculations show that the weak Ni···Ni interactions of 2.8 Å arise from a small but significant decrease of electron density from the Ni d_z2 orbitals (leading to partial Ni^{III} character for these ions, and therefore a partial bond). Wieghardt, K. personal communication.

[117] Oro, L. A.; Gómez-Beltrán, F.; Lahuerta-Peña, P.; González-Alvarez, D.; García-Fabián, L. *Rev. R. Acad. Cienc. Exactas, Fís., Quím. Nat. Zaragoza*, **1972**, *27*, 253.

[118] (*a*) Bellitto, C.; Dessy, G.; Fares, V. *Inorg. Chem*. **1985**, *24*, 2815. (*b*) Bellitto, C.; Dessy, G.; Fares, V. *Molec. Cryst. Liq. Cryst.* **1985**, *120*, 381.

[119] Cotton, F. A.; Murillo, C. A.; Reibenspies, J. H.; Villagrán, D.; Wang, X. P.; Wilkinson, C. C. *Inorg. Chem.* **2004**, *43*, 8373.

[120] Cotton, F. A.; Gruhn, N. E.; Gu, J. D.; Huang, P.; Lichtenberger, D. L.; Murillo, C. A.; Van Dorn, L. O.; Wilkinson, C. C. *Science* **2002**, *298*, 1971.

[121] Shadle, S. E.; Hedman, B.; Hodgson, K. O.; Solomon, E. I. *J. Am. Chem. Soc.* **1995**, *117*, 2259.

[122] In fact, recent results from UV photoelectron spectroscopy suggest that the first ionization of dinickel formamidinates is ligand based and that the ligand orbitals are therefore situated higher in energy than the corresponding nickel orbitals. Lichtenberger, D. L. personal communication.

[123] Berry, J. F.; Cotton, F. A.; Daniels, L. M.; Murillo, C. A.; Wang, X. P. *Inorg. Chem.* **2003**, *42*, 2418.

[124] Clérac, R.; Cotton, F. A.; Dunbar, K. R.; Murillo, C. A.; Pascual, I.; Wang, X. P. *Inorg. Chem.* **1999**, *38*, 2655.

[125] Berry, J. F.; Cotton, F. A.; Daniels, L. M.; Murillo, C. A. *J. Am. Chem. Soc.* **2002**, *124*, 3212.

[126] (*a*) Shieh, S. J.; Chou, C. C.; Lee, G. H.; Wang, C. C.; Peng, S. M. *Angew. Chem., Int. Ed. Engl.* **1997**, *36*, 56. (*b*) Peng, S. M.; Wang, C. C.; Jang, Y. L.; Chen, Y. H.; Li, F. Y.; Mou, C. Y.; Leung, M. K. *J. Magn. Magn. Mater.* **2000**, *209*, 80. (*c*) Lai, S. Y.; Wang, C. C.; Chen, Y. H.; Lee, C. C.; Liu, Y. H.; Peng, S. M. *J. Chin. Chem. Soc.* **1999**, *46*, 477.

[127] Berry, J. F.; Cotton, F. A.; Lei, P.; Lu, T. B.; Murillo, C. A. *Inorg. Chem.* **2003**, *42*, 3534.

[128] Kiehl, P.; Rohmer, M. M.; Bénard, M. *Inorg. Chem.* **2004**, *43*, 3151.

[129] Arnold, D. I.; Cotton, F. A.; Maloney, D. J.; Matonic, J. H. *Polyhedron* **1997**, *16*, 133.

[130] Lin, C.; Protasiewicz, J. D.; Ren, T. *Inorg. Chem.* **1996**, *35*, 7455.

[131] Nelkenbaum, E.; Kapon, M.; Eisen, M. S. *J. Organomet. Chem.* **2005**, *690*, 3154.

[132] Cotton, F. A.; Murillo, C. A.; Timmons, D. J. Unpublished results: Chemistry Department, Texas A&M University, College Station, TX.

[133] (*a*) Rappé, A. K.; Casewit, C. J.; Colwell, K. S.; Goddard, I., W. A.; Skiff, W. M. *J. Am. Chem. Soc.* **1992**, *114*, 10024. (*b*) Rappé, A. K.; Colwell, K. S. *Inorg. Chem.* **1993**, *32*, 3438.

[134] *Cerius2 Force-Field-Based Simulations*, Accelrys, Inc.:San Diego CA, 2001.

[135] (a) Stratmann, R. E.; Scuseria, G. E.; Frisch, M. J. *J. Chem. Phys.* **1998**, *109*, 8218. (b) Bauernschmitt, R.; Alrichs, R. *Chem. Phys. Lett.* **1996**, *256*, 454. (c) Casida, M. E.; Jamorski, C.; Casida, K. C.; Salahub, D. R. *J. Chem. Phys.* **1998**, *108*, 4439.

[136] Carty, P.; Dove, M. F. A. *J. Organomet. Chem.* **1971**, *28*, 125.

[137] (a) Carlson-Day, K. M.; Eglin, J. L.; Lin, C.; Smith, L. T.; Staples, R. J.; Wipf, D. O. *Polyhedron* **1999**, *18*, 817. (b) Cotton, F. A.; Ren, T. *J. Am. Chem. Soc.* **1992**, *114*, 2237.

[138] Cotton, F. A.; Daniels, L. M.; Huang, P. L.; Murillo, C. A. *Inorg. Chem.* **2002**, *41*, 317.

[139] Cotton, F. A.; Nocera, D. G. *Acc. Chem. Res.* **2000**, *33*, 483.

[140] It should be noted that the Ni−Ni distances in these Ni_2^{5+} species are significantly shorter than those in $Ni_2(S_2CCH_3)_4I$ (2.514(3) Å). See ref.118.

[141] Cotton, F. A.; Daniels, L. M.; Murillo, C. A.; Timmons, D. J.; Wilkinson, C. C. *J. Am. Chem. Soc.* **2002**, *124*, 9249.

[142] (*a*) Bailey, P. J.; Bone, S. F.; Mitchell, L. A.; Parsons, S.; Taylor, K. J.; Yellowlees, L. J. *Inorg. Chem.* **1997**, *36*, 5420. (*b*) Bailey, P. J.; Bone, S. F.; Mitchell, L. A.; Parsons, S.; Taylor, K. J.; Yellowlees, L. J. *Inorg. Chem.* **1997**, *36*, 867.

[143] (*a*) Han, B. C.; Shao, J. G.; Ou, Z. P.; Phan, T. D.; Shen, J.; Bear, J. L.; Kadish, K. M. *Inorg. Chem.* **2004**, *43*, 7741. (*b*) Kadish, K. M.; Phan, T. D.; Wang, L. L.; Giribabu, L.; Thuriere, A.; Wellhoff, J.; Huang, S. R.; Van Caemelbecke, E.; Bear, J. L. *Inorg. Chem.* **2004**, *43*, 4825. (*c*) Kadish, K. M.; Phan, T. D.; Giribabu, L.; Shao, J. G.; Wang, L. L.; Thuriere, A.; Van Caemelbecke, E.; Bear, J. L. *Inorg. Chem.* **2004**, *43*, 1012. (*d*) Kadish, K. M.; Phan, T. D.; Giribabu, L.; Van Caemelbecke, E.; Bear, J. L. *Inorg. Chem.* **2003**, *42*, 8663.

[144] Bailey, P. J.; Pace, S. *Coord. Chem. Rev*. **2001**, *214*, 91.

[145] For an account on well-known violations of Koopmans' theorem, see for example: Ferreira, R. *Struct. Bond*. **1976**, *31*, 1.

[146] From this point onwards, only the double-ζ basis set was used to allow swifter convergence and since the geometries calculated with the lager basis set are not significantly better in quality as compared to the experimental results.

[147] An indication that the nature of the substituents in the ligand has an important effect on the dimetal unit has been provided by the CVs of Ni_2(formamidinate)$_4$ compounds that showed a significant variation in the $E_{½}$ values as the value of the Hammet constant of the substituent is modified. See ref.130.

[148] Since the hydrogen atoms in the crystal structure are placed in calculated positions, the C–H bond distances are underestimated. Therefore, the hydrogen atom positions were optimized using the universal force field (UFF, see Experimental section) keeping the rest of the structure fixed.

[149] It should be noted that a previous Xα calculation on a simplified model had shown that the odd electron in the oxidized complex was in an orbital of δ* symmetry rather than one of σ* symmetry. See ref. 51*b*.

[150] See for example: Kokatam, S.; Weyhermüller, T.; Bothe, E.; Chaudhuri, P.; Wieghardt, K. *Inorg. Chem.* **2005**, *44*, 3709.

[151] Bottrill, M.; Gavens, P. D.; *Comprehensive Organometallic Chemistry*, Wilkinson, G., Ed.; Pergamon Press: Oxford, 1982.

[152] Hao, S.; Fegali, K.; Gambarotta, S. *Inorg. Chem.* **1997**, *36*, 1745.

[153] Utko, J.; Przybylak, S.; Jerzykiewicz, L. B.; Mierzwicki, K.; Latajka, Z.; Sobota, P. *Inorg. Chem.* **2003**, *42*, 267.

[154] Cotton, F. A.; Wojtczak, W. A. *Gazz. Chim. Ital.* **1993**, *123*, 499.

[155] (*a*) Horáček, M.; Kupfer, V.; Thewalt, U.; Štěpnička, P.; Polášek, M.; Mach, K. *J. Org. Chem.* **1999**, *584*, 286; (*b*) Sobota, P.; Ejfler, J.; Szafert, S.; Szczegot, K.; Sawka-

Dobrowolska, W., *J. Chem. Soc., Dalton Trans*., **1993**, *15*, 2353; (*c*) Alyea, E. C.; Bradley, D. C.; Lappert, M. F.; Sanger, A. R. *J. Chem. Soc. Chem. Commun.* **1969**, 1064; (*d*) Olthof, G. J. *J. Organomet. Chem.* **1977**, *128*, 367.

[156] Coles M. P.; Hitchcock P. B., *J. Chem. Soc., Dalton Trans.,* **2001**, 1169.

VITA

Sergey Ibragimov received his Master of Science degree in chemistry from Lomonosov Moscow State University in June of 2000. He began graduate study at Texas A&M University in September of 2001 and graduated with a Ph.D. His research interests include inorganic supramolecules and the formation of metal-metal bond in paddlewheel compounds.

Sergey Ibragimov may be reached at Moscow, Profsoyuznaya street, house 18, building 1, 117292, Russia.

Email address: ibragimov1979@rambler.ru